NTNU
Norwegian University of
Science and Technology

Voronoi Based Deployment for Multi-Agent Systems

Johan Hatleskog

Master of Science in Cybernetics and Robotics
Submission date: August 2018
Supervisor: Morten Hovd, ITK
Co-supervisor: Sorin Olaru, CentraleSupelec

Norwegian University of Science and Technology
Department of Engineering Cybernetics

Abstract

This thesis investigates convergence in the framework of Voronoi-based deployment of a multi-agent system to a convex polytopic multi-dimensional environment. The deployment objective is to drive the system into a stable static configuration which exhibits optimal coverage of the target environment. To this end, the system is subjected to a collection of decentralized control laws steering each agent towards a Chebyshev center of its associated time-varying polytopic Voronoi-neighborhood. In non-degenerate cases, so-called Chebyshev configurations of the multi-agent system achieves the above objective. In these configurations, all agents are at a Chebyshev center of their Voronoi-neighborhood. Proving convergence to the set of Chebyshev configurations is an open research question. This is the most pertinent issue with regards to the framework viability. While such a property is supported by simulations, neither complete formal convergence proofs nor formal characterizations of the equilibria to be achieved exist. This thesis is oriented towards strengthening the theoretical convergence results. For the special case of deployment to one-dimensional environments, we prove convergence to an unique static Chebyshev configuration. Moreover, we highlight connections to discrete time averaging systems and show how the system converges to consensus on the Chebyshev radii. The remaining results apply in the general case of multi-dimensional environments. We introduce a novel undirected interaction graph as a theoretical tool for a deeper understanding of the multi-agent system's functioning. Exploiting this graph, we prove that the set of static configurations are Chebyshev configurations in which all subsets of agents within the same connected component of the interaction graph are in consensus on their Chebyshev radii. Finally we prove convergence to a Chebyshev configuration, with consensus on the Chebyshev radii, provided the interaction graph is connected along the trajectories of the multi-agent system. Throughout the presentation, the theoretical results are motivated and supported by simulations.

Keywords: Deployment Problem, Coverage Problem, Dynamic Voronoi partition, Chebyshev Center, Decentralized control.

Sammendrag

Norwegian abstract

Denne avhandlingen omhandler konvergens innenfor et Voronoi-basert rammeverk for å utplassere et multi-agent system i et konvekst polytopisk mange-dimensjonalt område. Målet for utplasseringen er å styre systemet til en stabil og statisk konfigurasjon hvor agentene dekker området i en viss optimal forstand. For å oppnå dette, benyttes en samling av desentraliserte styringslover som styrer hver enkelt agent mot et Chebyshev-senter av dens tilhørende tidsvarierende polytopiske Voronoi-nabolag. I ikke-degenererte tilfeller blir nevnte mål oppnådd av såkalte Chebyshev-konfigurasjoner av systemet. I disse konfigurasjonene er alle agentene i et Chebyshev-senter av deres Voronoi-nabolag. Å bevise konvergens til slike konfigurasjoner er et åpent problem. En slik konvergens-egenskap er støttet av simuleringer, men det finnes ingen fullstendige formelle bevis. Denne avhandlingen er rettet mot å styrke de teoretiske konvergens-resultatene for rammeverket. For spesialtilfellet der multi-agent systemet utplasseres i et en-dimensjonalt område, beviser vi konvergens til en unik statisk Chebyshev-konfigurasjon. Videre trekker vi frem koblinger til konsensus-teori fra lineær distribuert reguleringsteori, og viser at systemet konvergerer til konsensus på agentenes Chebyshev-radius. De gjenværende resultatene gjelder i de mer generelle tilfellene der området agentene utplasseres i er mange-dimensjonalt. Vi introduserer en ny urettet interaksjons-graf. Ved å benytte denne grafen, viser vi at settet av statiske konfigurasjoner er Chebyshev-konfigurasjoner der alle subset av agenter innenfor samme sammenhengende sub-graf av den originale grafen har konsensus på deres tilhørende Chebyshev-radiuser. Til slutt beviser vi konvergens til en Chebyshev-konfigurasjon med konsensus på Chebyshev-radiuser i tilfeller hvor interaksjons-grafen er sammenhengende langs banen multi-agent systemet beveger seg i. De teoretiske resultatene er motivert av og underbygget av simuleringer.

Acknowledgments

This work has been conducted during the second of two semesters of visiting studies at the Centre National de la Recherche Scientifique (CNRS) Laboratoire des Signaux et Systèmes at CentraleSuplec, Gif-sur-Yvette, France. I would like to thank Professor Morten Hovd (NTNU) for his supervision and for facilitating the visiting studies. Furthermore, I am very grateful to my local supervisor Professor Sorin Olaru (CentraleSupelec) and the other members of the lab for welcoming me.

I would also like to thank my fiancé Sunniva.

Paris, August 26, 2018.

Contents

Preface

This preface provides background information on the thesis. In compliance with guidelines from the NTNU Department of Engineering Cybernetics, the preface content has been attested by the supervisors upon submission of the thesis.

Problem description: A common principle in a wide range of multi-agent system (MAS) applications is to let a group of mobile agents deploy in a predetermined target region with the objective of attaining a static configuration such that the coverage of the region is maximized. This problem is known as *the deployment problem*.

Most works in the deployment problem literature are so-called Voronoi partition based. At each time instant, a bounded convex polyhedral working region is partitioned using a Voronoi algorithm providing the agents with non-overlapping functioning zones. The deployment objective is achieved by using local stabilizing feedback control ensuring the convergence of each agent towards a geometric center of its associated time-varying functioning zone.

Many recent research works focus on driving the MAS into a centroidal Voronoi configuration in which the position of each agent coincides with the center of mass of its associated Voronoi cell. However, computing the center of mass of a polytope can be prohibitively expensive in terms of computational resources. To overcome this difficulty, other geometric centers have to be considered.

A pertinent candidate in this respect, is the Chebyshev center. This can be computed easily by a convex optimization. Consequently, the use of the Chebyshev center as an alternative target point has been investigated in recent works. Disregarding certain degenerate cases, simulations support the conjectured property of MAS convergence to particular optimal static configurations.

However, the pursuit after formal convergence proofs represent an open research problem. Due to the non-linear nature of the resulting MAS dynamics, with an optimization in the loop, convergence proofs are non-trivial to obtain. Few analytic expressions are available. Moreover, the involved quantities do not exhibit the monotonicity required for applying standard Lyapunov-like approaches. Complete proofs of convergence to optimal static configurations only exists for the trivial case of single-agent systems. As such, strengthening the convergence results is imperative for this research topic.

The purpose of this thesis is to move towards stronger convergence results. The first objective is to examine the closed loop functioning of the MAS under Chebyshev control schemes. The goal is to uncover additional mathematical structure to better understand the convergence properties of the MAS. The second objective is to widen the scope of assumptions under which convergence to Chebyshev configurations can be proven.

Academic background and context: This thesis is submitted in satisfaction of the requirements for the 30 ECTS credits course TTK4900 Engineering Cybernetics Master's thesis at NTNU. It is submitted in partial satisfaction of the requirements for NTNU's five years integrated Master of Science degree in Engineering Cybernetics.

The thesis work has been carried out during visiting studies at the Centre National de la Recherche Scientifique (CNRS) Laboratoire des Signaux et Systèmes at CentraleSupélec, Gif-sur-Yvette, France. It succeeds a student project by the thesis author, also conducted at CentraleSupélec, on the same deployment framework. Both this thesis as well as the student project can be regarded as a continuation of a line of research pursued in the PhD [Nguyen, 2016] under the supervision of Professor Sorin Olaru (CentraleSupélec).

The student project addressed the problem of finding particular unique geometric centers of polytopes within the subset of Chebyshev centers. It was also helpful in becoming familiar with the deployment problem. The direction of this thesis is motivated by simulation results from the project illustrating that former convergence results rely on assumptions which do not hold in the general case.

Results on convergence in the present manuscript were all obtained during the work on the Master's thesis. All novel results in this thesis have been obtained by the author during the course of the thesis work. The supervisors have served as discussion partners and have pointed the author to relevant literature on the area. No outside assistance has been received.

The work has been of a research oriented nature. Numerous theoretical approaches have been tried to tackle the objectives and simulation based benchmarks have been established. The presentation in this thesis builds on those which proved fruitful and relevant to the main results. A summary of the main thesis contributions is provided in section 1.1, and is also attested by the supervisors.

Prerequisites: The reader is assumed to be familiar with standard results and concepts from linear algebra, linear systems theory, real analysis, convex optimization and nonlinear systems and control.

Typesetting and figures: This document was typeset using the LaTeX typesetting system. The template is derived from the ETH IDSC LaTeX template [Ritter et al., 2017]. Several figures have been exported from Matlab using `matlab2tikz` [Schlömer, 2008]. Finally, many figures contain elements generated with the Multi-Parametric Toolbox 3 [Herceg et al., 2013].

Nomenclature

$\mathbb{N}$	Set of positive integers $\{1, 2, \dots\}$.
$\mathbb{N}_q$	Positive integers up to $q \in \mathbb{N}$, i.e. $\mathbb{N} = \{1, 2, \dots, q\}$.
$\mathbb{R}^d$	Space of reals of dimension $d \in \mathbb{N}$.
$\mathbb{R}_+$	Positive orthant of $\mathbb{R}$.
$\text{int}(S)$	Interior of the set S.
∂S	Boundary of the set S.
$A \subset B$	A is a proper subset of B.
$A \subseteq B$	A is an improper subset of B.
$A \oplus B$	Minkowski sum of the sets A and B.
$A \ominus B$	Pontryagin difference between the sets A and B.
$A \backslash B$	Set difference between the sets A and B.
$\dim(S)$	Dimension of the set S.
$\mathbb{1}$	Vector of all ones.
$\mathbb{0}$	Vector of all zeros.
e_i	Standard basis vector. The i'th entry is 1 while all other entries are zero.
A^T	Transpose of the matrix or vector A.
$\text{spec}(A)$	Spectrum of the matrix A.
$\rho(A)$	Spectral radius of the matrix A.
I	Identity matrix.
$\|x\|$	Euclidean norm of the vector x (unless otherwise stated).
$\mathbb{B}_r(x_0)$	Closed ball centered at x_0 with radius r
$\text{dist}(x, A)$	Euclidean distance between a point x and a set A.

$\text{depth}(x, A)$	Depth of x in the set A. I.e. $\text{dist}(x, \partial A)$ provided $x \in A$.
$\mathcal{G}$	Directed or undirected graph.
$\mathcal{V}$	Nodes of some graph $\mathcal{G}$.
$\mathcal{E}$	Edges of some graph $\mathcal{G}$.
$\bar{x}_i$	Some Chebyshev center associated with agent i.
$\mathbb{V}_i$	Voronoi cell associated with agent i.
r_i	Agent depth, defined as $\text{depth}(x_i, \mathbb{V}_i)$ where x_i is the agent state.
$\tilde{r}_i(k)$	Depth of agent state $x_i(k+1)$ relative to the Voronoi cell at time k, $\mathbb{V}_i(k)$.
$\bar{r}_i$	Chebyshev radius associated with agent i, defined as $\text{depth}(\bar{x}_i, \mathbb{V}_i)$.
r_m	Lower bound on r_i, $r_m = \min_i r_i$.
$\tilde{r}_m$	Lower bound on $\tilde{r}_i$, $\tilde{r}_m = \min_i \tilde{r}_i$.
$\bar{r}_m$	Lower bound on $\bar{r}_i$, $\bar{r}_m = \min_i \bar{r}_i$.
$\bar{r}_M$	Upper bound on $\bar{r}_i$, $\bar{r}_M = \max_i \bar{r}_i$.
$\mathcal{W}$	Environment to which the multi-agent system is deployed.
$\mathcal{X}_{\text{D}}$	Set of configurations with distinct agent states in $\mathcal{W}$.
$\mathcal{X}_{\text{SC}}$	Set of static configurations.
$\mathcal{X}_{\text{CC}}$	Set of Chebyshev Configurations.

Chapter 1

Introduction

Many tasks within mobile robotics are concerned with deploying a set of cooperating agents to a predetermined bounded environment of interest. Subject to constraints like collision avoidance [Tanner, 2004], minimum energy consumption [Schwager et al., 2011; Song et al., 2014] and robustness to disturbances [Bakolas and Tsiotras, 2013], the overarching goal is to attain a static configuration of the robots which maximizes the coverage of the target region. This principle is applicable in settings such as environmental monitoring, surveillance and rescue operations [Cortes et al., 2006; Murray, 2007; Tanner et al., 2007; Bullo et al., 2009].

In the control literature, this task is known under the names *the deployment problem* [Bullo et al., 2009] and *the coverage problem* [Mesbahi and Egerstedt, 2010]. In particular, several works within distributed control of multi-agent systems tackle this problem. These works limit admissible solutions to those amenable to a so-called distributed or decentralized implementation.

Standard control theory generally grants controllers for each subsystem access to the global system state, known as *centralized* control. This follows from assuming an information structure where either i) each controller may communicate with a central coordinator, or ii) all subsystems may communicate with each other over a fully connected network [Ren and Beard, 2008]. Contrary to centralized control, *distributed* controllers have weaker couplings. They do not communicate with a central coordinator, and the intra-subsystem communications structure is of a sparse nature.

In the context of multi-agent systems, the agents represent the subsystems. These can for instance be autonomous underwater vehicles, unmanned surface vehicles or unmanned aerial vehicles. In distributed control of multi-agent systems, each agent may only communicate with some, possibly time-varying, subset of its fellow agents. For the deployment problem, this typically translates to a communication structure where each agent may only communicate with the subset of agents defined to be its neighbors.

In decentralized control, the constraints on communications are stricter than for distributed control. Typically distributed control schemes involve some extent of intra-sample communication between agents. Distributed controllers may exploit this kind of communication to coordinate with controllers of neighboring agents. Decentralized controllers are not given this privilege [Nguyen, 2016].

In terms of optimal control, distributed and decentralized controllers will perform no better than those utilizing a centralized structure. This is a simple consequence of optimizing over a subset rather than the whole space of available control structures. As such, it is reasonable to ask what is gained by applying this restriction. For multi-agent systems, it is typically motivated by concerns related to scalability, fault tolerance, limited communication capabilities, range-limited sensing capabilities and scarceness of computational resources [Mesbahi and Egerstedt, 2010; Ren and Beard, 2008]. In many applications, including those categorized as deployment problems, knowledge of the entire system state is neither feasible nor desirable. Real world communication topologies are usually not fully connected, and utilizing a central coordinator involves risk of catastrophic system failure due to having a single point of failure [Ren and Beard, 2008]. Rather, the synthesized controllers should make the system converge to global optimality despite only relying on spatially local information and interactions.

To this end, most works within the deployment problem literature are variations about so-called Voronoi partition [Voronoï, 1908] based deployment. In these schemes, the polyhedral target region is partitioned into equally many cells as there are agents. For each agent, the interior of their corresponding cell contains all points to which the current agent is the closest. In this manner, the target region is partitioned into disjoint subsets where each subset has a corresponding agent responsible for its coverage. As the partition is with respect to the agents time-varying positions, it is itself time-varying. Thus it is a *dynamic Voronoi partition*. Decentralized control schemes tackling the deployment problem exploit the fact that any agent may compute its own Voronoi cell using exclusively local information. Specifically, knowledge of the borders of the target region and positions of agents in adjacent cells is sufficient for any agent to compute its own Voronoi cell. Next, most Voronoi based schemes pick some target geometric center within the agent's cell such that the convergence of each agent to its geometric center ensures the convergence of the global system to a static configuration. Again, the geometric centers will be time-varying due to the time-varying nature of its underlying structure. Thus the geometric center must itself converge while the agent converges towards it.

Much attention has been devoted to continuous and discrete time schemes utilizing the centroid as the geometric center [Cortes et al., 2004; Kwok and Martinez, 2010; Yan and Mostofi, 2012; Song et al., 2014; Moarref and Rodrigues, 2014]. The goal is to make the system converge to a *Centroidal Voronoi Configuration*, where the position of each agent corresponds to the centroid of its corresponding cell. Additionally, works such as [Cortes et al., 2002, 2005; Martinez et al., 2007] consider the extension where one endows the target region with a mass density function and steer the agents towards the center of mass of their cells.

However, computing the centroid and center of mass of a polytope is in general not easy. The complexity of computing the involved integrals increase with the dimension of the state space [Nguyen, 2016]. Closed form solutions for polytope centroids only exist for the one-dimensional and two-dimensional cases[1]. Numerical approximation schemes are necessary in high dimensional spaces. To overcome this difficulty, other geometric centers have been considered.

Nguyen and Maniu [2016] and Nguyen [2016] consider the use of a so-called Vertex-interpolated center in discrete time. At each time instant, all agents compute their respective target points by solving a quadratic program.

Cortes and Bullo [2005] use the circumcenter as the target point in the context of continuous time multi-agent systems deployed to the plane. The circumcenter is the minimal radius enclosing Euclidean ball of a polytope. In a discrete time implementation, the circumcenter can be found by solving an appropriate quadratically constrained linear program.

In this manuscript we consider the discrete time Voronoi-based framework in [Nguyen et al., 2017], this case being closer to a practical application where the control actions are computed in at a regularly spaced interval. The authors use the Chebyshev center of a cell, the center of an inscribed Euclidean ball of maximal radius, as the target. The radius of this ball is known as the Chebyshev radius. Finding a Chebyshev center and the corresponding Chebyshev radius amounts to solving a linear program with the representation of the agent's Voronoi cell as input. While linear programs have no explicit solutions, they are well known to be easy to solve [Boyd and Vandenberghe, 2004]. Thus this framework is an attractive alternative to centroid-based methods in terms of computational strain. Additionally, the controllers based on the Chebyshev center are indeed amenable to a decentralized implementation.

The use of Chebyshev centers in a deployment setting was first investigated by Cortes and Bullo [2005]. The authors consider a continuous time multi-agent system (MAS) in the plane where all agents adhere to single integrator dynamics. Moreover, a so-called *sphere packing multicenter function* is introduced. Evaluated at a particular MAS configuration, this multicenter function provides the largest radius guaranteeing that the equal-radius open spheres centered at the agent positions are contained in the target environment and are pairwise disjoint. By means of non-smooth analysis, the authors show that this multicenter function is monotonically optimized when utilizing specific control laws steering each agent towards some Voronoi cell Chebyshev center. This establishes the optimality of the MAS limit configurations.

However, proving convergence to a local optimum of the sphere packing multi-center function is not sufficient to establish stationarity. A necessary step in ensuring convergence to a static configuration is showing convergence to a so-called Chebyshev configuration [Nguyen et al., 2017]. The MAS is in a Chebyshev configuration when all agents are at a Chebyshev center of their respective Voronoi cells. In [Bullo et al., 2009] this is referred to as an open research question. This conjectured property is supported by simulations in [Nguyen et al., 2017; Bullo et al., 2009; Cortes and Bullo, 2005].

[1] See for instance Cortes et al. [2004] for explicit formulas in the $\mathbb{R}^2$ case.

The frameworks presented in Nguyen et al. [2017] and Cortes and Bullo [2005] are related by virtue of exploiting the same target point. Meanwhile they differ in the sense that the former paper i) considers discrete time dynamics, ii) accommodates a larger class of heterogeneous agent dynamics and iii) allows for deployment to both the plane as well as $\mathbb{R}^d$ for any finite $d \in \{1, 2, \dots\}$. Proving convergence to a Chebyshev configuration for discrete time MAS was thought to be solved by a result in [Nguyen et al., 2017]. In the prequel to the present thesis, the report [Hatleskog, 2017], said result came under scrutiny. There it is shown that the convergence result in [Nguyen et al., 2017] relies on an assumption which fails in several common cases. As a consequence, the most pertinent question related to the framework is currently the convergence to a Chebyshev configuration.

This thesis is oriented towards providing formal convergence results for the discrete time Voronoi-based MAS deployment framework. Thus we aim to cover some of the open research questions in Nguyen et al. [2017]. To this end, we thoroughly investigate the closed loop functioning of the MAS subject to such a decentralized Voronoi-based control scheme. Motivated by numerical illustrations, we uncover mathematical mechanisms and structure which steers the MAS towards some Chebyshev configuration. We show that the closed loop functioning of deployment in 1D can be analyzed with standard tools from discrete time averaging systems. By introducing novel graph theoretic notions, we characterize the topology of static MAS configurations and highlight connections to consensus algorithms. By exploiting the same graph theoretic notions, we illustrate how MAS behavior under deployment in multi-dimensional environments can be understood and analyzed with generalizations of the concepts exploited in the 1D case.

1.1 Contributions

This section summarizes the main contributions of the thesis. The first results apply when agents complying with discrete time single integrator dynamics are deployed to a 1-dimensional environment. The agents are subjected to linear time-invariant agent control laws steering each agent towards the current Chebyshev center of their Voronoi cells.

(i) It is shown that the MAS dynamics adhere to discrete time affine time-invariant dynamics. Analyzing the resulting systems of equations with tools and results from algebraic graph theory and discrete time averaging systems, we prove convergence of the MAS to an unique static Chebyshev configuration. Upon closer inspection we reveal that one cannot expect finite time convergence, rather the convergence is asymptotic.

(ii) The explicit discrete time linear time-invariant dynamic equation for the Chebyshev radii of the agents is derived. Upon analyzing the dynamics, we prove convergence to consensus on the Chebyshev radii. I.e. we prove that convergence to the unique static Chebyshev configuration implies convergence to equal Chebyshev radii for all agents.

To the best of the authors' and thesis supervisors knowledge, this is the first time such explicit connections between the present deployment framework and discrete time averag-

ing systems have been shown. Additionally, these are the first results proving convergence to a static Chebyshev Configuration in $\mathbb{R}$.

The remaining results apply in a more general context. We assume deployment to $\mathbb{R}^d$. All agents adhere to discrete time linear time-invariant dynamics and respect the same regularity conditions as imposed in [Nguyen et al., 2017]. The agents are subjected to control laws steering each agent to the subsets of their current Voronoi cells where the distances to the boundary is longer than, or otherwise at least as long as, the current distance from the agent to the boundary. Under these assumptions we first prove:

(iii) The non-decrease and convergence of the minimum distance any agent has to its cell boundary. This extends a result we derived for single integrator dynamics and linear controllers in [Hatleskog, 2017].

(iv) The convergence of the minimal Chebyshev radius.

Further to analyzing functioning of the framework, we introduce and exploit graph theoretic notions. In particular:

(v) We introduce the notion of an interaction graph to the framework, encoding the ability of agents to affect each others Chebyshev radii.

(vi) Exploiting the interaction graph, we examine the topology of static MAS configurations. We prove that these correspond to Chebyshev configurations where all agents within the same connected component of the interaction graph have consensus on their Chebyshev radii.

(vii) The main result in this thesis is a convergence proof exploiting the interaction graph. We prove convergence to a Chebyshev configuration whenever the time-varying interaction graph is connected along the trajectories of the MAS. Moreover, the connectedness of the interaction graph ensures convergence to consensus on agent Chebyshev radii.

These novel theoretical notions and the corresponding results are the most important thesis contributions.

The convergence results in $\mathbb{R}^d$ will also appear in the accepted paper:

- Johan Hatleskog, Sorin Olaru and Morten Hovd. Voronoi-based deployment of multi-agent systems. 57th IEEE Conference on Decision and Control (CDC), Florida, USA, 2018.

to be presented in December 2018.

1.2 Organization of the thesis

The outline of the thesis is as follows: In chapter 2 we provide an introduction to the Chebyshev center based deployment framework. Section 2.1 presents useful theoretical

background before the following framework introduction in sections 2.2-2.5. Next we motivate the theoretical developments with several numerical illustrations in section 2.7. A problem statement follows in section 2.8. Chapter 3 is devoted to convergence results. Additional theoretical background is presented in 3.1. Section 3.2 discussed preliminary convergence notions. Convergence results on for deployment in $\mathbb{R}$ are presented in 3.3 whereas $\mathbb{R}^d$-results are presented in section 3.4. Finally we conclude in chapter 4.

We end this introductory chapter with a brief section on mathematical notation and conventions.

1.3 Notation and conventions

Let $\mathbb{N} = \{1, 2, \dots\}$ be the set of natural numbers. We define $\mathbb{N}_l = \{1, 2, \dots, l\} \subset \mathbb{N}$ as the subset of natural number less or equal to $l \in \mathbb{N}$. The set of strictly positive real numbers is denoted by $\mathbb{R}^+$. The Minkowski sum and Pontryagin difference of two appropriate sets P, Q is $P \oplus Q$ and $P \ominus Q$ respectively. λP for $\lambda \in \mathbb{R}^+$ is a λ-scaling of the set P. The Minkowski sum, the Pontryagin difference and λ-scaling is introduced in section 2.1.4. Finally ∂P and $\text{int}(P)$ denotes respectively the boundary and the interior of the set P.

Unless otherwise specified, $\|\cdot\|$ is the standard Euclidean metric. $\mathbb{B}_r(x_0) \subset \mathbb{R}^d$ is a closed d-dimensional Euclidean ball centered at $x_0 \in \mathbb{R}^d$ with radius $r \in [0, \infty)$. We use the shorthand $\mathbb{B}_r = \mathbb{B}_r(0)$. The distance between a point $p \in \mathbb{R}^d$ and a set $Q \subset \mathbb{R}^d$ is defined as $\text{dist}(p, Q) = \inf\{\|p - q\| \mid q \in Q\}$.

$\mathbb{1}$ and $\mathbb{0}$ are appropriately sized column vectors of ones and zeros respectively. The i'th standard basis vector is e_i. I.e. $e_i^T e_i = 1$ and $e_i^T e_j = 0$ when $i \neq j$. Vector inequalities are to be understood element wise. E.g. for $u, v \in \mathbb{R}^d$, then $u \leqslant v \iff e_i^T u \leqslant e_i^T v \forall i \in \mathbb{N}_d$. I is an identity matrix of appropriate dimension. In general, dimensions will rarely be stated and should be understood from context.

Let $f(x_1, \dots, x_N)$ be some function. If one or more arguments are discrete time-varying, e.g. $x_i = x_i(k)$, then we often use $f(k) = f(x_1(k), \dots, x_N(k))$ as a shorthand for evaluating $f(\cdot)$ along the trajectories of its arguments. E.g. an energy function $V(x) = x^T x$ is time invariant, and has the shorthand $V(k) = V(x(k))$ when evaluating it along the trajectory $x(k)$.

Chapter 2

Framework description

In this chapter we introduce the Voronoi-based discrete time deployment framework following the setup proposed in [Nguyen et al., 2017; Nguyen, 2016]. Framework-related notions such as target environment and agent neighborhood will be formally defined. Additionally we introduce the depth of a point in polytope, Chebyshev centers, the polytopic set of Chebyshev centers and other important mathematical notions. Convergence proofs are deferred to chapter 3. We do however prove certain important framework properties, e.g. collision avoidance. Moreover, the forthcoming theoretical developments are motivated by numerical illustrations in section 2.7.

2.1 Theoretical background

In this section we provide a non-exhaustive treatment of topics and notions central to the framework. Sections 2.1.1 and 2.1.2 provides general theory on affine sets and polytopes. These can be skipped by readers familiar with the theory. Section 2.1.3 highlights a few useful connections between linear programming and the theory on polytopes. Section 2.1.4 introduces set theoretic notions such as the Minkowski sum, Pontryagin difference and contraction of a set. The most specialized section is 2.1.5. There we introduce the definition of a Chebyshev center as well as the of depth of a point in a polytope. Both notions will be used frequently in the sequel. For implementations of the framework, the linear program formulation for finding a Chebyshev center the Chebyshev radius of a polytope is also provided.

2.1.1 Affine sets

This section is devoted to recalling necessary set theoretic notions related to affine and convex sets. The section follows [Boyd and Vandenberghe, 2004].

An *affine combination* of points $x_1, \ldots, x_k$ is a linear combination of the points such that the coefficients sum to one. I.e.

$$\sum_i \theta_i x_i \text{ such that } \sum_i \theta = 1 \text{ with } \theta_i \in \mathbb{R}. \tag{2.1}$$

The definition is similar to that of a convex combination of points. However for convex combinations we require $\theta_i \geqslant 0$ while for affine combinations $\theta_i \in \mathbb{R}$. I.e. convex combinations are a subset of affine combinations.

A set $C \subset \mathbb{R}^d$ is *affine* if for any points $x_1, x_2 \in C$ all affine combinations of the same points are contained in C. Let C be an affine set, then

$$V(x_0) = \{x - x_0 \mid x \in C\}, x_0 \in C \tag{2.2}$$

is a subspace of $\mathbb{R}^d$. Conversely the affine set may be expressed as

$$C = \{v + x_0 \mid v \in V\}, x_0 \in C. \tag{2.3}$$

Hence an affine set is simply a subspace plus an offset. The offset may be selected as any arbitrary point in C. The dimension of an affine subset is, by definition, the dimension of its corresponding subspace. I.e.

$$\dim(C) = \dim(V(x_0)) \text{ with } x_0 \in C. \tag{2.4}$$

In determining the dimension of an affine set C, one may equivalently consider the number of affinely independent points in C. Let $\{p_0, \ldots, p_k\}$ be a set of distinct points. Then they are affinely independent if and only if

$$\sum_{i=1}^{k} \theta_i (p_i - p_0) = 0 \tag{2.5}$$

has the unique solution $\theta_1 = \cdots = \theta_k = 0$. If these $k + 1$ points are affinely independent, then the dimension of C is k. The link to linear independence of vectors in subspaces is apparent here. Intuitively one may think of the dimension of an affine set as the number of independent directions it is possible to move and still stay in the set when starting at an arbitrary point in the set. For instance any plane embedded in $\mathbb{R}^3$ is an affine set. Clearly the dimension of this affine set is two.

An ubiquitous example of an affine set is the solution set of linear equations, i.e.

$$C = \{x \in \mathbb{R}^d \mid Ax = b \in \mathbb{R}^m\} \tag{2.6}$$

In this case the subspace associated with C is the nullspace $N(A)$ of A. Every affine set may be expressed as the solution set of a system of linear equations.

Let P be a subset of $\mathbb{R}^d$. Then the affine hull of P, $\text{aff}(P)$, is the set of all affine combinations of points in P. That is

$$\text{aff}(P) = \{\theta_1 x_1 + \theta_2 x_2 + \cdots + \theta_k x_k \mid x_1, \ldots, x_k \in P, \theta_1 + \cdots + \theta_k = 1\}. \tag{2.7}$$

The affine dimension of a set $P \subset \mathbb{R}^d$ is defined as the dimension of its affine hull. I.e. $\text{affdim}(P) = \dim(\text{aff}(P))$. If a set $P \subset \mathbb{R}^d$ has $\text{affdim}(P) < d$ then $P \subset \text{aff}(P) \neq \mathbb{R}^d$. I.e. all $x \in P$ are constrained to a subset of an affine subset of $\mathbb{R}^d$. This concept is of particular importance in constrained optimization, where equality constraints may force feasible solutions $x_f \in \mathbb{R}^d$ to be in a set P of lower dimension than d. In these cases projecting onto a lower dimensional space may lead to an easier optimization problem.

Remark 2.1.1. *In some cases the affine dimension is inconsistent with our usual notions of dimension. One particular example: The affine dimension of $\varnothing$ is -1. This may make more sense after considering the link between an affine subset C consisting of a single point p and its corresponding subspace $V = V(x_0) = \{p' - p \mid p' \in C\} = \{0\}$. $V(p)$ clearly has dimension 0 in this case. I.e. an affine set consisting of a single point essentially corresponds to the zero vector.*

2.1.2 Polyhedra and polytopes

We define a *polyhedron* $P \subset \mathbb{R}^d$ as the set of solutions to the system of m linear inequalities[1][2]

$$P = \{x \in \mathbb{R}^d \mid Ax \leqslant b\} \tag{2.8}$$

with $A = \left[a_{i\in\mathbb{N}_m}^T\right] \in \mathbb{R}^{m\times n}$, $a_i \neq \mathbb{0}\ \forall\ i \in \mathbb{N}_m$ and $b \in \mathbb{R}^m$ [Fukuda, 2016]. This representation is called the H-representation, as it represents the polyhedron as the intersection of a finite number of half spaces. It is inherently convex as P is defined as the intersection of a finite number of convex sets. To simplify the presentation, it is often beneficial to assume that all rows,

$$\text{row}_i(A) = e_i^T A = a_i^T, \tag{2.9}$$

are normalized to unit length in the euclidean norm. I.e. $\|a_i\|_2 = 1$. Let $P = \{x \in \mathbb{R}^d \mid Ax \leqslant b \in \mathbb{R}^m\}$ be a polyhedron. Define $D = \text{diag}(\|a_1\|_2, \ldots, \|a_m\|_2)$. Furthermore let

$$\hat{A} = D^{-1}A \tag{2.10}$$

$$\hat{b} = D^{-1}b \tag{2.11}$$

Inherently the half space representation

$$a_i^T x \leqslant b \tag{2.12}$$

is invariant to scaling by a positive constant. Thus

$$P = \{x \mid Ax \leqslant b\} = \{x \mid \hat{A}x \leqslant \hat{b}\}. \tag{2.13}$$

[1] Some texts use the term *convex polyhedron(s)*. However with our definition of polyhedra the convexity is inherent and consequently we simply say polyhedron(s).

[2] Polyhedra is polyhedron in plural form.

Hence one may assume that polytopes are *normalized* according to the above procedure without loss of generality. Normalized or not, the H-representation is not unique. Eg. let $a_r^T x \leqslant b_r$ be some constraint which holds for all $x \in P$. The set P is invariant to the addition of any such *redundant* constraint to P in the sense that

$$P = (\cap_{i=1}^{m}\{x \mid a_i^T x \leqslant b_i\}) \cap \{x \mid a_r^T x \leqslant b_r\} = (\cap_{i=1}^{m}\{x \mid a_i^T x \leqslant b_i\}) = \{x \mid Ax \leqslant b\}. \tag{2.14}$$

Conversely, let P' be a polyhedron where one or more of the inequalities in the H-representaion of P are removed. If $P' = P$, the removed inequalities were redundant constraints of P.

A rich set of bounded and unbounded objects may be represented as polyhedra. For instance lines, planes, line-segments and all affine subspaces are polyhedra. Figure 2.1 shows three examples of polyhedra in $\mathbb{R}^2$.

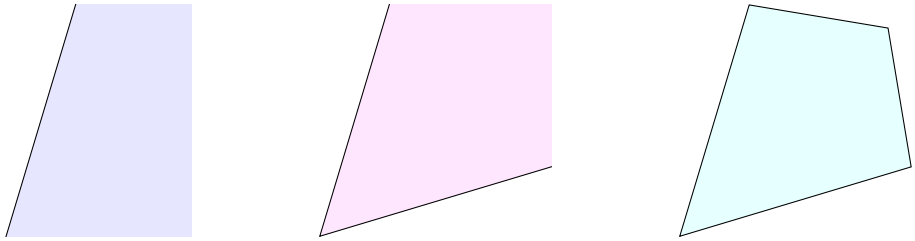

(a) Half space. (b) Cone. (c) Polytope.

Figure 2.1: Sample polyhedra in $\mathbb{R}^2$. The black line segments represent the boundaries whereas the colored region is the interior. Polyhedra may be both bounded and unbounded. In the former case, it is by definition a polytope.

An inequality $c^T x \leqslant \beta \in \mathbb{R}$ is *valid* for P provided that the inequality holds for all $x \in P$ [Fukuda, 2016]. Given a subset F of P, this is called a face of P if it is represented as

$$F = P \cap \{x \in \mathbb{R}^d \mid c^T x = \beta\} \tag{2.15}$$

for some valid inequality $c^T x \leqslant \beta$ [Fukuda, 2016]. Faces of dimension zero, i.e. points, are by definition *the vertices of* P. As intersections of polyhedra are polyhedra, F is itself a polyhedron. Relating the definition to figure 2.1c, the four corners of the polyhedron are its vertices. The vertices along with the four line segments on the boundary of the figure are all the so-called non-trivial faces. The trivial faces are the polytope itself together with the empty set.

We define $\dim(P) = \text{affdim}(P)$. A point $x \in P$ is on the boundary of P denoted ∂P if one or more of the inequalities in $Ax \leqslant b$ are tight. Conversely any face of P is on the boundary of P. If none of the constraints are tight at $x \in P$, i.e. $Ax < b$, then x is in the interior of P namely $\text{int}(P)$.

Remark 2.1.2. *A polyhedron $P \subset \mathbb{R}^d$ has a non-empty interior iff $\dim(P) = d$. In this case P is said to be full-dimensional.*

2.1.3 Linear programming

Consider the linear program (LP)

$$\min_x c^T x \text{ subject to } Ax \leqslant b. \tag{2.16}$$

We recognize that the constraint $Ax \leqslant b$ coincides with $x \in P$ for a polyhedron $P \subset \mathbb{R}^d$ defined by the same system of inequalities. The LP is *feasible* if $P \neq \varnothing$. Provided that the LP is feasible, we say that it is *bounded* if there exist some finite positive constant M such that $c^T x > -M \ \forall x \in P$. Otherwise it is *unbounded*. Intuitively all directions in which it is beneficial to move with respect to the objective function $c^T x$ must be bounded for the LP to be bounded.

Assume boundedness and consider an optimizer $x^\star$ of (2.16) with corresponding optimal value $p^\star = c^T x^\star$.

Proposition 2.1.1. *The optimizer of a feasible and bounded LP* (2.16) *will be on the boundary of the polyhedron* $P = \{x \in \mathbb{R}^d \mid Ax \leqslant b\}$.

Proof. Recall that $\|\cdot\|$ denotes the euclidean norm. Assume for the sake of contradiction that $x^\star \in \text{int}(P)$. Then there exists some $\epsilon > 0$ such that $x^\star + \Delta x \in P \ \forall \Delta x \in \{\Delta x \mid 0 < \|\Delta x\| < \epsilon\}$. Pick $\Delta x = -\frac{\epsilon}{2}\frac{\nabla c^T x}{\left\|\nabla c^T x\right\|} = -\frac{\epsilon}{2}\frac{c}{\|c\|}$. Now $\bar{p} = c^T(x^\star - \Delta x) = p^\star - \frac{\epsilon}{2}\|c\| < p^\star$ which is a contradiction. □

Clearly $c^T x \leqslant p^\star$ is a valid inequality for P and $x^\star \in F^\star = P \cap \{x \mid c^T x = p^\star\}$. Hence, by definition $x^\star$ is on the face $F^\star$ of P. As such the optimizer is unique provided $\dim(F^\star) = 0$. Otherwise there are infinitely many optimizers, namely all x on the face $F^\star$ of P. In any case we have $\dim(F^\star) \leqslant d - 1$ due to the equality constraint $c^T x = p^\star$.

As mentioned in [Boyd and Vandenberghe, 2004], solving linear programs is a mature technology. Even with hundreds of variables and thousands of constraints, todays solvers will produce a solution in a manner of seconds on ordinary desktop computers. Thus it is very attractive from a computational point of view if an optimization can be cast as a linear program.

2.1.4 Set theoretic prerequisites

The following standard set-theoretic definitions will be applied in the sequel.

Definition 2.1.1. *The Minkowski sum of the sets* A *and* B *is defined as*

$$A \oplus B = \{a + b \mid a \in A, b \in B\}. \tag{2.17}$$

See figure 2.2 for an illustration with the Minkowski sum of two polytopes. Minkowski sums can also be used to translate sets. Let $A \subset \mathbb{R}^d$ be a set and $v \in \mathbb{R}^d$ be some vector,

then

$$A \oplus \{v\} \tag{2.18}$$

is the translation of A by v. For our part this is particularly useful to *center* polyhedra such that they contain the origin. Let $v \in P$ of a polyhedron P, observe that the translated set

$$P \oplus \{-v\} \tag{2.19}$$

contains the origin.

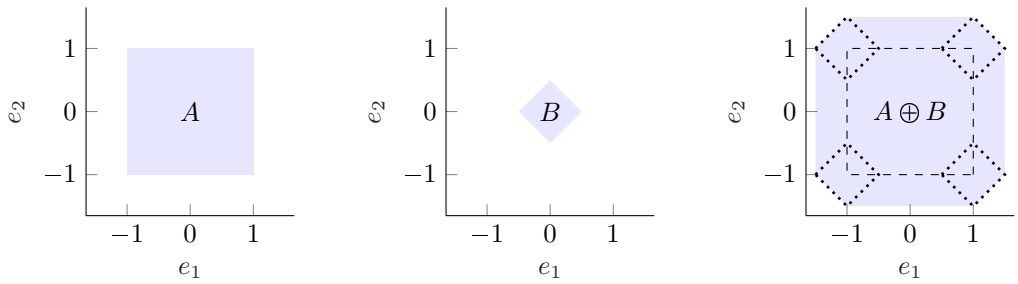

Figure 2.2: Illustration of the Minkowski sum of two polytopes A and B. The shaded area is the polyhedron. In the figure $A \oplus B$ the operands are superimposed. A is in its original position while B is translated to illustrate the operation.

This operation is needed in the context of *scaling* sets.

Definition 2.1.2. . *Let $A \subset \mathbb{R}^d$ be a set. Then the λ-scaling of A is*

$$\lambda A = \{x \in \mathbb{R}^d \mid x = \lambda a, a \in A\}. \tag{2.20}$$

When $\lambda \in (0, 1) \subset \mathbb{R}$ then the scaled set λA is called a λ-*contraction* of the set. Commonly we expect a contraction to be a subset of the original set, as illustrated in figure 2.3b. However, figure 2.3a illustrates that this is not the case in general. In fact, for $\lambda A \subset A$ when $\lambda \in (0, 1) \subset \mathbb{R}$ to hold, A has to contain the origin. Therefore we assume that the set being contracted contains the origin. This is without loss of generality due to the previously mentioned centering operation. A set which does not contain the origin can be contracted in the following manner,

$$\lambda(P \oplus \{-v\}) \oplus \{v\}, v \in P. \tag{2.21}$$

While this may look a bit involved, it simply amounts to centering the coordinate system at some $v \in P$, contracting this centered set and finally adding v back in. As figure 2.3c exemplifies, this yields the expected result. Namely a contracted set which is in the subset of its original set. Note however that the shape of the resulting polytope depends on the choice of v. E.g. if $v \neq (2, 2)$ in the example in figure 2.3c, then the shape would not be maintained.

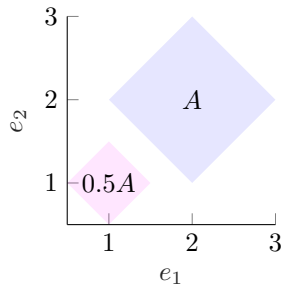

(a) λ-scaling with $\lambda \in \mathbb{R}_{(0,1)}$ of a set A not containing the origin. In this case $\lambda A \not\subset A$

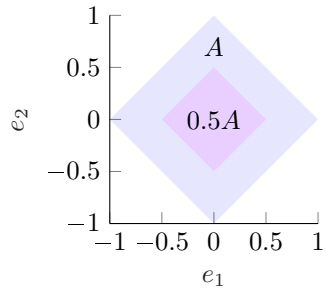

(b) λ-scaling with $\lambda \in \mathbb{R}_{(0,1)}$ of a set A containing the origin. In this case $\lambda A \subset A$.

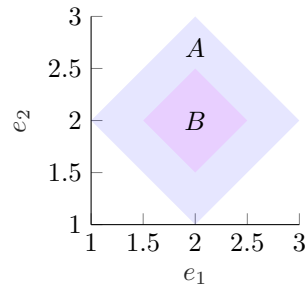

(c) Contracting a set A not contaning the origin. $B = 0.5(A \oplus \{-2\mathbb{1}\}) \oplus \{2\mathbb{1}\} \subset A$.

Figure 2.3: λ-scaling samples.

Applying the definition, the λ-scaling of a polyhedron $P = \{x \mid Ax \leqslant b\}$ is easily found to be

$$\lambda P = \{x \mid Ax \leqslant \lambda b\}. \tag{2.22}$$

Later on we will make use of the following contraction-related claim.

Proposition 2.1.2. *Let P be a non-empty full-dimensional polytope and assume, without loss of generality, $\mathbb{0} \in \text{int}(P)$. Consider some $x_0 \in P$. Then $x_0 \in \text{int}(P) \iff \exists \lambda \in (0,1) : x_0 \in \lambda P$.*

Proof. First, assume that x_0 is a non-zero point in the interior of P. Consider the ray αx_0, $\alpha \geqslant 0$. Since P is bounded and x_0 is in the interior of P, there exists some $\alpha_m > 1$ such that $\alpha_m x_0$ is at the boundary of P. Thus

$$\alpha_m x_0 \in P \implies x_0 \in \frac{1}{\alpha_m} P = \lambda P. \tag{2.23}$$

I.e. x_0 is contained in a contraction of P as claimed. If $x_0 = \mathbb{0}$ then trivially $x_0 \in \lambda P$ as $x_0 \in \text{int}(P) \iff \mathbb{0} < b$ yields $\mathbb{0} < \lambda b$ for any admissible λ. For the converse direction, let $x_0 \in \lambda P$ for some $\lambda \in (0,1)$ and assume for the sake of contradiction that $x_0 \in \partial P$. Since $x_0 \in \partial P$, at least one inequality in the H-representation of P is tight. I.e. $a_i^T x_0 = b_i > \lambda b_i$ for at least one i, contradicting $x_0 \in \lambda P$. The result follows. □

Finally we introduce the Pontryagin difference. This notion is complementary to the Minkowski sum.

Definition 2.1.3. . *The Pontryagin difference of the sets A and B is defined as*

$$A \ominus B = \{a \in A \mid a + b \in A \ \forall \ b \in B\}. \tag{2.24}$$

Intuitively the Pontryagin difference yields all the elements of A where one can add any element from B and still stay in A. This is illustrated in figure 2.4.

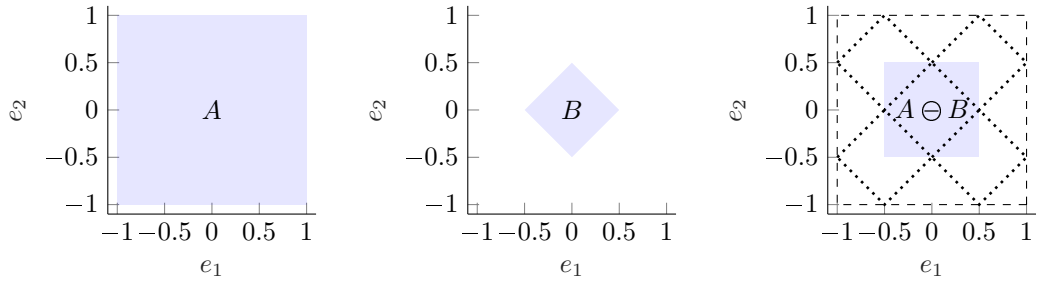

Figure 2.4: Illustration of the Pontryagin difference of two polytopes A and B. In $A \ominus B$ the operands are superimposed. A in its original position. B translated to illustrate the operation.

In the context of Chebyshev centers, the Pontryagin difference between a polytope and a ball tuns out to be of particular importance.

Proposition 2.1.3. *Let $P = \{x \in \mathbb{R}^d \mid Ax \leqslant b \in \mathbb{R}^m\} \subset \mathbb{R}^d$ be a non-empty polytope of dimension d and let $\mathbb{B}_r \subset \mathbb{R}^d$ be a d-dimensional ball centered at the origin with a particular radius $r \in \mathbb{R}_+$. Assume without loss of generality that all rows a_i^T of A satisfy $\|a_i\|_2 = 1$. Then*

$$P \ominus \mathbb{B}_r = \{x \in \mathbb{R}^d \mid Ax \leqslant b - r\mathbb{1}\} \tag{2.25}$$

Proof.

$$P \ominus \mathbb{B}_r = \{x \in P \mid x + u \in P \ \forall u \in \mathbb{B}_r\} \tag{2.26}$$

$$= \{x \in \mathbb{R}^d \mid A(x + u) \leqslant b \ \forall \|u\| \leqslant r\}. \tag{2.27}$$

For each row i,

$$e_i^T(Ax + u) = a_i^T x + a_i^T u \leqslant b_i \ \forall \|u\| \leqslant r \iff a_i^T x + r \leqslant b_i \tag{2.28}$$

since $r = \max\{a_i^T u \mid \|u\| \leqslant r\}$ when $\|a_i\| = 1$. Thus

$$P \ominus \mathbb{B}_r = \{x \in \mathbb{R}^d \mid Ax \leqslant b - r\mathbb{1}\}, \tag{2.29}$$

as claimed. □

Therefore $P \ominus \mathbb{B}_r$ is simply a tightened version of P. Let $r_1 > r_2 > 0$. Then

$$Ax \leqslant b - r_1\mathbb{1} \leqslant b - r_2\mathbb{1} \leqslant b, \tag{2.30}$$

illustrating the inclusions

$$P \ominus \mathbb{B}_{r_1} \subset P \ominus \mathbb{B}_{r_2} \subset P. \tag{2.31}$$

I.e. $P \ominus \mathbb{B}_{r_1}$ is a proper subset of $P \ominus \mathbb{B}_{r_2}$ provided $r_1 > r_2$, and both are proper subsets of P.

2.1.5 Depth, Chebyshev radius, and Chebyshev centers of a polytope

Let P be some non-empty polytope. Following [Boyd and Vandenberghe, 2004], we define the depth of a point x in P as

$$\operatorname{depth}(x, P) = \operatorname{dist}(x, \partial P) = \min\{\|x - x_{\partial P}\| \mid x_{\partial P} \in \partial P\} \text{ provided } x \in P. \tag{2.32}$$

That is, the depth of some $x \in P$ is the distance to its closest point on the boundary of P. Equivalently, $\operatorname{depth}(x, P)$ is the maximal radius r such that

$$\mathbb{B}_r(x) \subset P. \tag{2.33}$$

Exploiting the normalized H-representation of P,

$$\begin{aligned} \operatorname{depth}(x, P) &= \max\{r \in \mathbb{R} \mid A(x + u) \leqslant b \ \forall \|u\| \leqslant r\} && (2.34)\\ &= \max\{r \in \mathbb{R} \mid Ax + r\mathbb{1} \leqslant b\} && (2.35)\\ &= \max\{r \in \mathbb{R} \mid r\mathbb{1} \leqslant b - Ax\}. && (2.36) \end{aligned}$$

Thus the depth is simply the greatest lower bound on the slack of the constraints $a_i^T x \leqslant b_i$ at $x \in P$,

$$\operatorname{depth}(x, P) = \min_i e_i^T (b - Ax) = \min\{b_1 - a_1^T x, \ldots, b_m - a_m^T x\}. \tag{2.37}$$

Moreover, observe the useful connection to the Pontryagin difference $P \ominus \mathbb{B}_r$ via

$$\{x \in P \mid \operatorname{depth}(x, P) \geqslant r\} = \{x \mid Ax + r\mathbb{1} \leqslant b\} = P \ominus \mathbb{B}_r. \tag{2.38}$$

The Chebyshev radius of P, denoted by $r_c(P)$, is the maximal depth of any $x \in P$. Formally

$$r_c(P) = \max_{x \in P} \operatorname{depth}(x, P). \tag{2.39}$$

Equivalently,

$$r_c(P) = \max\{r \mid Ax + r\mathbb{1} \leqslant b \ \forall (x, r) \in \mathbb{R}^d \times \mathbb{R}\}. \tag{2.40}$$

Observe that this is simply the linear objective function r maximized over the polyhedron

$$\tilde{P} = \{(x, r) \in \mathbb{R}^d \times \mathbb{R} \mid Ax + r\mathbb{1} \leqslant b\}. \tag{2.41}$$

Thus the computation of $r_c(P)$ can be cast as the linear program

$$\begin{aligned} r_c(P) = \max_{x,r} \ & r \\ \text{such that } & Ax + r\mathbb{1} \leqslant b. \end{aligned} \tag{2.42}$$

Note that the linear program is bounded since the objective function value decreases in the only unbounded direction $-r$. Uniqueness of $r_c(P)$ follows from the uniqueness of the optimal value.

Since the depth notion is defined in terms of a distance $\text{dist}(x, \partial P)$, a negative $r_c(P)$ does not make sense. However, the constraint $r \geqslant 0$ is superfluous when P is non-empty. To see this, note that the point $(x, 0)$ provides the lower bound $r_c(P) \geqslant 0$ for any $x \in P$. If the optimization returns a negative r, then P must be empty. A negative r amounts to a relaxation of the constraints defining P.

Finally, the Chebyshev centers of P are the $x \in P$ with depth equal to the Chebyshev radius. Formally,

$$x_c \text{ is a Chebyshev center of } P \iff x_c \in P \ominus \mathbb{B}_{r_c(P)}. \tag{2.43}$$

Most algorithms for solving linear programs such as (2.42) would return both the optimal value $r_c(P)$ and a corresponding optimizer $(x^\star, r_c(P))$, with $x^\star \in P \ominus \mathbb{B}_{r_c(P)}$. However, the optimizer may not be unique. In fact, this holds if and only if $\dim(P \ominus \mathbb{B}_{r_c(P)}) = 0$. This may not be the case. However, the following proposition lets us bound $\dim(P \ominus \mathbb{B}_{r_c(P)})$.

Proposition 2.1.4. *Let $P = \{x \in \mathbb{R}^d \mid Ax \leqslant b\} \subset \mathbb{R}^d$ be a full-dimensional polytope with Chebyshev radius $r_c(P)$. Then $\dim(P \ominus \mathbb{B}_{r_c(P)}) \leqslant d - 1$.*

Proof. Assume, for the sake of contradiction, $\dim(P \ominus \mathbb{B}_{r_c(P)}) = d$. In this case $P \ominus \mathbb{B}_{r_c(P)}$ has a non-empty interior, and $\exists \bar{x} \in \mathbb{R}^d$ such that $Ax < b - \bar{r}_c(P)\mathbb{1}$. Pick any such $\bar{x}$. Then $\Delta r = \text{depth}(\bar{x}, P \ominus \mathbb{B}_{r_c(P)}) > 0$. By the definition of depth, $\bar{x}$ satisfies the system of inequalities

$$A\bar{x} + \Delta r \mathbb{1} \leqslant b - r_c(P)\mathbb{1} \iff A\bar{x} + (\Delta r + r_c(P)) \leqslant b \tag{2.44}$$

Thus $\text{depth}(\bar{x}, P) = \Delta r + r_c(P) > r_c(P)$, contradicting the definition of Chebyshev radius. Thus $\dim(P \ominus \mathbb{B}_{r_c(P)}) < d$, and the claim follows. □

For the purposes of control, we would like $\dim(P \ominus \mathbb{B}_{r_c(P)}) = 0$. This cannot hold in general for $d > 1$. As an example, consider the d-dimensional rectangle $P \ominus \mathbb{B}_r$ represented by the inequalities

$$|e_1^T x + r| \leqslant 2, \tag{2.45}$$

$$|e_i^T x + r| \leqslant 1, i \in \{2, 3, \ldots, d\}. \tag{2.46}$$

Clearly $r_c(P) = 1$ with corresponding Chebyshev centers $x \in \{[t, \mathbb{0}_{d-1}^T]^T \mid t \in [-1, 1]\}$.

2.2 System Dynamics

We consider a Multi-Agent System (MAS) consisting of a finite set of $N \in \mathbb{N}$ agents. For each agent $i \in \mathbb{N}_N = \{1, 2, \ldots, N\}$, its discrete-time linear time-invariant dynamics are governed by the equations

$$x_i(k+1) = f_i(x_i(k), u_i(k)) = A_i x_i(k) + B_i u_i(k) \in \mathbb{R}^d. \tag{2.47}$$

We impose the following regularity conditions[3]:

Assumption 2.2.1 (Regularity conditions)**.**

(i) The pair (A_i, B_i) are controllable for all $i \in \mathbb{N}_N$.

(ii) For all $\hat{x}_i \in \mathbb{R}^d$ and for all i, $\exists \hat{u}_i$ such that $\hat{x}_i = A_i \hat{x}_i + B_i \hat{u}_i$.

(iii) For all agents i, any full-dimensional convex set $P \subset \mathbb{R}^d$ is controlled λ-contractive [Blanchini and Miani, 2008] with respect to the agent dynamics. I.e. $\exists \hat{x}_i \in \text{int}(P)$ such that $\exists u_i(x_i)$ ensuring $f_i(x_i, u_i(x_i)) \in \hat{x}_i \oplus \lambda(P \oplus \{-\hat{x}_i\})$ for some $\lambda \in [0, 1)$ whenever $x_i \in P$.

The non-standard set-theoretic assumption on λ-contractiveness ensures that for any convex subset of $P \subset \mathbb{R}^d$, all agents have the control authority to move from the boundary ∂P into the strict interior $\text{int}(P)$ in one time step. This will be formally proven in the sequel for the special case of polytopes.

All assumptions are trivially satisfied when

$$x_i(k+1) = x_i(k) + u_i(k) \in \mathbb{R}^d. \tag{2.48}$$

In some sections we will assume compliance with these single-integrator dynamics. This allows us to focus on effects stemming from the particular framework at hand rather than variations in agent dynamics.

All agent states $x_i(k)$ evolve in a common space $\mathbb{R}^d$. It is instructive to think of the $x_i(k)$'s for $i \in \mathbb{N}_N$ as the d-dimensional positions of N robots at time k. While the framework is applicable regardless of $d \in \mathbb{N}$, examples in this thesis are restricted to $\mathbb{R}$ and $\mathbb{R}^2$ for obvious practical reasons.

We aggregate the states and inputs of the agents in the two vectors

$$x^T(k) = \left[x_1^T(k) \cdots x_N^T(k) \right], \tag{2.49}$$

$$u^T(k) = \left[u_1^T(k) \cdots u_N^T(k) \right]. \tag{2.50}$$

In the single integrator case, the aggregated dynamics of the entire MAS are described by

$$x(k+1) = x(k) + u(k) \in \mathbb{R}^{d \times N}. \tag{2.51}$$

[3] We refer to appendix A for generalization of the agent dynamics.

2.3 Environment

The agents are deployed to the static, convex, polytopic, full-dimensional and bounded set $\mathcal{W}$. We utilize the half-space representation of $\mathcal{W}$, i.e.

$$\mathcal{W} = \{x \in \mathbb{R}^d \mid Hx \leqslant \theta\} \subset \mathbb{R}^d. \tag{2.52}$$

for appropriate choices of $H \in \mathbb{R}^{m \times d}$ and $\theta \in \mathbb{R}^m$. Since $\mathcal{W}$ is a bounded polyhedron, it is by definition a polytope. Figure 2.5 illustrates a random polytopes in $\mathbb{R}^2 = \text{span}(e_1, e_2)$ which could serve as $\mathcal{W}$.

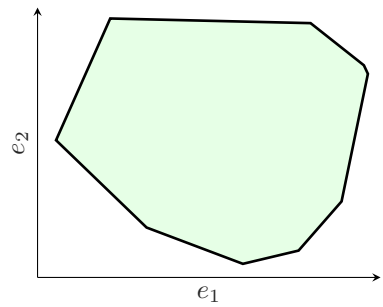

Figure 2.5: Sample polytopic environment.

Due to its static nature, we assume $\mathcal{W}$ to be known to all agents prior to deployment.

2.4 Agent Neighborhood

Consider now some MAS state vector $x(k)$ in which all $x_i(k)$'s are distinct elements in $\mathcal{W}$. To each agent we associate a *neighborhood* $\mathbb{V}_i$, about its position in the state space, defined as

$$\mathbb{V}_i(k) = \mathbb{V}_i(x(k), \mathcal{W}) = \{w \in \mathcal{W} \mid \|x_i(k) - w\| \leqslant \left\|x_j(k) - w\right\| \, \forall i \neq j\}. \tag{2.53}$$

Equivalently,

$$\mathbb{V}_i = \mathcal{W} \cap \{w \in \mathbb{R}^d \mid 2(x_j - x_i)^T w \leqslant \left\|x_j\right\|^2 - \|x_i\|^2 \, \forall j \neq i\}. \tag{2.54}$$

Inspecting (2.54), regarding all x_i's and x_j's as fixed, the polytopic nature of the $\mathbb{V}_i$'s is apparent from the structure of inequalities. The neighborhoods are inherently time varying by the dependence on $x(k)$.

The above definition of neighborhood is not well posed if two agents have the same state. We therefore assume distinct initial states $x_i(0)$. Formally we constrain the set of admissible initial states to $x(0) \in \mathcal{X}_\text{D}$, where $\mathcal{X}_\text{D}$ is defined as follows:

Definition 2.4.1 (MAS configurations with non-coincident agents)**.** *Let $\mathcal{X}_D$ be the set of MAS configurations such that all agent states are distinct members of the target environment $\mathcal{W}$. Formally,*

$$\mathcal{X}_D = \{x^T = \begin{bmatrix} x_1^T \cdots x_N^T \end{bmatrix}^T \mid x_i \in \mathcal{W} \ \forall i \in \mathbb{N}_N, x_i \neq x_j \ \forall j \neq i \in \mathbb{N}_N\}. \tag{2.55}$$

This constraint ensures well-posedness of agent neighborhoods at time $k = 0$. Distinctness beyond time $k = 0$ will be addressed when discussing the agent control laws.

Intuitively, points in $\mathcal{W}$ such that the i'th agent is the closest in euclidean distance are in the neighborhood of agent i. The exception to this is the set of points where several agents are equally distant from the point. This subset represents the boundaries/frontiers or borders between the agent neighborhoods.

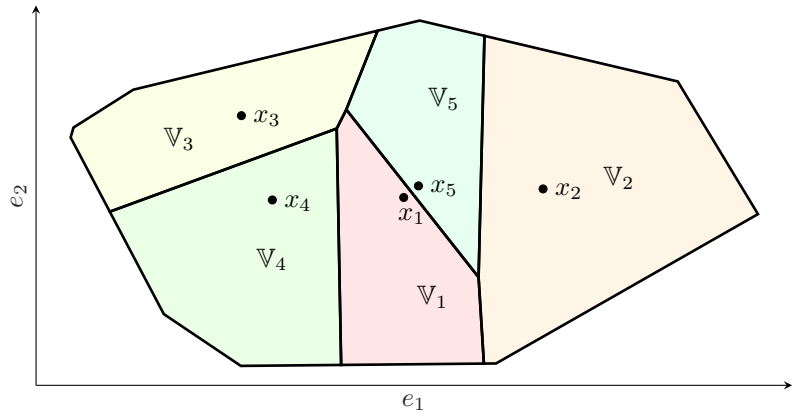

Figure 2.6: Sample agent neighborhoods. Agent positions and Voronoi cells are denoted by x_i and the $\mathbb{V}_i$ respectively. The union of all Voronoi cells $\mathbb{V}_i \in \mathbb{V}$ is the environment $\mathcal{W}$.

Since all points in $\mathcal{W}$ are closest to at least one agent, the $\mathbb{V}_i$'s partition $\mathcal{W}$. I.e.

$$\mathcal{W} = \cup_{i=1}^{N} \mathbb{V}_i. \tag{2.56}$$

As the reader might have noticed, this is the well-known Voronoi partition [Voronoï, 1908]. The $\mathbb{V}_i$'s are known as the Voronoi cells. The collection $\{\mathbb{V}_1(x, \mathcal{W}), \ldots, \mathbb{V}_N(x, \mathcal{W})\}$ represent the Voronoi partition of $\mathcal{W}$ with respect to $\{x_1, \ldots, x_N\}$.

The partitioning of $\mathcal{W}$ and the agent neighborhoods are illustrated in figure 2.6. Agreeing with our intuition, the borders between agents are located mid-way between neighboring agents. This can be seen in a more rigorous manner by rewriting the equation for $\mathbb{V}_i$ to the equivalent form

$$\mathbb{V}_i = \mathcal{W} \cap \{w \in \mathbb{R}^d \mid (x_j - x_i)^T w \leqslant (x_j - x_i)^T (\frac{x_i + x_j}{2}) \forall j \neq i\}. \tag{2.57}$$

Observe that the inequality corresponding to the j'th agent is tight whenever $w = \frac{x_i+x_j}{2}$.

The interior of any cell $\mathbb{V}_i$ is the set of points such that all inequalities in (2.53) are strict. Denote this interior by $\text{int}(\mathbb{V}_i)$ and note that

$$\begin{aligned}\text{int}(\mathbb{V}_i) \cap \text{int}(\mathbb{V}_j) \subset \{w \in \mathbb{R}^d \mid \|x_i - w\| < \left\|x_j - w\right\|, \\ \|x_i - w\| > \left\|x_j - w\right\| \ \} = \varnothing, i \neq j.\end{aligned} \tag{2.58}$$

I.e. the Voronoi cells have a mutually disjoint interior. We also note that the interior must be non-empty. When the x_i's are distinct, continuity ensures the existence of some $\epsilon > 0$ such that the ball $\mathbb{B}_\epsilon(x_i)$ does not touch any x_j's.

If two distinct agent neighborhoods $\mathbb{V}_i, \mathbb{V}_j$ have a non-empty intersection, i.e.

$$\mathbb{V}_i \cap \mathbb{V}_j \neq \varnothing, i \neq j, \tag{2.59}$$

we say that the agents are (Voronoi) neighbors. With regards to the intuitive explanation of agent neighborhoods above, informally agents are neighbors if they share a border. We denote the set of neighbors of an agent i by $\mathcal{N}_i$, i.e.

$$\mathcal{N}_i(k) = \mathcal{N}_i(x(k), \mathcal{W}) = \{j \neq i \in \mathbb{N}_N \mid \mathbb{V}_i(x(k), \mathcal{W}) \cap \mathbb{V}_j(x(k), \mathcal{W}) \neq \varnothing\}. \tag{2.60}$$

Like the Voronoi neighborhoods, $\mathcal{N}_i$ is time-varying via $x(k)$. Revisiting (2.53) and (2.54) we observe that if $j \notin \mathcal{N}_i$, the corresponding constraint is *redundant*. Removing the constraints corresponding to non-neighbor-agents has no effect on the set of feasible elements in $\mathbb{V}_i$. Considering $\mathbb{V}_i$ as a function of agent states and $\mathcal{W}$,

$$\mathbb{V}_i = \mathbb{V}_i(x, \mathcal{W}) = \mathbb{V}_i(\{x_j \mid j \in \mathcal{N}_i(x, \mathcal{W}) \cup \{i\}\}, \mathcal{W}). \tag{2.61}$$

Thus for any agent i, knowledge of its own state x_i states of neighbors x_j, $j \in \mathcal{N}_i$, is sufficient for computing $\mathbb{V}_i$. I.e. $\mathbb{V}_i$ can be computed in a decentralized manner. We add the following assumption to ensure that this is always possible:

Assumption 2.4.1. *All agents $i \in \mathbb{N}_N$ are equipped with sensors allowing them to determine their set of Voronoi neighbors $\mathcal{N}_i$ as well as $x_i(k)$ and $x_j(k)$ $\forall j \in \mathcal{N}_i$.*

2.5 Control laws

The objective of the agent control laws $\mathcal{K}_i(\cdot)$ for $i \in \mathbb{N}_N$ is to drive the MAS to an optimal static configuration. To this end, we utilize decentralized agent control laws steering each agent towards some Chebyshev center of its current neighborhood $\mathbb{V}_i(k)$.

We denote the Chebyshev radius and an associated Chebyshev center of $\mathbb{V}_i(k)$ by $\bar{r}_i(k)$ and $\bar{x}_i(k)$ respectively. That is

$$\bar{r}_i(k) = \bar{r}_i(\mathbb{V}_i(k)) = r_c(\mathbb{V}_i(k)), \tag{2.62}$$

$$\bar{x}_i(k) \in \mathbb{V}_i(k) \ominus \mathbb{B}_{\bar{r}_i(k)}. \tag{2.63}$$

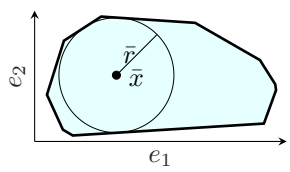

(a) A randomly generated polytope in the plane.

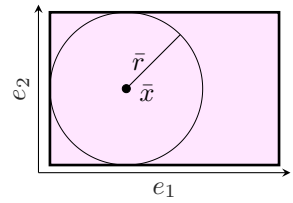

(b) A rectangle in the plane.

Figure 2.7: Chebyshev center $\bar{x}$, ball and radius $\bar{r}$ of two polytopes.

Since $\mathbb{V}_i(k)$ is time-varying, $\bar{x}_i(k)$ and $\bar{r}_i(k)$ will also be. Moreover, we refer to

$$\mathbb{B}_{\bar{r}_i(k)}(\bar{x}_i(k)) = \{w \in \mathbb{R}^d \mid \|\bar{x}_i(k) - w\|_2 \leqslant \bar{r}_i(k)\}, \tag{2.64}$$

as a Chebyshev ball of $\mathbb{V}_i(k)$. See figure 2.7 for an illustration. As shown in section 2.1.5, both the Chebyshev radius and an admissible Chebyshev center of a polytope can be found by solving a linear program.

We also define the depth of $x_i(k)$ and $x_i(k+1)$ with respect to $\mathbb{V}_i(k)$ by

$$r_i(k) = r_i(x_i(k), \mathbb{V}_i(k)) = \text{depth}(x_i(k), \mathbb{V}_i(k)), \tag{2.65}$$

$$\tilde{r}_i(k) = \tilde{r}_i(x_i(k), u_i(k), \mathbb{V}_i(k)) = \text{depth}(x_i(k+1), \mathbb{V}_i(k)), \tag{2.66}$$

respectively. Remark that $\bar{r}_i(k), \tilde{r}_i(k)$ and $r_i(k)$ are amenable to computation in a decentralized manner. The knowledge of $\mathbb{V}_i(k), u_i(k)$ and $x_i(k)$ is sufficient. Thus the decentralized property of the agent Voronoi cell computation carries over to agent control laws utilizing these quantities.

To drive each agent towards the set of Chebyshev center of its Voronoi cell, we therefore pick decentralized control laws

$$u_i(k) = \mathcal{K}_i(x(k), \mathcal{W}) = \mathcal{K}_i(x_i(k), \mathbb{V}_i(k)), \tag{2.67}$$

satisfying the requirements

$$\bar{r}_i(k) \neq r_i(k) \implies \tilde{r}_i(k) > r_i(k), \tag{2.68}$$

$$\bar{r}_i(k) = r_i(k) \implies \tilde{r}_i(k) = r_i(k) = \bar{r}_i(k). \tag{2.69}$$

Equivalently, we can impose the constraint

$$\exists \alpha_i(k) \in (0, 1] : \tilde{r}_i(k) = r_i(k) + \alpha_i(k)[\bar{r}_i(k) - r_i(k)]. \tag{2.70}$$

Unless the agent is at a Chebyshev center, an admissible control law steers the agent towards some $x_i(k+1) \in \mathbb{V}_i(k)$ such that the depth with respect to $\mathbb{V}_i(k)$ strictly increases.

An important consequence of imposing the above requirements is distinctness of agent states beyond time $k = 0$ provided the their initial states $x_i(0)$ are distinct elements in $\mathcal{W}$. I.e. collision avoidance is inherent. Recall $\mathcal{X}_{\text{D}}$ from definition 2.4.1, the set of MAS configurations such that all agent states are distinct members of the target environment $\mathcal{W}$.

Proposition 2.5.1. *$x(0) \in \mathcal{X}_D \implies x(k) \in \mathcal{X}_D$ for all $k > 0$ provided the collection of control laws $\{\mathcal{K}_1(\cdot), \ldots, \mathcal{K}_N(\cdot)\}$ satisfies requirements* (2.68) *and* (2.69).

Proof. Assume $x(k) \in \mathcal{X}_\mathrm{D}$ for some k. Since all $x_i(k)$'s are distinct members of $\mathcal{W}$, $\mathbb{V}_i(k)$ is well defined and $\mathrm{int}(\mathbb{V}_i(k)) \neq \varnothing$ for all agents i. By the control law requirements, $\tilde{r}_i(k) > 0$. Moreover, $\tilde{r}_i(k) > 0$ if and only if $x_i(k+1) \in \mathrm{int}(\mathbb{V}_i(k))$ by the definition of depth. Thus $x_i(k+1) \neq x_j(k+1)$ for all $i \neq j$ as $\mathrm{int}(\mathbb{V}_i(k)) \cap \mathrm{int}(\mathbb{V}_j(k)) = \varnothing$ would be contradicted otherwise. I.e. $x(k) \in \mathcal{X}_\mathrm{D} \implies x(k+1) \in \mathcal{X}_\mathrm{D}$. Since $x(0) \in \mathcal{X}_\mathrm{D}$ holds by assumption at $k = 0$, $x(k) \in \mathcal{X}_\mathrm{D}$ holds by induction for all $k > 0$. □

The feasibility of agent control laws satisfying (2.68)-(2.70) is ensured by assumption 2.2.1.

Proposition 2.5.2. *For any full-dimensional convex polytope P, $\forall x(k) \in P\ \exists x_i(k+1) \in \mathrm{int}(P)$ whenever the agent dynamics satisfies the regularity conditions in assumption 2.2.1.*

Proof. Since P is full-dimensional, its interior is non-empty. First assume that $x_i(k) \in \mathrm{int}(P)$. Then $\exists x_i(k+1) \in \mathrm{int}(P)$ by (ii) in assumption 2.2.1 since $\exists u_i(k)$ such that $x_i(k+1) = x_i(k)$. Next assume $x_i(k) \in \partial P$. By (iii) in assumption 2.2.1 there exists a point $\hat{x}_i \in \mathrm{int}(P)$ such that $x_i(k+1) = f_i(x_i(k), u_i(x_i(k))) \in \hat{x}_i \oplus \lambda(P \oplus \{-\hat{x}_i\})$ for some $\lambda \in (0, 1]$. For clarity we assume, without loss of generality, $\hat{x} = \mathbb{0}$. Simply translate the involved variables if this assumption does not hold. Then $\exists \lambda \in (0, 1]$ such that $x_i(k+1) \in \lambda P$. By proposition 2.1.2, $x \in \lambda P \implies x \in \mathrm{int}(P)\ \forall x \in \lambda P$, thus $\exists x_i(k+1) \in \mathrm{int}(P)$ as claimed. □

Proposition 2.5.2 ensures that the requirement (2.68) can be satisfied, since any agent has the control authority to move from $\mathbb{V}_i(k) \ominus \mathbb{B}_{r_i(k)}$ to some $x_i(k+1) \in \mathrm{int}(\mathbb{V}_i(k) \ominus \mathbb{B}_{r_i(k)})$. Such a successor state $x_i(k+1)$ necessarily satisfies $\tilde{r}_i(x_i(k+1), \mathbb{V}_i(k)) > r_i(k)$ by virtue of being in the strict interior of $\mathbb{V}_i(k) \ominus \mathbb{B}_{r_i(k)}$. The requirement in (2.69) is trivially satisfied since any agent may pick $x_i(k+1) = x_i(k)$ by (ii) in assumption 2.2.1.

The agent control law requirements can be fulfilled by picking any control $u_i(k) \in \mathcal{U}_i(k)$ where

$$\mathcal{U}_i(k) = \{u_i \mid x_i(k+1) \in \mathrm{int}(\mathbb{V}_i(k) \ominus \mathbb{B}_{r_i(k)}) \cup \mathbb{V}_i(k) \ominus \mathbb{B}_{\bar{r}_i(k)}\}. \tag{2.71}$$

The particular controller implementation can for instance be based on optimization over the feasible set of control actions $\mathcal{U}_i(k)$. In this manner, constraints as well as costs on states and penalty on the energy of the control actions can be accommodated. For the single integrator dynamics (2.48) the linear controller

$$\mathcal{K}_i(x_i(k), \mathbb{V}_i(k)) = \alpha_i(\bar{x}_i(k) - x_i(k)), \alpha_i \in (0, 1] \tag{2.72}$$

is admissible.

Proposition 2.5.3. *Assume that $x_i(k+1) = x_i(k) + u_i(k) \in \mathbb{R}^d$ for some agent $i \in \mathbb{N}$. Then the controller $u_i(k) = \mathcal{K}_i(x_i(k), \mathbb{V}_i(k)) = \alpha_i(\bar{x}_i(k) - x_i(k))$ with $\alpha_i \in (0, 1]$ satisfies the controller requirements* (2.68)-(2.70).

Proof. The corresponding agent closed loop dynamics are

$$x_i(k+1) = x_i(k) + \alpha_i(\bar{x}_i(k) - x_i(k)) \tag{2.73}$$
$$= (1-\alpha_i)x_i(k) + \alpha_i\bar{x}_i(k). \tag{2.74}$$

Consider the normalized H-representation of the agent's Voronoi cell, $\mathbb{V}_i(k) = \{w \mid H_i(k)w \leqslant \xi_i(k)\}$. Inserting $w = x_i(k+1)$ in the system of inequalities defining $\mathbb{V}_i(k)$ yields

$$H_i(k)x_i(k+1) = H_i(k)[(1-\alpha_i)x_i(k) + \alpha_i\bar{x}_i(k)] \tag{2.75}$$
$$\leqslant \xi_i(k) - [(1-\alpha_i)r_i(k) + \alpha_i\bar{r}_i(k)]\mathbb{1}, \tag{2.76}$$

by

$$H_i(k)x_i(k) \leqslant \xi_i(k) - r_i(k)\mathbb{1}, \tag{2.77}$$
$$H_i(k)\bar{x}_i(k) \leqslant \xi_i(k) - \bar{r}_i(k)\mathbb{1}. \tag{2.78}$$

Consequently $\tilde{r}_i(k) = r_i(k) + \alpha_i[\bar{r}_i(k) - r_i(k)]$ with $\alpha \in (0,1]$, ensuring the satisfaction of all control law requirements. □

Remark 2.5.1. *The framework can be generalized with respect to agent dynamics provided the requirements in* (2.68)-(2.70) *are satisfied. See for instance the generalization proposed in appendix A. Arguably* (2.68) *is the most restrictive. E.g. nonholonomic systems cannot satisfy* (2.68)*, and would require a more comprehensive generalization of the framework.*

2.6 Formal MAS control law objectives

Having formalized the local agent control law requirements, we proceed by properly defining the global control law objectives at the MAS-level. We are interested in convergence with respect to the following sets of MAS configurations.

Definition 2.6.1 (Static configuration [Nguyen et al., 2017])**.** *Let $\mathcal{X}_{SC}$ be the set of static MAS configurations under the collection of control laws $\{\mathcal{K}_1, \ldots, \mathcal{K}_N\}$. Formally,*

$$\mathcal{X}_{SC} = \{x \mid x_i = f_i(x_i, \mathcal{K}_i(x_i, \mathbb{V}_i))\ \forall i \in \mathbb{N}_N\}. \tag{2.79}$$

If $x \in \mathcal{X}_{SC}$ then the MAS is in a static configuration*.*

Definition 2.6.2 (Chebyshev configuration [Nguyen et al., 2017])**.** *Let $\mathcal{X}_{CC}$ be the set of Chebychev configurations. Formally,*

$$\mathcal{X}_{CC} = \{x \mid \bar{r}_i(\mathbb{V}_i(x, \mathcal{W})) = r_i(x_i, \mathbb{V}_i(x, \mathcal{W}))\ \forall i \in \mathbb{N}_N\}. \tag{2.80}$$

If $x \in \mathcal{X}_{CC}$ then the MAS is in a Chebyshev configuration*.*

Definition 2.6.3 (Static Chebyshev configuration)**.** *Let $\mathcal{X}^\star$ be the set of static Chebyshev configurations. Formally,*

$$\mathcal{X}^\star = \mathcal{X}_{CC} \cap \mathcal{X}_{SC}. \tag{2.81}$$

If $x \in \mathcal{X}^\star$ then the MAS is in a static Chebyshev configuration*.*

Formally we seek a collection of decentralized controllers $\{\mathcal{K}_1, \ldots, \mathcal{K}_N\}$ such that

$$\lim_{k\to\infty} x(k) \in \mathcal{X}^\star = \mathcal{X}_{\mathrm{CC}} \cap \mathcal{X}_{\mathrm{SC}}. \tag{2.82}$$

Motivated by $\bar{r}_i(\mathbb{V}_i(x, \mathcal{W}))) = r_i(x_i, \mathbb{V}_i(x, \mathcal{W})))$ for all MAS configurations $x \in \mathcal{X}_{\mathrm{CC}}$, we define the following energy-like function

$$V(x(k), \mathcal{W}) = \sum_{i\in\mathbb{N}_N} \bar{r}_i(\mathbb{V}_i(x(k), \mathcal{W})) - r_i(x_i(k), \mathbb{V}_i(x(k), \mathcal{W})). \tag{2.83}$$

The use of such an energy function was first suggested in [Nguyen et al., 2017]. Observe that $V(x, \mathcal{W}) \geqslant 0$ since $\bar{r}_i \geqslant r_i$ for all $i \in \mathbb{N}_N$. The properties of $V(x, \mathcal{W})$ allow us to characterize convergence to some $x(k) \in \mathcal{X}_{\mathrm{CC}}$ via the convergence of $V(x(k), \mathcal{W})$ to zero.

Proposition 2.6.1. *$V(x, \mathcal{W}) = \sum_{i\in\mathbb{N}_N} \bar{r}_i(\mathbb{V}_i(x, \mathcal{W})) - r_i(x_i, \mathbb{V}_i(x, \mathcal{W})) = 0$ if and only if $x \in \mathcal{X}_{CC}$.*

Proof. $x \in \mathcal{X}_{\mathrm{CC}} \implies \bar{r}_i = r_i \ \forall i \in \mathbb{N}_N \implies V(x, \mathcal{W}) = 0$. For the converse direction, assume $\mathbb{V}(x, \mathcal{W}) = 0$ and $x \notin \mathcal{X}_{\mathrm{CC}}$. Then $\bar{r}_i \neq r_i$ for at least one $i \in \mathbb{N}_N$ contradicting $V(x, \mathcal{W}) = 0$. The result follows. □

In turn

$$\lim_{k\to\infty} x(k) \in \mathcal{X}_{\mathrm{CC}} \iff \lim_{k\to\infty} V(x(k), \mathcal{W}) = 0. \tag{2.84}$$

Therefore we can utilize $V(x, \mathcal{W})$ to measure MAS performance with respect to the objective of attaining a Chebyshev configuration.

Consider now $\mathcal{X}_{\mathrm{SC}}$, the set of static configurations under the particular collection of control laws. By (ii) in assumption 2.2.1, the MAS has sufficient control authority to make any $x \in \mathcal{X}_{\mathrm{CC}}$ a static configuration. In this respect the restriction to $\mathcal{X}_{\mathrm{SC}}$ may seem superfluous. As we will illustrate in the forthcoming section, convergence to $x \in \mathcal{X}_{\mathrm{CC}}$ does not imply convergence to a static configuration in degenerate cases where $\dim(\mathbb{V}_i \ominus \mathbb{B}_{\bar{r}_i}) > 0$. Whenever this occurs, it is necessary to introduce some scheme ensuring convergence to a static configuration within the set $\mathcal{X}_{\mathrm{CC}}$.

As mentioned, we desire convergence to an optimal MAS configuration. As opposed to an a priori performance requirement, the optimality of the limit configurations stems from the imposed control law requirements. This optimality will be discussed in section 3.4.3.

The convergence of the MAS to some $x \in \mathcal{X}_{\mathrm{CC}}$ is an open research problem, and will be the main topic of this thesis. To motivate the forthcoming theoretical developments, we proceed to numerical illustrations.

2.7 Motivating examples

The following numerical illustrations in 1D and 2D will be used as running examples throughout the thesis. Initially we will use the simulation results to conjecture mathematical properties. The two forthcoming sections present 1D and 2D simulations respectfully. Finally we summarize the most important observations from these motivating examples in section 2.7.3.

2.7.1 1D numerical illustrations

First we simulate N agents in $\mathbb{R}$. All agents adhere to the single integrator dynamics

$$x_i(k+1) = x_i(k) + u_i(k) \in \mathbb{R}, \tag{2.85}$$

and utilize decentralized controllers

$$u_i(k) = \mathcal{K}_i(x_i(k), \mathbb{V}_i(k), k) = \alpha_i(k)(\bar{x}_i(k) - x_i(k)). \tag{2.86}$$

Let the target environment be $\mathcal{W} = [x_l, x_u] = [0, 1]$. We assume, without loss of generality, that $0 \leqslant x_1(0) < x_2(0) < \cdots < x_N(0) \leqslant 1$. Since $x_i(k+1) \in \text{int}(\mathbb{V}_i(k))$ for all i and for all k, the ordering will also be respected for all $k \geqslant 0$. To avoid clutter we therefore omit agent indices in most figures as these are apparent from the ordering of agents in $[0, 1]$.

Remark 2.7.1. *By scale and translation invariance of the present framework, we can pick $\mathcal{W} = [0, 1]$ as target environment in $\mathbb{R}$ without loss of generality. Assume $\tilde{\mathcal{W}} = [\tilde{x}_l, \tilde{x}_u] \neq [0, 1]$. Any $x_{\tilde{\mathcal{W}}} \in \tilde{\mathcal{W}}$ has a bijective mapping to an unique $x_{\mathcal{W}} \in \mathcal{W}$ via $x_{\mathcal{W}}(x_{\tilde{\mathcal{W}}}) = \frac{x_{\tilde{\mathcal{W}}} - \tilde{x}_l}{\tilde{x}_u - \tilde{x}_l}$. Conversely $x_{\tilde{\mathcal{W}}}(x_{\mathcal{W}}) = (\tilde{x}_u - \tilde{x}_l)x_{\mathcal{W}} + \tilde{x}_l$.*

Figure 2.9a shows the simulation results when simulating $N = 10$ agents from randomly chosen initial positions in $(0, 1)$. Two different runs are superimposed. One run with $\alpha_i(k) = \alpha = 0.4$ and a second run where $\alpha_i(k) = \alpha = 1.0$. These are shown in red and black respectively. Regardless of the particular α, both runs exhibit convergence to the configuration x^{ss}, illustrated in figure 2.8, where $\bar{r}_i(k) = \bar{r}_i(k) = 1/2N$. I.e. the agents asymptotically reach consensus on $\bar{r}_i$ and r_i with a consensus value of $1/2N$. Moreover, evaluating the energy function $V(x, \mathcal{W})$ at x^{ss} yields $V(x^{ss}, \mathcal{W}) = 0$ implying $x^{ss} \in \mathcal{X}_{\text{CC}}$ as desired. The choice of α does however appear to affect the speed of convergence. Figure 2.9a suggests asymptotic convergence with improvements in convergence factor when increasing α. This agrees with intuition. If the $\bar{x}_i(k)$'s were fixed and $u_i(k) = \alpha(\bar{x}_i - x_i(k))$, then increasing α from zero and towards 1 would clearly improve the convergence rate.

Figure 2.9b shows simulation results when simulating $N = 10$ agents from a different random choice of initial conditions. This time with gains $\alpha = 0.4$ and $\alpha = 1.0$, shown in red and black respectively. Despite the change in initial conditions from the simulations in figure 2.9a, the MAS still exhibit convergence to x^{ss}. Moreover, we see the same pattern with respect to change increased gain α and speed of convergence. On the other hand,

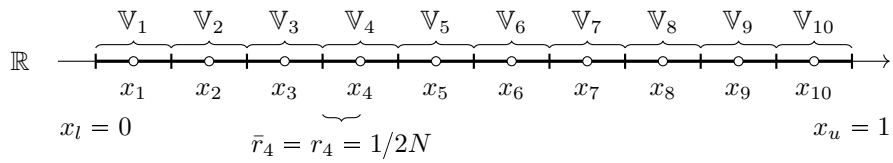

Figure 2.8: Steady state configuration x^{ss} for $N = 10$ agents in $\mathcal{W} = [0, 1] \subset \mathbb{R}$. Here $\bar{r}_i = r_i = 1/2N$ for all agents i.

this simulation illustrates the limits of the analogy to systems with fixed target positions. If the $\bar{x}_i(k)$'s were fixed, then the control action $u_i(0) = (\bar{x}_i - x_i(k))$ would lead to finite time convergence with $x_i(1) = \bar{x}_i$. However, the results in figure 2.9b suggest asymptotic convergence regardless of $\alpha = 1$. The time-varying nature of $\bar{x}_i(k)$'s seemingly induce asymptotic rather than finite time convergence of the MAS.

Next we investigate invariance of the final configuration with respect to the choice of controllers. In particular we utilize time-varying linear controllers in the sense that for each agent i the gain $\alpha_i(k)$ is drawn from the uniform random distribution on $(0, 1)$ at each time step k. To guard against chance, we simulate 200 runs with $N = 5$ agents. For each run, the initial condition $x(0)$ is determined by picking five random numbers independently and identically distributed from the uniform distribution on $(0, 1)$ and sorting these numbers such that $x_1(0) < x_2(0) < \cdots < x_5(0)$. Figure 2.9c shows the simulation results. The simulations support asymptotic convergence to expected configuration, where $\bar{r}_i = r_i = 1/2N$ for all agents i, invariant to initial conditions and the time-varying nature of the controllers.

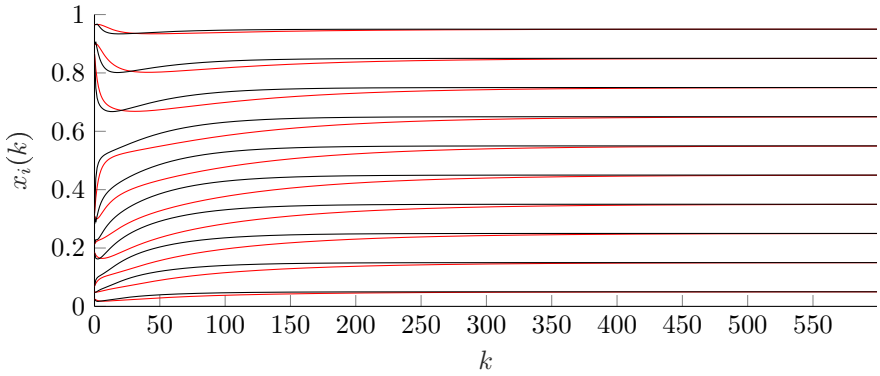

(a) $N = 10$. Two runs with equal initial conditions. $\alpha = 0.4$ in red and $\alpha = 0.9$ in black.

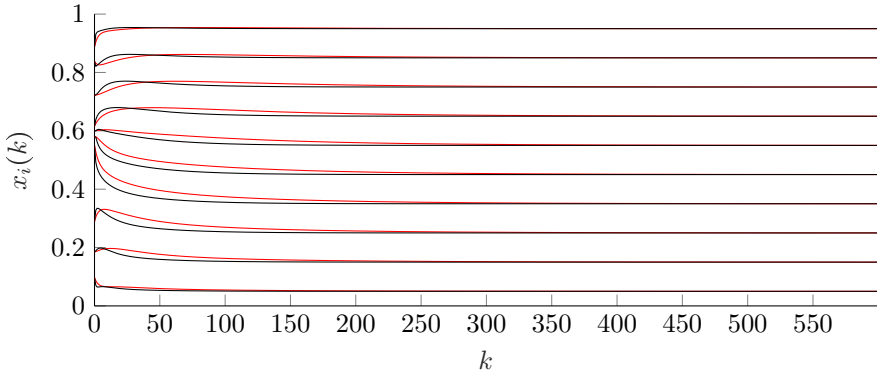

(b) $N = 10$. Two runs with equal initial conditions. $\alpha = 0.4$ in red and $\alpha = 1.0$ in black.

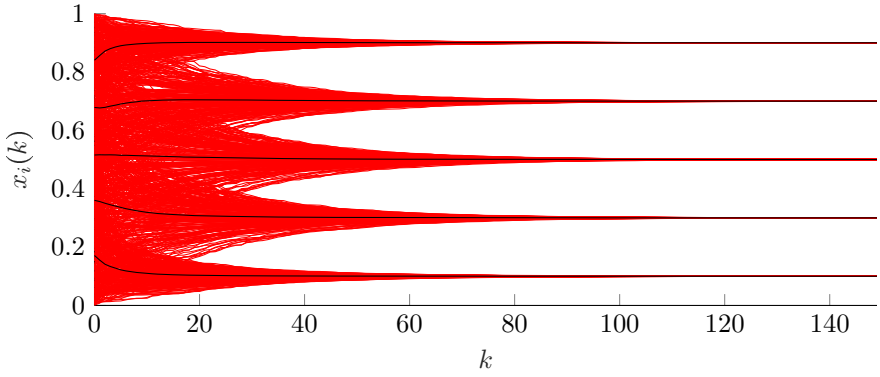

(c) $N = 5$. 200 runs with random initial conditions in $(0, 1)$ and random $\alpha_i(k)$ in $(0, 1)$. Individual runs shown in red. The average of all runs shown in black.

Figure 2.9: 1D simulations.

The final 1D example is related to the concept of information propagation in the MAS. Consider figure 2.10. In the illustrated configuration, $r_i = \bar{r}_i$ for agents $i = 2, \ldots, 5$. However, for agent 1 it is clearly possible to increase r_1 by moving to the left. We are interested in knowing how many time steps that are required before all agents are affected by the fact that the MAS is not in a steady state configuration. Figure 2.11 shows the first few time steps when simulating a five-agent MAS initialized with the configuration from figure 2.10 and with $\alpha_i(k) = \alpha = 1$. Observe that, in this particular simulation, $\bar{x}_i(k) \neq x_i(0)$ only if $k = i-1$ for $i = 1, \ldots, 5$. Since $x_i(k+1) \neq x_i(k)$ only if $\bar{x}_i(k) \neq x_i(k)$, $x_i(k) \neq x_i(0)$ only if $k = i$. Thus it takes $k = N = 5$ time steps before agent 1's deviation from its Chebyshev center propagates through the entire MAS in the sense that all agents move away from their initial positions. While we will not pursue any formal proofs in the present section, it is not hard to imagine that the relation $x_i(k) \neq x_i(0)$ only if $k = i$ holds for any finite number of agents N provided agent 1 is the sole agent where $\bar{r}_i(0) \neq r_i(0)$. The simulation indicates that the convergence factor for the system worsens with increased number of agents N. Moreover, it illustrates that a deviation $\bar{r}_i(0) > r_i(0)$ for some agent i not necessarily leads to immediate change in $\bar{x}_i, x_i, \bar{r}_i$ or r_i for other agents. Rather the propagation is, at best, in finite time. A natural question is the generalization of such a property to the multi-dimensional case.

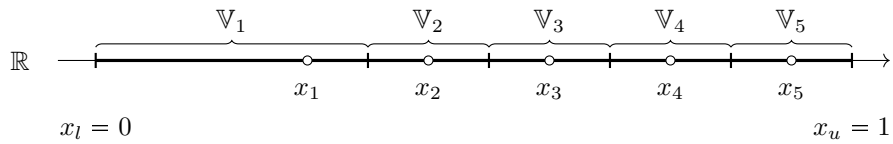

Figure 2.10: $N = 5$ agents where all but agent $i = 1$ have $\bar{r}_i = r_i$.

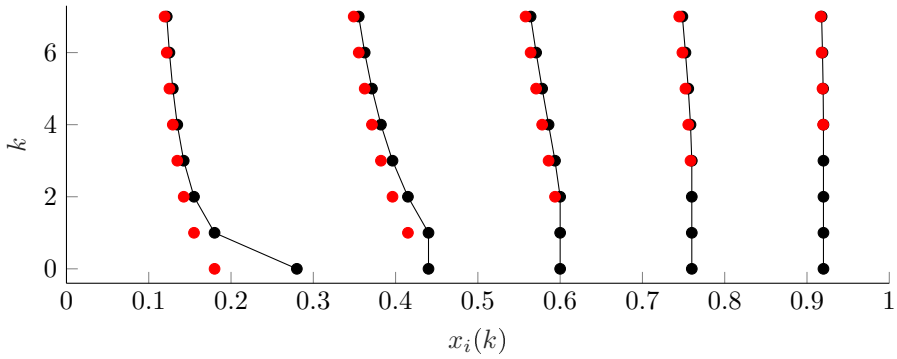

Figure 2.11: $N = 5$ agents with an initial condition where all but agent $i = 1$ have $\bar{r}_i(0) = r_i(0)$. $x_i(k)$'s marked by black dots. $\bar{x}_i(k)$'s are marked with red dots whenever $\bar{x}_i(k) \neq x_i(k)$.

2.7.2 2D numerical illustrations

We simulate N agents in a target environment $\mathcal{W} \subset \mathbb{R}^2$. All agents adhere to the single integrator dynamics

$$x_i(k+1) = x_i(k) + u_i(k) \in \mathbb{R}^2 \tag{2.87}$$

and utilize decentralized controllers

$$u_i(k) = \mathcal{K}_i(x_i(k), \mathbb{V}_i(k)) = \alpha_i(\bar{x}_i(k) - x_i(k)). \tag{2.88}$$

Initially we pick $\mathcal{W} = \{x \in \mathbb{R}^2 \mid \|x\|_\infty \leqslant 1\}$, with $\|\cdot\|_\infty$ being the infinity norm, as the target environment.

Figures 2.12 and 2.13 illustrate two particular simulations. $\alpha = 0.5$ in both cases, while the initial conditions $x(0)$ are different. Figures 2.12a and 2.13a show the initial positions and trajectories in $\mathcal{W}$. In both simulations, the MAS exhibits convergence to a static configuration with $\bar{r}_i(k) = r_i(k)\ \forall i \in \mathbb{N}_N$. Observe from figure 2.12b and figure 2.13b respectively that these differ. Figure 2.14 shows the results from a third simulation with equal initial conditions $x(0)$ as in figure 2.13, but with $\alpha = 1$ rather than 0.5. In this case the MAS exhibits convergence to a third steady state configuration, shown in figure 2.14b, different from the two previous simulations. All three simulations suggest the desired property of convergence to a static Chebyshev configuration. However, the final configuration of the MAS is seemingly not invariant to neither initial positions $x(0)$ nor the choice of admissible controller.

Inspecting the trajectories of r_i reveals other interesting patterns. First define the time varying bounds

$$\bar{r}_M(k) = \max_{i \in \mathbb{N}_N} \bar{r}_i(k), \qquad r_m(k) = \min_{i \in \mathbb{N}_N} r_i(k). \tag{2.89}$$

By construction

$$\bar{r}_M(k) \geqslant \bar{r}_i(k) \geqslant r_i(k) \geqslant r_m(k),\ \forall i \in \mathbb{N}_N. \tag{2.90}$$

Figure 2.15 shows the trajectories of both the bounds and individual $r_i(k)$'s for the simulation in figure 2.12. In this case it appears like $\bar{r}_M(k) \to r_m(k)$ as $k \to \infty$ which by (2.90) leads to $r_i = \bar{r}_M = r_m$ for all agents $i \in \mathbb{N}_N$. I.e. the agents achieve consensus on r_i. This is not the case in the simulation in figure 2.13. Revisiting 2.13b, we see that agents 1 and 5 have r_i's strictly larger than that of the remaining agents. This is reflected in figure 2.16, showing the trajectories of r_i. Seemingly

$$\max_{i \in \{2,5\}} \bar{r}_i(k) \to \min_{i \in \{2,5\}} r_i(k) \tag{2.91}$$

and

$$\max_{i \in \mathbb{N}_{10} \setminus \{2,5\}} \bar{r}_i(k) \to \min_{i \in \mathbb{N}_{10} \setminus \{2,5\}} r_i(k). \tag{2.92}$$

That is, the simulations suggest the existence of some mathematical structure steering subsets of agents to consensus on $\bar{r}_i$ and r_i.

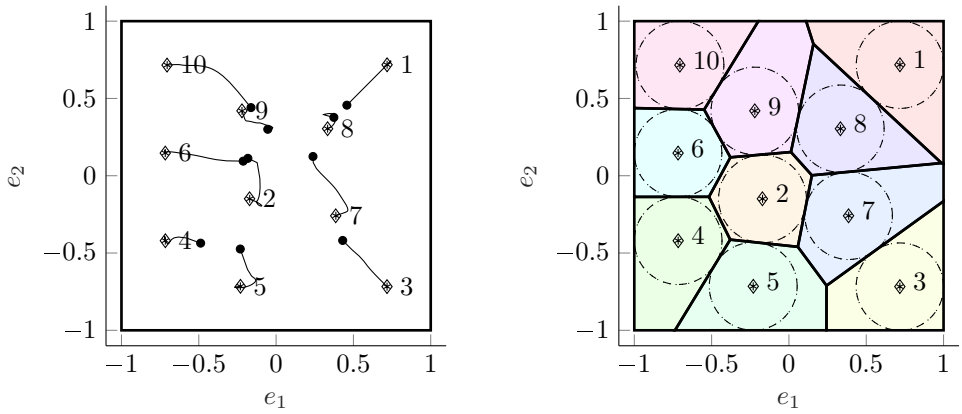

(a) Agent trajectories $x_i(k)$ are given by the solid lines. Dots indicate initial agent positions.

(b) The final MAS configuration. The circles are agent Chebyshev balls. Colored regions indicate agent Voronoi cells.

Figure 2.12: 2D simulation 1. $\alpha = 0.5$. The diamonds and asterisks are final agent Chebyshev centers and positions respectively.

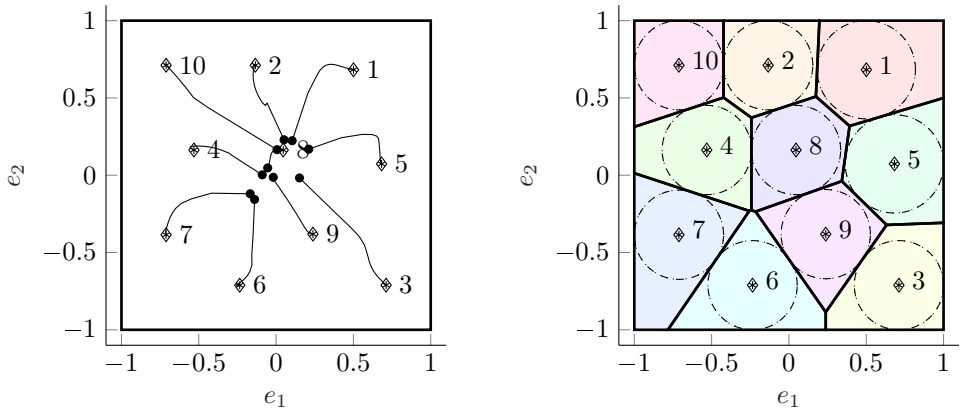

(a) Agent trajectories $x_i(k)$ are given by the solid lines. Dots indicate initial agent positions. The diamonds and asterisks are final agent Chebyshev centers and positions respectively.

(b) The final MAS configuration. The circles are agent Chebyshev balls. Colored regions indicate agent Voronoi cells.

Figure 2.13: 2D simulation 2. $\alpha = 0.5$.

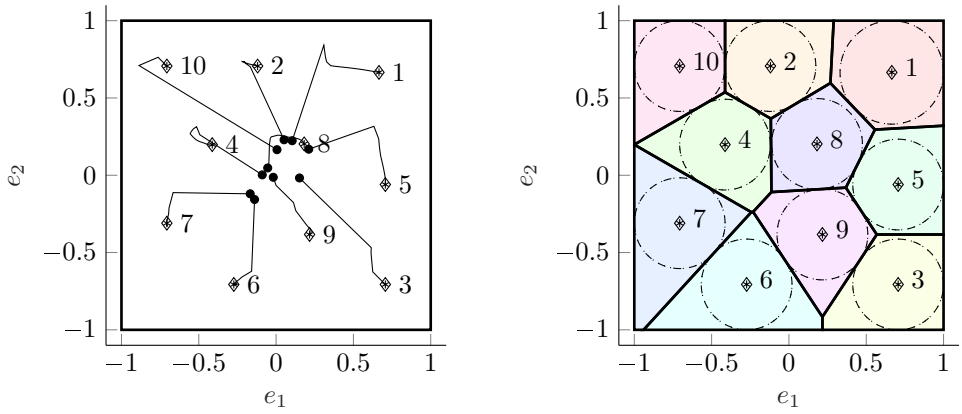

(a) Agent trajectories $x_i(k)$ are given by the solid lines. Dots indicate initial agent positions.

(b) The final MAS configuration. The circles are agent Chebyshev balls. Colored regions indicate agent Voronoi cells.

Figure 2.14: 2D simulation 3. $\alpha = 1$. The diamonds and asterisks are final agent Chebyshev centers and positions respectively.

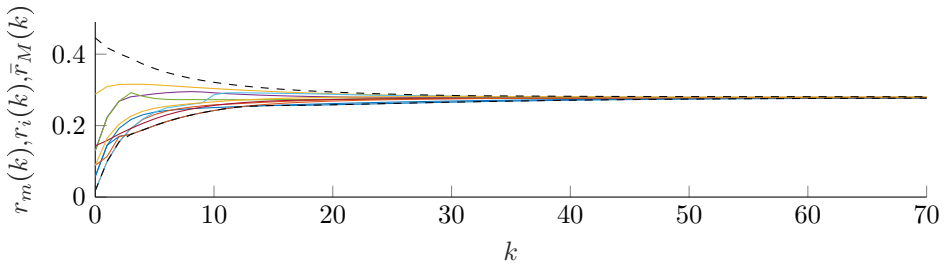

Figure 2.15: 2D simulation 1. Agent depth trajectories. $r_i(k)$'s given by colored lines. Agent indices are not important and therefore omitted. The upper and lower dashed lines are $\bar{r}_M(k)$ and $r_m(k)$ respectively.

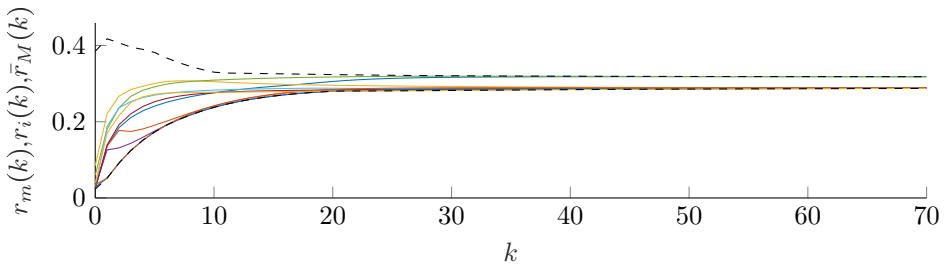

Figure 2.16: 2D simulation 2. Agent depth trajectories. $r_i(k)$'s given by colored lines. Agent indices are not important and therefore omitted. The upper and lower dashed lines are $\bar{r}_M(k)$ and $r_m(k)$ respectively.

Next we illustrate a degenerate case where the MAS exhibits convergence to the set of Chebyshev centers, but does not converge to a static configuration. $N = 2$ agents are deployed to the rectangle $\mathcal{W} = w \in \mathbb{R}^2 \mid |e_1^T x| \leqslant 3, |e_2^T x| \leqslant 1$ with agent controller gains $\alpha = 0.5$. Figure 2.17 shows the simulation results. Eventually $\bar{r}_i(k) = r_i(k) = 1$ for both agents. Consequently $V(x(k), \mathcal{W}) \to 0$. In this sense the simulation supports the hypothesis of convergence to the set of Chebyshev configurations,

$$\lim_{k \to \infty} x(k) \in \mathcal{X}_{\mathrm{CC}}. \tag{2.93}$$

However, the trajectories in figure 2.17a exemplifies how satisfying (2.93) does not guarantee convergence to a static configuration. The cause is apparent when considering the rectangular polytope in figure 2.18. It is possible to place a ball of radius $\bar{r}$ anywhere along the purple line, thus $\bar{x}$ is not unique. A similar observation holds for the trajectories of the MAS in figure 2.17a. Even when $\bar{r}_1(k) = \bar{r}_2(k) = r_1(k) = r_2(k) = 1$, the agents may move in a subset of the purple line. The control law requirements (2.68)-(2.70) are not sufficient to ensure the convergence of the MAS to a static configuration whenever non-uniqueness of Chebyshev centers arises.

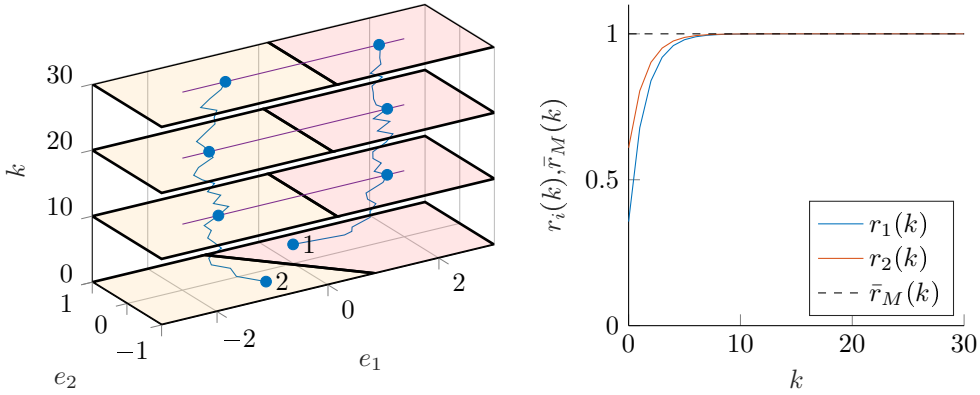

(a) The blue lines show the trajectories $x_i(k)$. (b) Trajectories of $r_1(k)$, $r_2(k)$ and $r_M(k)$. Shaded areas represent agent Voronoi cells at $r_M(k)$ is constant throughout the simulation. the k's indicated by the k-axis labels.

Figure 2.17: 2D simulation 4.

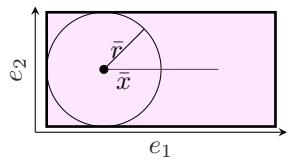

Figure 2.18: A rectangle in the plane illustrating the non-uniqueness of the Chebyshev center. Any $\bar{x}$ on the purple line is a valid placement for a ball with radius $\bar{r}$.

2.7.3 Concluding remarks on motivating examples

The preceding numerical illustrations inform our expectations as to which convergence properties we believe can be proved. All simulations support the hypothesis

$$\lim_{k\to\infty} x(k) \in \mathcal{X}_{\mathrm{CC}}. \tag{2.94}$$

In 1D, convergence to $\mathcal{X}_{\mathrm{CC}}$ appears to:

(i) Coincide with convergence to a static configuration.

(ii) Coincide with convergence to consensus on r_i.

(iii) Be asymptotic rather than finite time.

Moreover:

(iv) The steady state configuration of the MAS in 1D appears to be unique modulus boundaries x_l, x_u of $\mathcal{W} = [x_l, x_u]$ and number of agents N. I.e. $\mathcal{X}_{\mathrm{CC}}$ consists of a single configuration.

(v) $\bar{r}_M(k) > r_i(k)$ for all agents i appears to propagate to an increase in all r_i's in at most N steps.

Judging from the 2D simulations, several of these properties do not generalize beyond $\mathbb{R}$. Importantly the simulations in $\mathbb{R}^2$ illustrate:

(vi) $\mathcal{X}_{\mathrm{CC}}$ will in general not be a singleton set.

(vii) If the MAS converges to a particular Chebyshev configuration, the configuration to which it converges is not invariant to neither initial conditions nor choice of admissible agent controllers.

(viii) Convergence to $\mathcal{X}_{\mathrm{CC}}$ does not guarantee convergence to static configurations in degenerate cases.

(ix) The agents can in general not be expected to achieve consensus on $\bar{r}_i$ and r_i.

Meanwhile the same simulations support:

(ix) Convergence to a static configuration provided the agent Chebyshev centers are unique.

(x) The existence of some structure steering the MAS to consensus on $\bar{r}_i$ and r_i among subsets of neighboring agents.

In a sense, we expect the framework to exhibit mathematical properties in the multi-dimensional case which are similar but more general than in the 1D-case.

2.8 Problem statement

The main objective of the forthcoming theoretical developments is to revisit convergence results and address a series of open problems in this framework. Further to the observations in the motivating examples, we approach this objective by first investigating the special case of convergence under deployment to one-dimensional environments and next pursue similar yet more general results for the multi-dimensional case.

Thus the first objective is to formally prove convergence to the set of Chebyshev centers in the one-dimensional case. Related objectives are proofs of properties (i)-(iv) from section 2.7.3. Next we seek generalizations which are applicable also in the multi-dimensional case. In this respect, the consensus-like behavior is the most pertinent candidate for generalization. It is reasonable to expect that the mechanics driving the consensus-like behavior in 2D are the same driving the 1D MAS to consensus on Chebyshev radii. Thus uncovering the structure by which subsets of MAS agents are steered to consensus on Chebyshev radii and depths will be central to the developments. As a starting point, we aim to characterize the static MAS configurations in a manner which underpins the consensus among subsets of agents in higher dimensions. We expect the same characterization to yield consensus among all agents in static 1D configurations and additional unicity properties. Moreover, this line of research is motivated by the hypothesis that the consensus-like behavior is essential in driving the MAS to a Chebyshev configuration. To this end, information propagation between agents will be scrutinized. Under assumptions which resemble the 1D-conditions, we aim to prove convergence to a Chebyshev configuration with consensus on Chebyshev radii in the multi-dimensional case.

An important point of view due to the optimization-based nature of the Chebyshev center, is the effect of unicity properties of the optimizer with respect to MAS convergence. Convergence to a Chebyshev configuration is not sufficient for convergence to the set of static configurations in degenerated cases. A complete treatment of this issue is left as a future research direction. We do however suggest specific promising modifications to the framework in order to mitigate the problem.

Further to strengthening formal convergence results, we also aim to show convergence to globally optimal configurations in the general case. Specifically, we seek results showing that limit configurations of the MAS corresponds to local optima of the sphere packing function presented in [Cortes and Bullo, 2005].

The derivation of convergence results will be the topic of chapter 3.

2.9 Chapter notes

The theory on polyhedra and polytopes in section 2.1.2 is only a small excerpt of a rich theory. For instance we have left out the important Minkowski-Weyl theorem from which we know that all polyhedra admit both an H-representation and a so-called *vertex-representation*, abbreviated V-rep. In this latter representation, the polyhedron is represented as as the Minkowski sum of the set of convex combinations of its vertices and the set of conic[4] combinations of a particular set of rays. For theoretical purposes it is often useful to go back and forth between the two representations, but in practical applications this can be very computationally demanding. See for instance [Ziegler, 2012] or [Grünbaum, 2003] for more on polyhedra.

Linear programming has been extensively studied and is considered to be well understood. For more on linear programming, both [Boyd and Vandenberghe, 2004] and [Nocedal and Wright, 2006] are recommended. We assume that the reader is familiar with linear programming from before, and therefore limit the presentation to illustrating some of the many connections between polyhedra and linear programming.

Assuming single integrator agent dynamics may seem restrictive. However, this simplification is quite common in the literature on distributed control. Bruce Francis explains a possible justification for this in his 2014 Bode lecture [Francis, 2014]. He shows how a large class of mobile robots can be modeled as so-called unicycles. A particular linearization of the unicycle model, originally suggested by Yun and Yamamoto [1992], is in fact a single integrator system.

The Voronoi partition is also called a Voronoi tessellation, diagram or decomposition. While one may consider the partition with respect to other norms, the euclidean norm is the standard choice. In this case the so-called Delaunay complex is the dual of the Voronoi diagram [Rakovic et al., 2004]. The Delaunay Complex is commonly called The Delaunay triangulation. It does in fact not satisfy the formal requirements for being a triangulation unless the set of points generating the complex satisfy certain regularity conditions. A *cell complex* or just *complex* is a collection of polytopes with some additional mutual structure. See for instance [Fukuda, 2016] for a definition. The collection of Voronoi cells is in fact a cell complex, hence the name Voronoi cell.

The Delaunay graph [Bullo et al., 2009] is an undirected graph in which the nodes are the points generating the Voronoi diagram and for all nodes i there is an edge to node $j \neq i$ if $\mathbb{V}_i \cap \mathbb{V}_j \neq \varnothing$. Thus the set of neighbors $\mathcal{N}_i$ is implicitly derived from this graph. It is related to the Delaunay complex not only by name, but we will not discuss these connections any further. Computing $\mathcal{N}_i$ amounts to determining the set of edges connected to node i in the Delaunay graph. A method for doing this is presented in [Fukuda, 2004]. Essentially one has to determine the set of irredundant constraints in the half-space representation of $\mathbb{V}_i$. Existing methods are well documented. Thus we will not present any such methods here, but refer the reader to [Fukuda, 2004].

[4]The conic combinations of a set $\mathcal{P}$ of points/rays/vectors are linear combinations of the elements in $\mathcal{P}$ where all coefficients are non-negative.

Neither will we present methods for computing the complete Voronoi diagram. We have applied it to make some of the illustration in this report (e.g. figure 2.6). However, it is not applied in the theoretical developments and thus excluded from the presentation. We refer the reader to Rakovic et al. [2004] where it is shown how one may compute both Voronoi diagrams and Delaunay Triangulations for arbitrary high dimensional spaces by solving a parametric linear program. Conveniently this method is implemented in the open source Matlab toolbox Multi-Parametric Toolbox 3 [Herceg et al., 2013]. All Voronoi diagrams in the various figures in this report have been computed in this manner.

As apparent from the framework description, we do however depend on the agents being able to construct their individual Voronoi cells. While assumption 2.4.1 is sufficient in this respect, it may be replaced by other assumptions. In [Bash and Desnoyers, 2007] and [Alsalih et al., 2008], they show efficient methods for computing $\mathbb{V}_i$ provided the agents can transmit their positions to each other over a connected communications graph. This assumption is not necessarily weaker than assumption 2.4.1, but the abstraction it relies on can be more plausible or convenient in practical situations.

The assumption of distinct agents states may be dropped by introducing appropriate schemes for handling situations where agents are superimposed. For instance [Nguyen, 2016] suggest a scheme where one first partitions $\mathcal{W}$ with respect to the (possibly improper) subset of distinct agents states and next sub-partition Voronoi cells corresponding to states with multiplicity higher than one. Therefore this assumption is not critical, but simplifies the presentation. Moreover, it is obviously a reasonable assumptions in scenarios where the state of an agent its position in the room or in the plane.

With regards to the Chebyshev configurations observed in the 2D simulations in figure 2.7, it would in fact be reasonable to expect non-unique Chebyshev and static configurations from the outset. Due to the choice of squared environment $\mathcal{W}$, it is easy to see that reflecting any Chebyshev configuration about the e_1 and/or e_2 axis yields a new Chebyshev configuration. It is quite typical for formation control type frameworks to exhibit symmetries related to rotation, reflection and permutations of agent indices. As such, the interesting nature of the non-uniqueness of the Chebyshev configurations is the fact that considering Chebyshev configurations modulus these three classes of symmetries is not sufficient to recover uniqueness.

Chapter 3

Convergence

In this chapter we derive theoretical convergence results for the framework presented in chapter 2. After discussing preliminary convergence notions in section 3.2, we analyze deployment to $\mathbb{R}$ in section 3.3. As we will see, the framework has several useful connections to discrete time averaging systems. This is particularly prominent when deploying to $\mathbb{R}$. In fact the MAS dynamics can be analyzed with standard tools from linear discrete time averaging systems. Section 3.4 is devoted the more complicated case of deployment to $\mathbb{R}^d$. While the tools for analyzing stability of linear dynamical systems cannot be applied here, several concepts carry over. We start by providing additional theoretical background in section 3.1.

3.1 Theoretical background

Standard definitions, results and notions from theory on non-negative matrices and graphs are introduced in sections 3.1.1 and 3.1.2 respectively. Section 3.1.2 also discusses elements of algebraic graph theory. In particular we present results on adjacency matrices. Sections 3.1.1 and 3.1.2 are the foundation for the discrete time linear averaging part in section 3.1.3. A complete introduction to the topics are beyond the scope of thesis, and we refer to [Bullo, 2018] for a comprehensive treatment. The theory on discrete time linear averaging is applicable when analyzing deployment to $\mathbb{R}$. However, we need a different set of tools when analyzing the more complex case of deployment to $\mathbb{R}^d$. To this end, section 3.1.4 presents a few selected results from real analysis.

3.1.1 Matrix theory

We start by introducing elements of matrix theory - with emphasis on theory related to non-negative matrices.

Let $A \in \mathbb{R}^{n\times n}$ be a square matrix with elements $(A)_{ij} = e_i^T A e_j \in \mathbb{R}$.

We characterize the convergence of A^k, with $k \in \mathbb{N}$, via the following definitions:

Definition 3.1.1 (Semi-convergent and convergent matrices)**.** *The square matrix $A \in \mathbb{R}^{n\times n}$ is*

(i) semi-convergent if $\lim_{k\to\infty} A^k$ exists.

(ii) convergent if $\lim_{k\to\infty} A^k = \mathbb{0}_{n\times n}$.

E.g.

$$A_1 = \begin{bmatrix} 1 & 0 \\ 0 & 0.3 \end{bmatrix}, \qquad A_2 = \begin{bmatrix} 0.9 & 0 \\ 0 & 0.3 \end{bmatrix}, \qquad A_3 = \begin{bmatrix} 0 & 1 \\ 1 & 0 \end{bmatrix}, \tag{3.1}$$

are respectively semi-convergent, convergent and neither convergent nor semi-convergent.

As known from standard linear algebra, the convergence properties of A is related to its eigenstructure. In this respect, we rely on the following definitions:

Definition 3.1.2 (Spectrum and spectral radius)**.** *Let $A \in \mathbb{R}^{n\times n}$ be a square matrix.*

(i) The spectrum, $\mathrm{spec}(A)$, of A is the set of eigenvalues of A.

(ii) The spectral radius $\rho(A)$ of A is the maximum modulus of any eigenvalue of A. I.e.

$$\rho(A) = \max\{|\lambda| \mid \lambda \in \mathrm{spec}(A)\}. \tag{3.2}$$

E.g. $\mathrm{spec}(A_1) = \{1, 0.3\}$ and $\rho(A_1) = 1$. An eigenvalue is simple if its algebraic and geometric multiplicities are equal to one. It is semi-simple if its algebraic and geometric multiplicities are equal.

The spectrum can, to some extent, be localized via the very important Gershgorin Disks Theorem.

Theorem 3.1 (Gershgorin Disks Theorem, theorem 2.8 in [Bullo, 2018])**.** *For any square matrix $A \in \mathbb{R}^{n\times n}$ with $a_{ij} = (A)_{ij}$,*

$$\mathrm{spec}(A) \subset \bigcup_{i\in\mathbb{N}_n} \{z \in \mathbb{C} \mid |z - a_{ii}| \leqslant \sum_{j\in\mathbb{N}_n\setminus\{i\}} |a_{ij}|\}. \tag{3.3}$$

We will use this useful theorem to locate the spectrum of matrices in the MAS framework under consideration. Remark that it plays an important role in the proofs of several standard results from discrete time averaging systems. In particular it is vital for characterizing the spectrum of stochastic matrices. Stochastic matrices as well as the related classes of non-negative and positive matrices are defined as follows:

Definition 3.1.3 (Non-negative and positive matrices)**.** *The square matrix $A \in \mathbb{R}^{n\times n}$ is*

(i) non-negative if $(A)_{ij} \geqslant 0$ for all i, j in $\mathbb{N}_n$, denoted by $A \geqslant 0$.

(ii) positive if $(A)_{ij} > 0$ for all i, j in $\mathbb{N}_n$, denoted by by $A > 0$.

Definition 3.1.4 (Stochastic matrices)**.** *The non-negative matrix $A \in \mathbb{R}^{n\times n}$ is*

(i) row-stochastic if $A\mathbb{1} = \mathbb{1}$.

(ii) column-stochastic if $A^T\mathbb{1} = \mathbb{1}$.

(iii) doubly stochastic if $A \geqslant 0$ and $A^T\mathbb{1} = A\mathbb{1} = \mathbb{1}$. I.e. a doubly stochastic matrix is both row- and column-stochastic.

We omit the result for brevity, but remark that theorem 3.1 can be used to show that the spectrum of any stochastic matrix is contained in the unit disk. Also, observe that $(1, \mathbb{1})$ is a right eigenpair of any row-stochastic matrix by definition. Similarly, $(1, \mathbb{1}^T)$ is a left eigenpair of a column-stochastic matrix. Another related class of matrices, is that of sub-stochastic matrices:

Definition 3.1.5 (Row-substochastic matrix)**.** *The non-negative matrix $A \in \mathbb{R}^{n\times n}$ is row-substochastic if*

(i) $A\mathbb{1} \leqslant \mathbb{1}$, and

(ii) $e_i^T A\mathbb{1} < 1$ for at least one $i \in \mathbb{N}_n$.

In determining the convergence properties of non-negative matrices, the following characterizations are vital:

Definition 3.1.6 (Irreducible and primitive matrices)**.** *Let $A \in \mathbb{R}^{n\times n}$ be a non-negative matrix where $n > 1$. A is*

1. *irreducible if*

$$\sum_{k=0}^{n-1} A^k > 0, \tag{3.4}$$

2. *primitive if there exists $k \in \mathbb{N}$ such that*

$$A^k > 0. \tag{3.5}$$

A non-negative matrix is reducible *if it is not irreducible.*

Neither definition is particularly intuitive on first sight. However, they are easier to understand after linking them to specific graph theoretical concepts. This will be the topic of the next section.

3.1.2 Graph theory

Let $\mathcal{G} = (\mathcal{V}, \mathcal{E})$ be a graph with nodes $\mathcal{V} \subset \mathbb{N}$ and edges $\mathcal{E} \subset \mathcal{V} \times \mathcal{V}$. $\mathcal{G}$ can either be directed or undirected. In the latter case, $(u, v) \in \mathcal{E} \iff (v, u) \in \mathcal{E}$ and $(u, u) \notin \mathcal{E}$ (i.e. no self loops). Both cases are illustrated in figure 3.1. For the directed case, we follow the

convention where $(i, j) \in \mathcal{E}$ is represented by arrow from i to j. This should be interpreted as i "listens to" or "is affected by" j. For instance node 1 in figure 3.1a listens to nodes 2 and 5.

Remark 3.1.1. *Beware that this convention can be counter-intuitive on first glance. We have chosen to be consistent with [Bullo, 2018]. Later we will introduce the adjacency matrix $A(\mathcal{G})$ associated with a graph $\mathcal{G}$. The convention makes sense when using this adjacency matrix in discrete time systems on the form $x(k+1) = A(\mathcal{G})x(k)$. The presence of an edge (i, j) ensures that $A(\mathcal{G})_{ij} > 0$ and in turn leads to $x_i(k + 1)$ being directly affected by $x_j(k)$.*

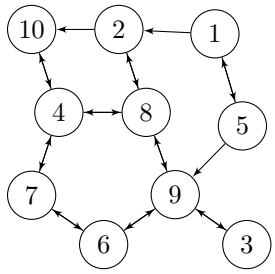

(a) Sample directed graph. Arrows show directionality.

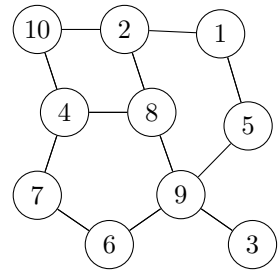

(b) Sample undirected graph.

Figure 3.1: Sample graphs embedded in the plane. A line between two nodes show the existence of edges between them.

Selecting subsets of nodes allow us to consider so-called subgraphs of $\mathcal{G}$. The formal definition is as follows.

Definition 3.1.7 (Subgraph)**.** *Graph $\mathcal{G}' = (\mathcal{V}', \mathcal{E}')$ is a subgraph of $\mathcal{G}$ provided*

(i) $\mathcal{V}' \subset \mathcal{V}$, and

(ii) $\mathcal{E}' \subset \mathcal{E}$ and $(i, j) \in \mathcal{E}'$ only if $i \in \mathcal{V}'$ and $j \in \mathcal{V}'$.

The subgraph of $\mathcal{G}$ induced by $\mathcal{V}'$ is the graph $\mathcal{G}' = (\mathcal{V}', \mathcal{E}')$ where $\mathcal{E}' = \{(i, j) \in \mathcal{E} \mid i \in \mathcal{V}', j \in \mathcal{V}'\}$. We say that a sub-graph $\mathcal{G}' = (\mathcal{V}', \mathcal{E}')$ strictly contains *the sub-graph $\mathcal{G}'' = (\mathcal{V}'', \mathcal{E}'')$ provided $\mathcal{V}'' \subseteq \mathcal{V}'$ and $\mathcal{E}'' \subseteq \mathcal{E}'$.*

Figure 3.2 shows two subgraphs of the graphs in figure 3.1.

For our purposes, graph connectivity notions are of particular importance. They determine the ability for information to propagate through the graph. Graph connectivity is defined via so-called paths.

Definition 3.1.8 (Path)**.** *Let $\mathcal{G} = (\mathcal{V}, \mathcal{E})$ be a graph. A path in $\mathcal{G}$ is a finite sequence $\{v_m\}_{m=0}^{M}$ of nodes $v_m \in \mathcal{V}$ such that any two consecutive nodes in the sequence are connected by an edge. I.e. $(v_{m-1}, v_m) \in \mathcal{E}$ for all $m \in \mathbb{N}_M$.*

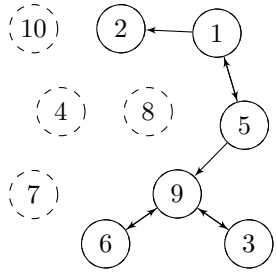

(a) Sub-graph induced by $\mathcal{V}' = \{1, 2, 3, 5, 6, 9\}$.

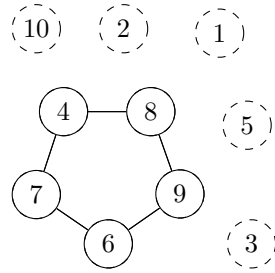

(b) Sub-graph induced by $\mathcal{V}' = \{4, 6, 7, 8, 9\}$.

Figure 3.2: Sub-graphs of the graphs in figure 3.1.

E.g. the sequence of nodes $1, 2, 10, 4, 8$ is a path in both graphs in figure 3.1a. As customary we define separate graph connectivity notions for directed and undirected graphs.

Definition 3.1.9 (Connected undirected graph)**.** *An undirected graph is connected if for any pair of nodes $i \neq j$ with $i, j \in \mathcal{V}$ there exists a path from i to j.*

If an undirected graph is not connected, we say that it is *disconnected*.

Figure 3.3 shows a connected and disconnected directed graph in figure 3.3a and figure 3.3b respectively. The graph in figure 3.3b is disconnected as nodes $i \in \mathbb{N}_{10} \backslash \{1, 5\}$ have no path to agents 1 and 5.

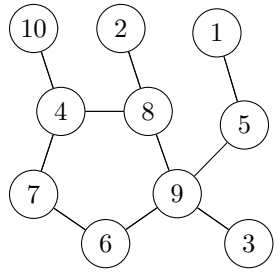

(a) A connected undirected graph.

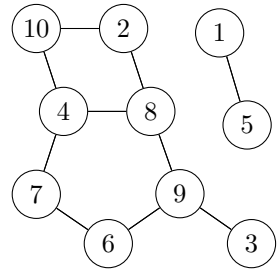

(b) A disconnected undirected graph.

Figure 3.3: Connectivity notions for undirected graphs.

Due to the addition of directionality, directed graphs have more elaborate connectivity notions.

Definition 3.1.10 (Connectivity notions for directed graphs)**.** *Given a directed graph $\mathcal{G} = (\mathcal{V}, \mathcal{E})$,*

(i) $\mathcal{G}$ is strongly connected if for all ordered pair of nodes $(i, j) \in \mathcal{V} \times \mathcal{V}$ there exists a path from i to j.

(ii) $\mathcal{G}$ *has a* globally reachable node *if there exists a node* $i \in \mathcal{V}$ *such that for all* $j \in \mathcal{V}\backslash\{i\}$ *there exists a path from* j *to* i.

Figure 3.4 illustrates these connectivity notions. The graph in figure 3.4a is strongly connected as there exists a path from any start node $i \in \mathbb{N}_{10}$ to any end node $j \in \mathbb{N}_{10}$. However, the strongly connected property is lost if one, for instance, removes the edge $(2, 1)$. This is the case in figure 3.4b. Nodes $i \in \mathbb{N}_{10}\backslash\{1, 5\}$ have no path to nodes 1 and 5. On the other hand, all nodes $i \in \mathbb{N}_{10}\backslash\{1, 5\}$ can be reached via a path from any node $j \in \mathbb{N}_{10}$ and thus the graph has several globally reachable nodes. Finally, the graph in figure 3.4c is neither strongly connected nor contains a globally reachable node due to the lack of edges between $i \in \{1, 5\}$ and $j \in \mathbb{N}_{10}\backslash\{1, 5\}$.

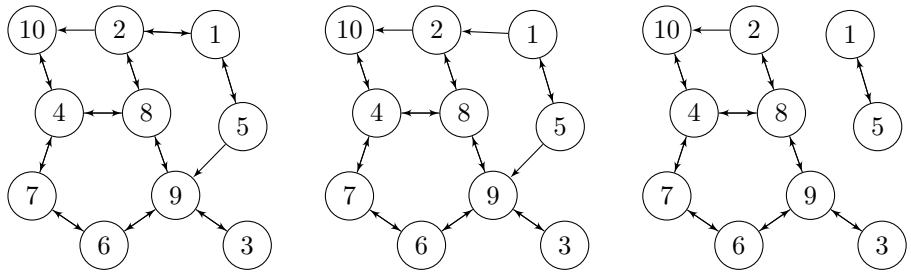

(a) A strongly connected directed graph.

(b) A directed graph with a globally reachable node.

(c) A directed graph which is not strongly connected and with no globally reachable nodes.

Figure 3.4: Connectivity notions for directed graphs.

Even if an undirected graph is not connected, it may contain subgraphs which are connected. Analogously, directed graphs may contain strongly connected subgraphs even when the graph itself is not strongly connected. Interpreting edges between nodes as encoding dependencies, it is often vital to uncover the subsets of nodes which depend on each other. Utilizing the notions of *connected components* and *strongly connected components*, for undirected and directed graphs respectively, allows us to identify large scale dependency patterns between subsets of nodes.

Definition 3.1.11 (Strongly connected and connected components)**.**

(i) A subgraph $\mathcal{G}'$ *is a connected component of the undirected graph* $\mathcal{G}$ *if* $\mathcal{G}'$ *is connected and any other subgraph of* $\mathcal{G}$ *strictly containing* $\mathcal{G}'$ *is not connected.*

(ii) A subgraph $\mathcal{G}'$ *is a strongly connected component of the directed graph* $\mathcal{G}$ *if* $\mathcal{G}'$ *is strongly connected and any other subgraph of* $\mathcal{G}$ *strictly containing* $\mathcal{G}'$ *is not strongly connected.*

E.g. the undirected graph in figure 3.3a consists of a single connected component whereas the graph in figure 3.3b has two connected components. In the latter case, the connected components are the subgraphs induced by the nodes $\mathbb{N}_{10}\backslash\{1, 5\}$ and $\{1, 5\}$ respectively.

As for the directed case, we observe that the graphs in figures 3.4b and 3.4c both have two strongly connected components. Again, these are the subgraphs induced by the nodes $\mathbb{N}_{10}\backslash\{1,5\}$ and $\{1,5\}$ respectively

If an undirected graph consists of more than one connected component, then graph is simply the union of the disjoint subgraphs contained in its collection of connected components. The subgraphs are disjoint in the sense that there are no edges between these subgraphs - the connected components do not interact at all. Strongly connected components in directed graphs may interact, but only in an asymmetric way. E.g. in figure 3.4b nodes $\{1,5\}$ are affected by nodes in $\mathbb{N}_{10}\backslash\{1,5\}$, but not vice versa. Given two separate strongly connected components $\mathcal{G}_1'$ and $\mathcal{G}_2'$ of a directed graph $\mathcal{G}$, there may exist a path from $\mathcal{G}_1'$ to $\mathcal{G}_2'$ or from $\mathcal{G}_2'$ to $\mathcal{G}_1'$ or no path between them at all. The latter is the case in figure 3.4c.

Next we introduce the notion of weighted directed graphs and their so-called adjacency matrix representation.

Definition 3.1.12 (Weighted directed graph)**.** *A weighted directed graph, represented by the triple $\mathcal{G} = (\mathcal{V}, \mathcal{E}, \{a_{ij}\}_{(i,j)\in\mathcal{E}})$, is a directed graph where each edge $(i,j) \in \mathcal{E}$ has an associated positive weight $a_{ij} > 0$.*

Definition 3.1.13 (Adjacency matrix)**.** *Let $\mathcal{G} = (\mathcal{V}, \mathcal{E}, \{a_{ij}\}_{(i,j)\in\mathcal{E}})$ be a weighted directed graph. Then the adjacency matrix associated with $\mathcal{G}$ is the square matrix $A \in \mathbb{R}^{|\mathcal{V}|\times|\mathcal{V}|}$ where*

(i) $(A)_{ij} = a_{ij}$ *for all* $(i,j) \in \mathcal{E}$*, and*

(ii) $(A)_{ij} = 0$ *otherwise.*

Conversely we associate a directed graph to all non-negative matrices.

Definition 3.1.14 (Weighted directed graph associated with non-negative matrix)**.** *Let $A \in \mathbb{R}^{n\times n}$ be a non-negative matrix, then its associated graph $\mathcal{G}$ is the weighted directed graph $\mathcal{G} = (\mathcal{V}, \mathcal{E}, \{a_{ij}\}_{(i,j)\in\mathcal{E}})$ where*

(i) $\mathcal{V} = \mathbb{N}_n$,

(ii) $\mathcal{E} = \{(i,j) \mid (A)_{ij} > 0\}$,

(iii) $a_{ij} = (A)_{ij}$ *for all* $(i,j) \in \mathcal{E}$.

See figure 3.5 for an example of a graph $\mathcal{G}$ and its associated adjacency matrix A.

Observe that:

- $e_i^T A = \mathrm{row}_i(A)$ contains the weights of edges leaving node i.
- $Ae_i = \mathrm{col}_i(A)$ contains the weights of edges entering node i.

We also remark that an adjacency matrix A associated with an undirected graph $\mathcal{G} = (\mathcal{V}, \mathcal{E})$ has to satisfy the following additional structural requirements:

(i) Diagonal entries of A are all zero, to satisfy the requirement of no self loops.

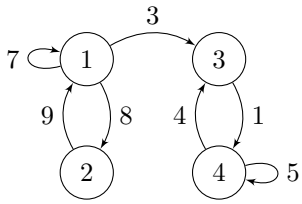

(a) $\mathcal{G} = \mathcal{G}(A)$, the graph induced by the adjacency matrix A.

$$A = \begin{bmatrix} 7 & 8 & 3 & 0 \\ 9 & 0 & 0 & 0 \\ 0 & 0 & 0 & 1 \\ 0 & 0 & 4 & 5 \end{bmatrix}$$

(b) The adjacency matrix A associated with $\mathcal{G}$.

Figure 3.5: A weighted graph $\mathcal{G}$ and its associated adjacency matrix.

(ii) $A^T = A$, i.e. the adjacency matrix is symmetric. This requirement is somewhat stronger than $(i,j) \in \mathcal{E} \iff (j,i) \in \mathcal{E}$ since the weights have to be equal, but is the natural and common extension of weighted graphs to the undirected case.

Even if a directed or undirected graph is unweighted, we may use an adjacency matrix to encode the presence of edges between nodes. In this case one usually considers the so-called binary adjacency matrix $A_{0,1}$ where $a_{ij} = 1$ provided $(i,j) \in \mathcal{E}$ and $a_{ij} = 0$ otherwise.

The ability to go back and forth between the graph representation $\mathcal{G}$ and the adjacency matrix A enables us to use properties of the graph to show properties of the adjacency matrix, and vice versa. First we relate non-zero entries in A^k with the existence of a length k path between nodes i and j where $(A^k)_{ij} > 0$.

Consider an adjacency matrix $A \in \mathbb{R}^{n \times n}$ and its associated graph $\mathcal{G}(A) = (\mathcal{V}, \mathcal{E})$. Remark that $e_i^T A e_j > 0$ if and only if $(i,j) \in \mathcal{E}$. I.e. $e_i^T A e_j > 0$ implies the existence of a length-1 path from i to j. Now consider

$$e_i^T A^2 e_j = \underbrace{\mathrm{row}_i(A)}_{\text{Edges exiting node } i} \cdot \underbrace{\mathrm{col}_j(A)}_{\text{Edges entering node } j} = \sum_{l=1}^{n} (e_i^T A e_l)(e_l^T A e_j). \tag{3.6}$$

Thus $e_i^T A^2 e_j > 0$ if and only if node i has a length one path to at least one node l with a length one path to node j. I.e. $e_i^T A^2 e_j > 0$ if and only if there exists at least one length-2 path from node i to j. Formalizing and extending this line of reasoning yields the following result:

Lemma 3.1.1 (Paths and powers of the adjacency matrix, lemma 4.2 in [Bullo, 2018])**.** *Let $\mathcal{G}$ be a weighted directed graph with the associated adjacency matrix $A \in \mathbb{R}^{n \times n}$. Then*

(i) the entry $e_i^T A^k e_j > 0$ if and only if there exists at least one length-k path from node i to node j.

Moreover, let $A_{0,1} \in \mathbb{R}^{n \times n}$ be the binary adjacency matrix of $\mathcal{G}$ where $e_i^T A_{0,1} e_j = 1$ if $e_i^T A e_j > 0$ and $e_i^T A_{0,1} e_j = 0$ otherwise. Then

(ii) the entry $e_i^T A^k e_j$ equals the number of length-k paths from node i to node j.

We refer to [Bullo, 2018] for more info on this lemma. With this result in mind, the following important result is not surprising:

Theorem 3.2 (Connectivity properties of the digraph and irreducibility of the adjacency matrix, theorem 4.2 in [Bullo, 2018])**.** *Let $\mathcal{G} = (\mathcal{V}, \mathcal{E})$ be a weighted directed graph where $|\mathcal{V}| > 1$ and let $A \in \mathbb{R}^{|\mathcal{V}| \times |\mathcal{V}|}$ be its associated adjacency matrix. The following statements are equivalent:*

(i) A is irreducible, i.e. $\sum_{i=0}^{|\mathcal{V}|-1} A^k > 0$.

(ii) $\mathcal{G}$ is strongly connected.

(iii) For all partitions $\{\mathcal{I}, \mathcal{J}\}$ of the index set $\{1, 2, \dots, |\mathcal{V}|\}$ there exists $i \in \mathcal{I}$ and $j \in \mathcal{J}$ such that $a_{ij} > 0$. I.e. there exists and edge $(i, j) \in \mathcal{E}$.

We refer the reader to [Bullo, 2018] for a proof. However, it is quite easy to grasp the intuition of (i) $\iff$ (ii) in light of lemma 3.1.1. Since $e_i^T A^k e_j > 0$ if and only if there exists a length-k path from i to j, then $e_i^T (\sum_{i=0}^{|\mathcal{V}|-1} A^k) e_j = \sum_{i=0}^{|\mathcal{V}|-1} e_i^T A^k e_j > 0$ if and only if there exists one or more paths with maximal length $|\mathcal{V}|$ from node i to node j. Remark that it is sufficient to consider paths of maximal length $|\mathcal{V}|$ when checking if $\mathcal{G}$ is strongly connected, since longer paths necessarily will contain repetitions of one or more nodes.

Importantly, the theorem allows us to relate irreducibility as a matrix property with connectivity properties of the associated graph. We can gain some intuition about irreducibility by considering the dynamical system $x(k+1) = Ax(k)$. In this case, irreducibility entails communication back and forth between all sub-systems. Eg. an irreducible matrix A can not have a structure such as

$$A = \begin{bmatrix} A^{(11)}_{r \times r} & A^{(12)}_{r \times (n-r)} \\ \mathbb{0}_{(n-r) \times r} & A^{(22)}_{(n-r) \times (n-r)} \end{bmatrix} \in \mathbb{R}^{n \times n}. \tag{3.7}$$

The subscripts indicate the sizes of the sub-matrices of A. Let $\mathcal{G}(A) = (\mathcal{V}, \mathcal{E})$ be the graph associated with A. Note that the partitioning $\mathcal{J} = \{1, \dots, r\}$, $\mathcal{I} = \{r+1, \dots, n\}$ yields $\nexists (i, j) \in \mathcal{E} : i \in \mathcal{I}, j \in \mathcal{J}$, contradicting theorem 3.2. Assuming the sub-matrices $A^{(11)}$ and $A^{(12)}$ are irreducible, the matrix structure in (3.7) corresponds to a graph with two strongly connected components. If $A^{(12)} \neq \mathbb{0}$, then $\mathcal{G}(A)$ contains a globally reachable node. To see this, observe that all nodes $i \in \{1, \dots, r\}$ can reach nodes $j \in \{r+1, \dots, n\}$ via some edge represented by $A^{(12)}$. Figure 3.5 can be revisited for an example of this situation. In turn, the nodes $j \in \mathcal{J}$ are unaffected by the nodes in $\mathcal{I}$. Specifically

$$x(k+1) = \begin{bmatrix} x^{(1)}(k+1) \\ x^{(2)}(k+1) \end{bmatrix} = \begin{bmatrix} A^{(11)} x^{(1)}(k) + A^{(12)} x^{(2)}(k) \\ A^{(22)} x^{(2)}(k) \end{bmatrix}. \tag{3.8}$$

I.e. $x^{(2)}(k)$ is independent of $x^{(1)}(k)$ for all k.

Irreducibility is of particular importance when investigating the semi-convergence of stochastic matrices. However, the system

$$x(k+1) = \underbrace{\begin{bmatrix} 0 & 1 \\ 1 & 0 \end{bmatrix}}_{P} x(k) \tag{3.9}$$

illustrates that irreducibility is not sufficient. The permutation matrix P is clearly doubly stochastic and irreducible. Meanwhile it is neither convergent or semi-convergent. The deficiency of P is related to the notion of graph periodicity. This is defined via graph cycles.

Definition 3.1.15 (Cycle in directed graph)**.** *A cycle in a directed graph $\mathcal{G} = (\mathcal{V}, \mathcal{E})$ is a path $\{v_m\}_{m=0}^{M}$, $M \geqslant 0$, such that:*

(i) $v_0 = v_M$, i.e. the initial and final node is the same.

(ii) Apart from the final node which is equal to the initial node, no node in the path appears more than once. More precisely $v_i \in \mathcal{V}$ and $v_i \neq v_j$ for all $i \neq j$ in $\{0, 1, 2, \ldots, M-1\}$ and $v_M = v_0$ when $M > 0$. If $M = 0$ then the initial and final node have the same index and are trivially equal.

By definition the cycle length is $M + 1$.

E.g. $6, 9, 8, 4, 7, 6$ is a cycle of the graph in figure 3.4a.

Definition 3.1.16 (Periodicity of directed graphs)**.** *The strongly connected directed graph $\mathcal{G}$ is periodic if there exists some $k > 1$ dividing the length of every cycle in the graph. If $\mathcal{G}$ is not periodic, it is aperiodic.*

Given some directed graph $\mathcal{G} = (\mathcal{V}, \mathcal{E})$, assume that some node $i \in \mathcal{V}$ has a self-loop. That is, $(i, i) \in \mathcal{E}$. In this case $\mathcal{G}$ has at least one length-1 cycle $\{v_i\}$. Therefore the presence of at least one self-loop in $\mathcal{G}$ is sufficient to ensure aperiodicity. See 3.6 for examples. The graph illustrated in 3.6a is periodic since both cycles $1, 2, 1$ and $2, 1, 2$ have cycle lengths divisible by 3. On the other hand, the presence of a self-loop in the graph in figure 3.6b ensures its aperiodicity.

(a) A periodic graph. (b) An aperiodic graph.

Figure 3.6: Graph periodicity examples.

The notion of periodicity allows us to provide a graph theoretic characterization of primitive matrices.

Theorem 3.3 (Graph theoretical characterization of primitive matrices, theorem 4.7 in [Bullo, 2018])**.** *Let $\mathcal{G}$ be a weighted directed graph with $|\mathcal{V}| > 1$ and an associated adjacency matrix A. The following two statements are equivalent:*

(i) $\mathcal{G}$ *is strongly connected and aperiodic.*

(ii) A *is primitive. I.e.* $\exists k \in \mathbb{N}$ *such that* $A^k > 0$.

A complete proof of this theorem is beyond the scope of the thesis, and we once again refer to Bullo [2018]. However, considering a simple case can provide a bit of intuition regarding why (i) $\implies$ (ii). Recall that $e_i^T A^k e_j > 0$ if and only if there exists at least one length k path from i to j. Since $\mathcal{G}$ is connected, A is irreducible. In turn $\exists k$ such that $e_i^T A^k e_j > 0$ for any pair of nodes (i, j). Assuming no path from i to j of length $k+1$ exists, then the corresponding entry will go from positive to zero from A^k to A^{k+1}. Now assume that all nodes have a self-loop, then $e_i^T A^k e_j > 0 \implies e_i^T A^{k+1} e_j > 0$ since any path of length k from i to j can be extended to a length $k+1$ path from i to j by following the edge (j, j). Aperiodicity ensures that eventually, for a large enough k, all elements of A^k of an irreducible matrix A remain non-zero for increasing k.

Next we turn to applications of the newly presented theory in the context of discrete time averaging systems.

3.1.3 Discrete time averaging systems

We now combine the graph theoretical concepts with stochastic matrices and present results on discrete time averaging systems. For brevity we do not pursue any proofs, but refer to Bullo [2018]. Consider the discrete time linear time-invariant system

$$x(k+1) = Ax(k) \tag{3.10}$$

where $A \in \mathbb{R}^{n \times n}$ is row-stochastic. We say that the dynamical system *achieves consensus* and that $x(k)$ *converges to consensus* provided

$$\lim_{k \to \infty} x(k) = (w^T x(0))\mathbb{1}. \tag{3.11}$$

If additionally $w^T = \frac{1}{N}\mathbb{1}$, then the dynamical system achieves *average consensus*.

The following theorem relates the primitivity of the matrix A to consensus.

Theorem 3.4 (Consensus for primitive row-stochastic matrices, corollary 2.14 in [Bullo, 2018])**.** *Let* A *be a primitive row-stochastic matrix. Then the following properties hold:*

(i) The eigenvalue 1 *is simple and has strictly larger magnitude than all other eigenvalues of* A.

(ii) $\lim_{k \to \infty} A^k = \mathbb{1}w^T$ *where* $w \geqslant \mathbb{0}$ *is the left eigenvector corresponding to the eigenvalue* 1. *I.e.* $w^T A = w^T$. *Additionally* w *satisfies* $\mathbb{1}^T w = 1$.

(iii) The limit of $x(k+1) = Ax(k)$ *satisfies*

$$\lim_{k \to \infty} x(k) = (w^T x(0))\mathbb{1}. \tag{3.12}$$

I.e. $x(k)$ *converges to consensus with consensus value* $w^T x(0)$. *Moreover, the consensus value is a convex combination of the elements in* $x(0)$.

(iv) If A is additionally doubly stochastic, then $w = \frac{1}{n}\mathbb{1}$ and therefore

$$\lim_{k\to\infty} x(k) = \frac{1}{n}\mathbb{1}^T x(0)\mathbb{1} = \text{average}(x(0))\mathbb{1}. \tag{3.13}$$

I.e. $x(k)$ converges to consensus with $\text{average}(x(0))$ as the consensus value.

In terms of achieving consensus, A being row-stochastic and primitive is sufficient but not necessary. For instance

$$x(k+1) = \begin{bmatrix} 1 & 0 \\ 1 & 0 \end{bmatrix} x(k) \tag{3.14}$$

converges to consensus despite having its dynamics governed by a reducible matrix. The following result is a generalization of theorem 3.4:

Theorem 3.5 (Consensus for row-stochastic matrices, theorem 5.1 in [Bullo, 2018])**.** *Let $A \in \mathbb{R}^{n\times n}$ be some row-stochastic matrix and let $\mathcal{G}$ be its associated directed graph. The following statements are equivalent:*

(i) The eigenvalue 1 is simple and all other eigenvalues have magnitude less than 1.

(ii) A is semi-convergent and $\lim_{k\to\infty} A^k = \mathbb{1}_n w^T$ for some $w \in \mathbb{R}^n$ satisfying $w \geqslant \mathbb{0}$ and $\mathbb{1}^T w = 1$.

(iii) $\mathcal{G}$ contains at least one globally reachable node and the subgraph of globally reachable nodes is aperiodic.

If any, and therefore all, of the previous statements are true then A is said to be indecomposable and the following properties hold:

(i) $w \geqslant \mathbb{0}$ is the left eigenvector corresponding to the eigenvalue 1 and $w_i > 0$ if and only if node i is globally reachable.

(ii) $x(k+1) = Ax(k)$ satisfies

$$\lim_{k\to\infty} x(k) = (w^T x(0))\mathbb{1}. \tag{3.15}$$

I.e. $x(k)$ converges to consensus with consensus value $w^T x(0)$. Moreover, the consensus value is a convex combination of the elements in $x(0)$.

(iii) If A is additionally doubly stochastic, then $w = \frac{1}{n}\mathbb{1}$ and therefore

$$\lim_{k\to\infty} x(k) = \frac{1}{n}\mathbb{1}^T x(0)\mathbb{1} = \text{average}(x(0))\mathbb{1}. \tag{3.16}$$

I.e. $x(k)$ converges to consensus with $\text{average}(x(0))$ as the consensus value.

The system in (3.14) is covered by this theorem. Moreover, the following theorem is a corollary:

Corollary 3.5.1 (Convergent row-substochastic matrices, corollary 4.10 in [Bullo, 2018])**.** *A row-substochastic matrix is convergent if and only if it is irreducible.*

To gain some insight into this corollary, consider the $x(k+1) = Ax(k)$ with $A \in \mathbb{R}^{n\times n}$ being row-substochastic and irreducible. Observe that the augmented system

$$\begin{bmatrix} x(k+1) \\ x_{n+1}(k+1) \end{bmatrix} = \underbrace{\begin{bmatrix} A & (I-A)\mathbb{1} \\ \mathbb{0}_n^T & 1 \end{bmatrix}}_{A_{\text{aug}}} \begin{bmatrix} x(k) \\ x_{n+1}(k) \end{bmatrix} \tag{3.17}$$

yields equivalent trajectories $x(k)$ provided $x_{n+1}(0) = 0$. Clearly A_{aug} is row-stochastic. Moreover, node $n+1$ is globally reachable since $\mathcal{G}(A)$ is strongly connected and $(I-A)\mathbb{1}$ has at least one positive entry by respectively the irreducibility and substochasticity of A. $n+1$ is the only globally reachable node since there does not exists any paths from node $n+1$ to the others. The self-loop at $n+1$ ensures aperiodicity of the subgraph of globally reachable nodes. By theorem 3.5, the left eigenvector corresponding to the eigenvalue 1 is $w^T = \begin{bmatrix} \mathbb{0}^T, & 1 \end{bmatrix}$ and

$$\lim_{k\to\infty} x_i(k) = (w^T x(0)) = x_{n+1}(0) = 0 \ \forall i \in \mathbb{N}_{N+1}. \tag{3.18}$$

This concludes the theoretical background on discrete-time averaging systems. We continue by presenting elements of real analysis.

3.1.4 Real analysis

In this final section on theoretical background, we briefly introduce a few concepts from real analysis.

We consider real sequences $\{a_k\}_{k=1}^{\infty}$ with $a_k \in \mathbb{R}$. A sequence is bounded provided it is bounded from above and below. Formally, $\{a_k\}_{k=1}^{\infty}$ is bounded if

$$\sup_k a_k = U < \infty \text{ and } \inf_k a_k = L > -\infty \tag{3.19}$$

for finite constants U and L. The sequence is convergent provided the limit

$$\lim_{k\to\infty} a_k \tag{3.20}$$

exists. Even if the sequence is not convergent, it may contain convergent *subsequences*. A subsequence is defined as follows:

Definition 3.1.17 (Subsequence)**.** *$\{b_l\}_{l=1}^{\infty}$ is a subsequence of $\{a_k\}_{k=1}^{\infty}$ if $b_l = a_{k_l}$ with $k_1 < k_2 < k_3 < \cdots$.*

If a subsequence converges, i.e. if $\lim_{l\to\infty} a_{k_l}$ exists, then the limit is called an accumulation point of the original sequence $\{a_k\}_{k=1}^{\infty}$.

Definition 3.1.18 (Accumulation point)**.** *a_0 is an accumulation point of $\{a_k\}_{k=1}^{\infty}$ if and only if there exist some subsequence $\{a_{k_l}\}_{l=1}^{\infty}$ such that $\lim_{l\to\infty} a_{k_l} = a_0$.*

Consider for instance the sequence $\{a_k\}_{k=1}^{\infty} = \{1, 0, -1, 0, 1, 0, -1, 0, \dots\}$ with

$$a_k = \cos(k\frac{\pi}{2}). \tag{3.21}$$

While this sequence does not converge, the following subsequences illustrate the existence of three accumulation points $1, 0, -1$.

$$\{\cos((0+2l)\frac{\pi}{2}\}_{l=1}^{\infty} = \{0\}_{l=1}^{\infty}, \tag{3.22}$$

$$\{\cos((1+4l)\frac{\pi}{2}\}_{l=1}^{\infty} = \{1\}_{l=1}^{\infty}, \tag{3.23}$$

$$\{\cos((2+4l)\frac{\pi}{2}\}_{l=1}^{\infty} = \{-1\}_{l=1}^{\infty}. \tag{3.24}$$

As the famous Bolzano-Weierstrass theorem shows, any bounded sequence has at least one accumulation point.

Theorem 3.6 (Bolzano-Weierstrass theorem)**.** *All bounded sequences in $\mathbb{R}^d$ have a convergent subsequence.*

We refer to the literature on real analysis for a proof. See for instance [Kolmogorov and Fomin, 1975]. By the following theorem, a bounded sequence is convergent if and only if it has a single unique accumulation point.

Lemma 3.1.2 (Unique accumulation point)**.** *A bounded sequence is convergent if and only if it has exactly one accumulation point.*

Proof. Assume that the sequence $\{a_k\}_{k=1}^{\infty}$ is convergent and converges to the limit a_0. Then for any $\epsilon > 0$ there exists $k' \in \mathbb{N}$ such that $\|a_k - a_0\| < \epsilon \ \forall k > k'$. Consider any subsequence of $\{a_{k_l}\}_{l=1}^{\infty}$ and note that for all $k_l > k'$ also $\left\|a_{k_l} - a_0\right\| < \epsilon$. Since this holds for arbitrarily small ϵ and for any subsequence, convergence of all subsequences to the accumulation point a_0 follows.

Consider now the converse direction. Assume for the sake of contradiction the existence a subsequence $\{a_{k_l}\}_{l=1}^{\infty}$ which does not converge to the unique accumulation point a_0. In this case, there exists some $\epsilon > 0$ such that $||a_{k_l^\star} - a_0|| > \epsilon$ for infinitely many indices $k_l^\star$. Pick these indices, denoted by $k_1^\star, k_2^\star, \dots$. Then $\{a_{k_l^\star}\}_{l=1}^{\infty}$ is a new sub-sequence of $\{a_k\}_{k=1}^{\infty}$. By theorem 3.6, the boundedness of this latter subsequence if sufficient to ensure the existence of an accumulation point. And by construction, the accumulation point must be different than the a_0. This contradicts the uniqueness of the accumulation point a_0. Thus all subsequences converge to a_0. Note that $\{a_k\}_{k=1}^{\infty}$ is a subsequence of itself. Thus it is convergent. □

Thus convergence of all subsequences to the same accumulation point is sufficient to show convergence of the original sequence. Finally we include the definition of a peak of a sequence.

Definition 3.1.19 (Peak of sequence)**.** *An index k is a peak of $\{a_k\}_{k=1}^{\infty}$ if $a_k > a_{k'}$ for all $k' > k$.*

E.g. the peaks $l_1, l_2, \dots$ of $\{a_k\}_{k=1}^{\infty} = \{(-1)^k \exp(-\frac{1}{25}k)\}_{k=1}^{\infty}$ are given by $l_i = 2i, i \in \mathbb{N}$. See figure 3.7 for a visual example.

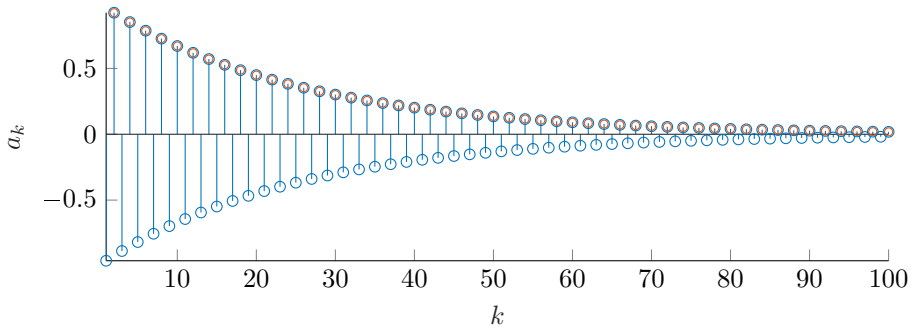

Figure 3.7: Plot of the first few elements of the sequence with $a_k = (-1)^k \exp(-\frac{1}{25}k)$. Even k are the peaks of the sequence.

This concludes the theoretical background for the convergence chapter. The remaining chapter sections are devoted to theoretical developments directly related to the MAS framework, and will be using the notions and results presented up to this point.

3.2 Preliminaries

In the following sections we will discuss convergence of the MAS with respect to the sets of configurations:

- $\mathcal{X}_{\mathrm{SC}}$, static configurations (see definition 2.6.1).
- $\mathcal{X}_{\mathrm{CC}}$, Chebyshev configurations (see definition 2.6.2).
- $\mathcal{X}^\star = \mathcal{X}_{\mathrm{CC}} \cap \mathcal{X}_{\mathrm{SC}}$, static Chebyshev configurations (see definition 2.6.3).

With regards to the deployment objective of attaining an optimal static configuration, the ultimate goal is to attain a static Chebyshev configuration. We defer the discussion of optimality of such configurations to section 3.4.3. Rather we start by highlighting relations between the sets $\mathcal{X}_{\mathrm{SC}}$ and $\mathcal{X}_{\mathrm{CC}}$. The following result is of particular importance.

Proposition 3.2.1. *The MAS subject to the agent controllers $\mathcal{K}_1, \dots, \mathcal{K}_N$ satisfying the control law requirements* (2.68)-(2.70) *is in a static configuration only if it is in a Chebyshev configuration.*

Proof. Assume that the MAS is in a static configuration which is not a Chebyshev configuration. Then $\exists i \in \mathbb{N}_N$, $\bar{r}_i(k) > r_i(k)$. By the control law requirement (2.68), $x_i(k+1) \in \mathrm{int}(\mathbb{V}_i(k) \ominus \mathbb{B}_{r_i(k)})$ for this particular agent. Meanwhile $x_i(k) \in \partial(\mathbb{V}_i(k) \ominus \mathbb{B}_{r_i(k)})$ by construction and $\mathrm{int}(\mathbb{V}_i(k) \ominus \mathbb{B}_{r_i(k)}) \cap \partial(\mathbb{V}_i(k) \ominus \mathbb{B}_{r_i(k)}) = \varnothing$. Thus $x_i(k+1) \neq x_i(k)$, which proves the claim by contradiction. □

I.e. the convergence to some $x \in \mathcal{X}_{\text{CC}}$ is necessary for convergence to some $x \in \mathcal{X}_{\text{SC}}$. That is $\mathcal{X}_{\text{SC}} \subseteq \mathcal{X}_{\text{CC}}$. From the motivating examples in section 2.7, we know that the converse is not true. In particular the simulation in figure 2.17 illustrated that non-uniqueness of the Chebyshev centers may preclude convergence to a static configuration. We consider the case where one or more Chebyshev centers are non-unique as degenerate. In the present chapter we sometimes assume non-degeneracy by invoking the following assumption:

Assumption 3.2.1. *The Chebyshev centers $\bar{x}_i(k)$ are assumed to be unique for all i for all k. I.e. while the Chebyshev centers may be time-varying, they are unique at each time step.*

Whenever assumption 3.2.1 holds, a strengthened version of proposition 3.2.1 applies.

Proposition 3.2.2. *Consider some MAS with agent controllers $\mathcal{K}_1, \ldots, \mathcal{K}_N$ satisfying the control law requirements* (2.68)-(2.70)*. Assume $x \in \mathcal{X}_{CC}$ where $\dim(\mathbb{V}_i \ominus \mathbb{B}_{\bar{r}_i}) = 0 \; \forall i \in \mathbb{N}_N$. I.e. the Chebyshev centers are unique for all agents at the particular Chebyshev configuration x. Then $x \in \mathcal{X}_{SC}$.*

Proof. By control law requirement (2.69), $\tilde{r}_i(k) = \bar{r}_i(k)$. By construction, $\tilde{r}_i(k) = \bar{r}_i(k) \iff x(k+1) \in \mathbb{V}_i(k) \ominus \mathbb{B}_{\bar{r}_i(k)}$. Since $\dim(\mathbb{V}_i(k) \ominus \mathbb{B}_{\bar{r}_i(k)}) = 0$, $\mathbb{V}_i(k) \ominus \mathbb{B}_{\bar{r}_i(k)}$ consists of a single point. Thus $x_i(k+1) = x_i(k)$ for all $i \in \mathbb{N}_N$. The result follows. □

Thus whenever assumption 3.2.1 applies, convergence to a Chebyshev configuration is equivalent to convergence to a static configuration. To some extent, this explains the steady state configurations in all but the last 2D simulations in section 2.7. The Chebyshev centers are unique in the final configuration of the respective simulations.

Remark 3.2.1. *Note that the MAS may be in a static configuration despite degeneracy. If $\bar{r}_i(k) = r_i(k)$ for all agents $i \in \mathbb{N}_N$, then $x_i(k+1) = x_i(k)$ would be a valid control action in order to satisfy the requirement $r_i(k) = r_i(k) \implies \tilde{r}_i(k) = r_i(k) = \bar{r}_i(k)$. This is true even when the Chebyshev center is non-unique for one or more agents. See figure 3.8 for an example.*

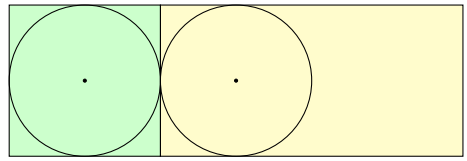

Figure 3.8: A possible static configuration with non-unique Chebyshev center for the rightmost agent. Dots represent agent positions and the circles are the respective agent Chebyshev balls. Colored regions indicate Voronoi cells.

The results in this section are valid regardless of the dimension of the target environment. We now turn to more specialized results for deployment to 1D in section 3.3 before returning to arbitrarily-dimensional environments in section 3.4.

3.3 Convergence in one-dimensional environments

First we consider deployment to the one-dimensional environment $\mathcal{W} \subset \mathbb{R}$. This has several advantages:

- It is possible to derive simple explicit expressions for $\mathbb{V}_i(k)$, $\bar{x}_i(k)$ and $\bar{r}_i(k)$.
- We can derive linear affine time-invariant equations for the closed loop dynamics of $x_i(k)$ and $\bar{r}_i(k)$.
- Standard results from linear systems theory and algebraic graph theory may be used to rigorously characterize MAS convergence.

As such, considering the one-dimensional case is an accessible manner of gaining insight and intuition about the inner workings of the framework. Furthermore, the additional mathematical structure available when deploying to $\mathbb{R}$ allows us to prove stronger results than in the multi-dimensional case.

Let $\mathcal{W} = [x_l, x_u] \subset \mathbb{R}$ with $x_l < x_u$. We disregard the trivial case of $N = 1$, and consider a MAS with $N > 1$ agents whose distinct initial positions are $x_1(0), \dots, x_N(0) \in \mathcal{W}$. Assume, without loss of generality, the ordering $x_1(0) < x_2(0) < \cdots < x_N(0)$. To focus the presentation on effects stemming from the particular framework rather than variations in agent dynamics, we pick single integrator dynamics

$$x_i(k+1) = x_i(k) + u_i(k) \in \mathbb{R} \tag{3.25}$$

for all agents $i \in \mathbb{N}_N$. Further to the same goal, we pick linear agent controllers

$$u_i(k) = \mathcal{K}(x_i(k), \mathbb{V}_i(k)) = \alpha(\bar{x}_i(k) - x_i(k)), \alpha \in [0, 1) \tag{3.26}$$

for all $i \in \mathbb{N}_N$.

3.3.1 Agent neighborhoods

In $\mathbb{R}$, each Voronoi cell $\mathbb{V}_i$ is simply a sub-interval of $\mathcal{W}$. First consider agents $i \in \{2, \dots, N-1\}$. From the definition of $\mathbb{V}_i$ in (2.54) it is apparent that

$$\mathbb{V}_i = [\frac{x_i + x_{i-1}}{2}, \frac{x_i + x_{i+1}}{2}]. \tag{3.27}$$

By the same equation, the Voronoi cells of the first and last agents are

$$\mathbb{V}_1 = [x_l, \frac{x_1 + x_2}{2}], \tag{3.28}$$

$$\mathbb{V}_N = [\frac{x_{N-1} + x_N}{2}, x_u]. \tag{3.29}$$

See figure 3.9 for a minimal example where all three cases are illustrated.

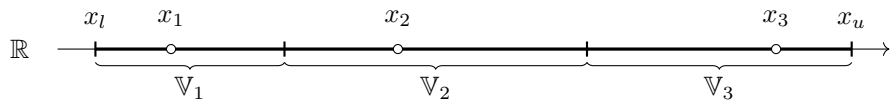

Figure 3.9: $N = 3$ agents deployed to a subset $\mathcal{W}$ of $\mathbb{R}$ and their respective Voronoi cells.

3.3.2 Agent depth, Chebyshev center and Chebyshev radius

The Chebyshev center of a line segment $[a, b]$, $a < b$, is particularly easy to compute. We start by finding its Chebyshev radius. First compute

$$[a, b] \ominus \mathbb{B}_r = [a + r, b - r]. \tag{3.30}$$

I.e. $x \in [a, b] \ominus \mathbb{B}_r$ if and only if

$$a + r \leqslant x \leqslant b - r, \tag{3.31}$$

implying

$$r \leqslant \frac{b - a}{2}. \tag{3.32}$$

This yields a maximal depth of

$$r_c([a, b]) = \frac{b - a}{2}. \tag{3.33}$$

Since $\dim([a, b]) = 1$, we know from proposition 2.1.4 that $\dim([a, b] \ominus \mathbb{B}_{r_c(P)}) = 0$. I.e. the Chebyshev center $x_c([a, b])$ must be unique. This is also obvious when inserting $r = r_c([a, b])$ in (3.31), then $(a + b)/2 \leqslant x_c([a, b]) \leqslant (a + b)/2$ and

$$x_c([a, b]) = \frac{a + b}{2}. \tag{3.34}$$

The depth of a point q in $[a, b]$, denoted $\text{depth}(q, [a, b])$, is also easy to define but somewhat more complicated to compute. It is not linear in a and b. Applying the definition and exploiting that $q \geqslant a$ and $b \geqslant q$ yields

$$\text{depth}(q, [a, b]) = \min\{\|q - q_{\partial P}\| \mid q_{\partial P} \in \partial[a, b] = \{a, b\}\}, \tag{3.35}$$

$$= \min\{|a - q|, |b - q|\} = \min\{q - a, b - q\}. \tag{3.36}$$

Figure 3.10 illustrates the various notions. With this figure in mind, it is easy to follow the preceding results graphically.

Applying (3.33) to the expressions for $\mathbb{V}_i$ yields the following linear equations for the Chebyshev centers.

$$\bar{x}_1 = \frac{1}{2}x_l \quad + \frac{1}{4}x_1 + \frac{1}{4}x_2, \tag{3.37}$$

$$\bar{x}_i = \frac{1}{4}x_{i-1} + \frac{1}{2}x_i + \frac{1}{4}x_{i+1} \text{ when } i \in \mathbb{N}_N \backslash \{1, N\}, \tag{3.38}$$

$$\bar{x}_N = \frac{1}{4}x_{N-1} + \frac{1}{4}x_N + \frac{1}{2}x_u. \tag{3.39}$$

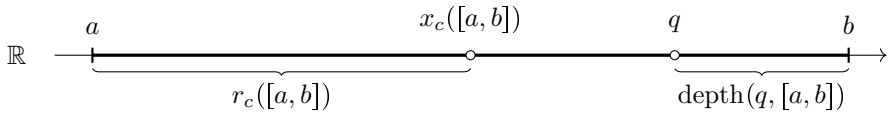

Figure 3.10: A line segment $[a,b] \subset \mathbb{R}$ and its associated Chebyshev center x_c and Chebyshev radius r_c. Additionally, the depth of an arbitrary point $q \in [a,b]$ is illustrated.

Moreover, the uniqueness of the Chebyshev centers affords us the following result.

Proposition 3.3.1. *The configuration $x \in \mathbb{R}^N$ of N agents in $\mathbb{R}$ with positions $x_1, \ldots, x_N \in \mathbb{R}$ is a Chebyshev configuration if and only if it is a static configuration. I.e. $x \in \mathcal{X}_{SC} \iff x \in \mathcal{X}_{CC}$.*

Proof. $x \in \mathcal{X}_{\text{SC}} \implies \mathcal{X}_{\text{CC}}$ follows from proposition 3.2.1. The converse direction follows from proposition 3.2.2 since the assumption of unique Chebyshev centers always holds in $\mathbb{R}$. □

Moving on to the Chebyshev radii, applying (3.34) to $\mathbb{V}_1, \ldots, \mathbb{V}_N$ yields the following linear equations

$$\bar{r}_1 = \frac{x_1 + x_2}{4} - \frac{x_l}{2}, \tag{3.40}$$

$$\bar{r}_i = \frac{x_{i+1} - x_{i-1}}{4} \text{ when } i \in \mathbb{N}_N \backslash \{1, N\}, \tag{3.41}$$

$$\bar{r}_N = \frac{x_u}{2} - \frac{x_{N-1} + x_N}{4}. \tag{3.42}$$

While the equations for $\bar{x}_i$ and $\bar{r}_i$ are linear, equations for r_i's are more involved. Applying (3.36) with $q = x_i$ and $[a,b] = \mathbb{V}_i$ yields

$$r_1 = \frac{1}{2}\min\{x_2 - x_1, 2(x_1 - x_l)\}, \tag{3.43}$$

$$r_i = \frac{1}{2}\min\{x_{i+1} - x_i, x_i - x_{i-1}\} \text{ when } i \in \mathbb{N}_N \backslash \{1, N\}, \tag{3.44}$$

$$r_N = \frac{1}{2}\min\{2(x_u - x_N), x_N - x_{N-1}\}. \tag{3.45}$$

3.3.3 Closed loop position dynamics

By (3.37)-(3.39), it is possible to express $\bar{x}^T(k) = [\bar{x}_1(k) \ldots \bar{x}_N(k)]^T$ with the following affine equation

$$\bar{x}(k) = Ax(k) + b, \tag{3.46}$$

where

$$A = \begin{bmatrix} 0.25 & 0.25 & & & & \\ 0.25 & 0.50 & 0.25 & & & \\ & 0.25 & 0.50 & 0.25 & & \\ & & \ddots & \ddots & \ddots & \\ & & 0.25 & 0.50 & 0.25 & \\ & & & 0.25 & 0.25 & \end{bmatrix} \in \mathbb{R}^{N\times N}, \qquad b = \begin{bmatrix} 0.5x_l \\ \mathbb{0}_{N-2} \\ 0.5x_u \end{bmatrix} \in \mathbb{R}^N. \tag{3.47}$$

Exploiting (3.46) yields the following closed loop MAS dynamics.

$$\begin{aligned} x(k+1) &= x(k) + \alpha(\bar{x}(k) - x(k)) = && (3.48)\\ &= (1-\alpha)x(k) + \alpha(Ax(k) + b) && (3.49)\\ &= \underbrace{(\alpha A + (1-\alpha)I)}_{A(\alpha)} x(k) + \alpha b = A(\alpha)x(k) + \alpha b && (3.50) \end{aligned}$$

Remark 3.3.1. *Beware that* (3.50) *might give the misleading impression that its steady state solution (assuming it exists) depends on α due to the excitation αb. As we will see later on, the α cancels out when computing the steady state value.*

From the motivating examples in section 2.7, we expect (3.48) to have an unique steady state value x^{ss} for any choice of $\alpha \in (0, 1]$. For this to hold, $A(\alpha)$ must be convergent. Considering $\alpha = 1$ in particular, the following result is therefore expected.

Lemma 3.3.1. *The matrix A as given by* (3.47) *is convergent.*

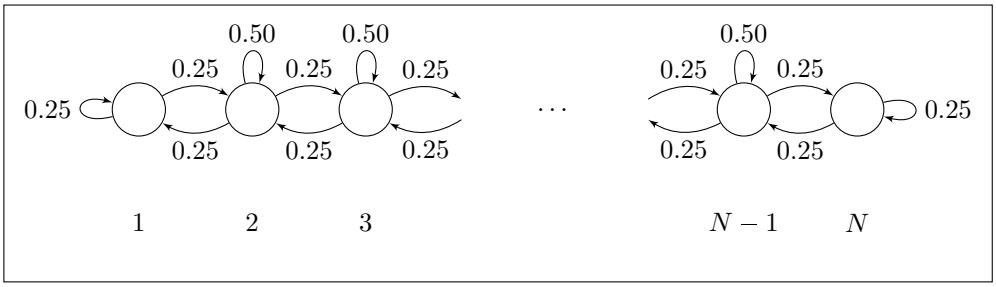

Figure 3.11: The graph associated with the matrix A.

Proof. Inspecting the structural properties of A reveals:

(i) A is row-substochastic,

$$A\mathbb{1}_N = \begin{bmatrix} 1/4 \\ \mathbb{1}_{N-2} \\ 1/4 \end{bmatrix}. \tag{3.51}$$

(ii) A is irreducible. To see this, consider the graph $\mathcal{G}(A)$ associated with the positive matrix A. This is illustrated in figure 3.11. For all pairs of vertices (i, j) with $i \neq j$ there exists a path from vertex i to vertex j. I.e. $\mathcal{G}(A)$ is strongly connected and therefore A is irreducible by theorem 3.2.

By these properties, A satisfies the assumptions of corollary 3.5.1 and is therefore convergent. □

Tuning α between $(0, 1]$ simply interpolates between the identity matrix and A. It is easy to verify that row-substochasticity is maintained for $A(\alpha)$. In turn, $A(\alpha)$ is also convergent. We prove this, as well as some other interesting properties of $A(\alpha)$, in the following lemma.

Lemma 3.3.2. *The matrix $A(\alpha) = \alpha A + (1-\alpha)I$, $\alpha \in (0, 1]$, with A given by (3.47) and eigenvalues $\lambda_1^\alpha, \ldots, \lambda_N^\alpha$ satisfies the following properties:*

(i) $\lambda_1^\alpha, \ldots, \lambda_N^\alpha \in \mathbb{R}$.

(ii) $\lambda_i^\alpha = \alpha\lambda_i + (1-\alpha)$ $\forall i \in \mathbb{N}_N$, *where λ_i are the eigenvalues of A.*

(iii) $\lambda_i^\alpha \in [(1-\alpha), 1)$ $\forall i \in \mathbb{N}_N$.

(iv) $A(\alpha)$ is convergent.

Proof. The first property follows from the fact that A and I and therefore also their convex combination $A(\alpha)$ is symmetric real. Since A is symmetric real, it admits the modal decomposition $A = VDV^T$ where $D = \operatorname{diag}(\lambda_1, \ldots, \lambda_N)$ and $VV^T = V^TV = I$. Therefore

$$A(\alpha) = \alpha VDV^T + (1-\alpha)VV^T \tag{3.52}$$

$$= V(\alpha D + (1-\alpha)I)V^T. \tag{3.53}$$

Let

$$D(\alpha) = V^T A(\alpha) V = \alpha D + (1-\alpha)I. \tag{3.54}$$

Since eigenvalues are invariant to similarity transformations, it is clear that the eigenvalues of $A(\alpha)$ are given by

$$\lambda_i^\alpha = e_i^T D(\alpha) e_i = \alpha\lambda_i + (1-\alpha). \tag{3.55}$$

This proves the second property. To show the third property, we first consider the matrix A in light of theorem 3.1.

$$\operatorname{spec}(A) \subset \cup_{i\in\mathbb{N}_N}\{z \in \mathbb{C} \mid |z - a_{ii}| \leqslant \sum_{j\in\mathbb{N}_N\setminus\{i\}} |a_{ij}|\} \tag{3.56}$$

$$\subset (\cup_{i=1}^2 \{z \in \mathbb{C} \mid |z - \frac{1}{4}| \leqslant \frac{1}{4}\}) \cup (\cup_{i\in\mathbb{N}_N\setminus\{1,2\}}\{z \in \mathbb{C} \mid |z - \frac{1}{2}| \leqslant \frac{1}{2}\}). \tag{3.57}$$

Since additionally the λ_i's are real and A is convergent, $\lambda_i \in [0, 1)$. Consequently

$$\min_i \lambda_i^\alpha \geqslant \alpha \cdot 0 + (1 - \alpha) = (1 - \alpha), \tag{3.58}$$

$$\max_i \lambda_i^\alpha < \alpha \cdot 1 + (1 - \alpha) = 1, \tag{3.59}$$

proving the third property. The fourth property follows from $\rho(A(\alpha)) = \max_i \lambda_i^\alpha < 1$. □

In turn, $A(\alpha)$ being convergent is sufficient to ensure the existence of a steady state value x^{ss} of the closed loop MAS dynamics,

$$x^{ss} = (\alpha A + (1 - \alpha)I)x^{ss} + \alpha b, \tag{3.60}$$

$$\alpha(I - A)x^{ss} = \alpha b, \tag{3.61}$$

$$x^{ss} = (I - A)^{-1} b. \tag{3.62}$$

Note that the inverse is well defined as $(I - A)$ is non-singular by $\rho(A) < 1$. Consider the error coordinates $e(k) = x(k) - x^{ss}$. The error dynamics are

$$e(k + 1) = x(k + 1) - x^{ss} \tag{3.63}$$

$$= (\alpha A + (1 - \alpha)I)x(k) + \alpha b - \big[(\alpha A + (1 - \alpha)I)x^{ss} + \alpha b\big] \tag{3.64}$$

$$= (\alpha A + (1 - \alpha)I) = A(\alpha)e(k) \tag{3.65}$$

Lemma 3.3.2 and the error dynamics (3.65) form the basis for the main result of this section.

Theorem 3.7 (MAS convergence in 1D)**.** *The MAS with agent dynamics $x_i(k + 1) = x_i(k) + u_i(k)$ and agent controllers $u_i(k) = \mathcal{K}_i(x_i(k), \mathbb{V}_i(k)) = \alpha(\bar{x}_i(k) - x_i(k))$, $\alpha \in (0, 1]$, converges to the steady state value x^{ss} where $x_i^{ss} = (2i - 1)\frac{x_u - x_l}{2N} + x_l$.*

Proof. Since $A(\alpha)$ is convergent for any $\alpha \in (0, 1]$,

$$\lim_{k \to \infty} e(k) = \mathbb{0}. \tag{3.66}$$

Furthermore, $e(k) = \mathbb{0} \iff x(k) = x^{ss}$. I.e. the convergence of $e(k)$ to zero ensures the convergence of $x(k)$ to x^{ss}. Note that x^{ss} is unique, e.g. by checking that $(I - A)$ is invertible. Thus if we find any configuration x such that $x = A(\alpha)x + \alpha b$ then $x = x^{ss}$. As a qualified guess, let $x_i = e_i^T x = (2i - 1)\frac{x_u - x_l}{2N} + x_l$. Inserting this expression into (3.37)-(3.39) yields $x = A(\alpha)x + \alpha b$. I.e. $x = x^{ss}$. The result follows. □

The steady state configuration x^{ss} is illustrated in figure 3.12.

This result coincides with our expectations from the first two 1D simulations in section 2.7. Invariant to the initial configuration, $x(k) \to x^{ss}$. We still need to analyze the effect of changing α. To this end, consider convergence factor of $e(k)$.

Theorem 3.8 (Asymptotic MAS convergence in 1D)**.** *Let λ_M be the maximal eigenvalue of A. The MAS converges asymptotically to the steady state value x^{ss} with a convergence factor of $\rho(A(\alpha)) = \alpha\lambda_M + (1 - \alpha)$.*

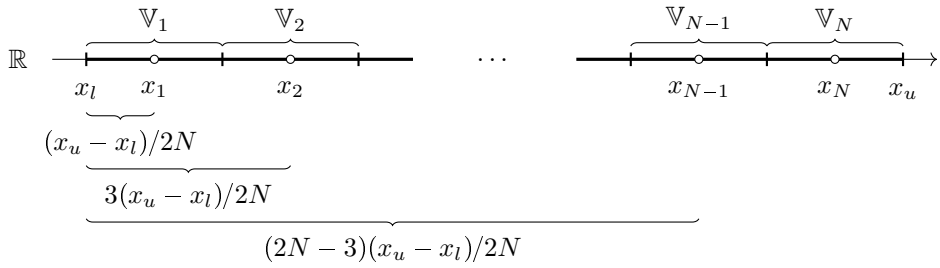

Figure 3.12: The steady state configuration x^{ss} for N agents in $\mathbb{R}$.

Proof. Recall that $A(\alpha)$ being symmetric real ensures the existence of a modal decomposition $A(\alpha) = VD(\alpha)V^T$ where $D(\alpha) = \text{diag}(\lambda_1^\alpha, \dots, \lambda_N^\alpha)$ and $VV^T = V^TV = I$. Considering the norm of $e(k)$ yields

$$\|e(k)\| = \left\|A^k(\alpha)e(0)\right\| = \left\|VD^k(\alpha)V^Te(0)\right\| \tag{3.67}$$

$$= \sqrt{e^T(0)VD^k(\alpha)V^TVD^k(\alpha)V^Te(0)} = \sqrt{e^T(0)VD^{2k}(\alpha)V^Te(0)} \tag{3.68}$$

$$\leqslant \rho^k(A(\alpha))\sqrt{e^T(0)VV^Te(0)} = \rho^k(A(\alpha))\sqrt{e^T(0)e(0)} = \rho^k(A(\alpha))\|e(0)\|\,. \tag{3.69}$$

From lemma 3.3.2 we know that $\rho(A(\alpha)) = \max_i[\alpha\lambda_i + (1-\alpha)] = \alpha\lambda_M + (1-\alpha)$. Note that we do not need to take the modulus of the eigenvalues of $A(\alpha)$ in this maximization since they are real and non-negative. Thus

$$\frac{\|e(k)\|}{\|e(0)\|} \leqslant (\alpha\lambda_M + (1-\alpha))^k. \tag{3.70}$$

□

Theorem 3.8 is consistent with expectations from the 1D simulations in section 2.7, and verifies the correctness of our presumptions regarding the role of α.

Further to the investigations of the nature of convergence, we provide an example showing that one cannot expect finite time convergence even when $\alpha = 1$. Consider a MAS with $N = 2$ agents deployed to $\mathcal{W} = [0, 1]$. Then

$$x_1(k+1) = \frac{1}{4}x_1(k) + \frac{1}{4}x_2(k) \tag{3.71}$$

$$x_2(k+1) = \frac{1}{4}x_1(k) + \frac{1}{4}x_2(k) + \frac{1}{2}. \tag{3.72}$$

By theorem 3.7, the steady state value is simply $x^{ss} = \left[1/4, 3/4\right]^T$. Let $h = \frac{1}{2}(x_1 + x_2)$. This is the position of the border between the two agents. In the steady state configuration, h is 1/2. Consider the trajectories of h,

$$h(k+1) = \frac{1}{2}(x_1(k+1) + x_2(k+1)) = \frac{1}{4}(x_1(k) + x_2(k)) + \frac{1}{4} = \frac{1}{2}h(k) + \frac{1}{4}. \tag{3.73}$$

In error coordinates $e_h = h - 1/2$,

$$e_h(k+1) = \frac{1}{2}h(k) - \frac{1}{4} = \frac{1}{2}e_h(k). \tag{3.74}$$

Thus for any initial value but $e_h(0) = 0$, $h(k)$ will not converge in finite time. Rewriting the dynamics of x_1,x_2 in terms of $h(k)$ yields

$$x_1(k+1) = \frac{1}{2}h(k), \tag{3.75}$$

$$x_2(k+1) = \frac{1}{2}h(k) + \frac{1}{2}. \tag{3.76}$$

Thus finite time convergence cannot hold for $x_1(k), x_2(k)$ either whenever $h(0) \neq 1/2$. However, the same example illustrates finite time convergence in certain symmetric cases. If the agent positions are symmetric about 1/2, e.g. $x(0) = \begin{bmatrix}0, 1\end{bmatrix}^T$, then $h(0) = 1/2$. In turn $x(1) = x^{ss}$ for this two-agent system.

Note that this example is consistent with 1D simulation 2 in 2.7. Recall the results from figure 2.9b. The simulation exhibits asymptotic convergence despite unitary gains α_i. The example sheds some light on why this is the case. Finite time convergence is precluded by the fact that the Voronoi cells converge asymptotically rather than in finite time.

The third 1D-simulation from section 2.7, with time-varying agent gains $\alpha_i(k)$, is not covered by the results in the present section. Rather we will apply the forthcoming results on $\mathbb{R}^d$-convergence to explain the behavior. For now we continue by pursuing results on convergence of $\bar{r}_i$ and r_i in 1D.

3.3.4 Closed loop Chebyshev radii dynamics

From the convergence $x(k) \to x^{ss}$ we expect similar convergence results for the Chebyshev radii $\bar{r}^T(k) = [\bar{r}_1(k), \ldots, \bar{r}_N(k)]^T$. As we will see, we can derive linear time-invariant dynamics $\bar{r}(k+1) = A_{\bar{r}}(\alpha)\bar{r}(k)$ which provably converges to consensus. First we consider convergence of Chebyshev radii and agent depth in light of the preceding results on closed loop position dynamics.

The convergence of the agent positions $x_1, \ldots, x_N$ provides plenty of information regarding the convergence of $\bar{r}_1, \ldots, \bar{r}_N$. By proposition 3.3.1,

$$\lim_{k\to\infty} x(k) = x^{ss} \implies \lim_{k\to\infty} \bar{r}_i(k) = \lim_{k\to\infty} r_i(k) = \bar{r}_i^{\infty} \ \forall i \in \mathbb{N}_N. \tag{3.77}$$

We can obtain stronger results by exploiting other relations between $x(k)$ and $\bar{r}(k)$. Observe that translating (3.40)-(3.42) to matrix form yields

$$\bar{r}(k) = Cx(k) + d \in \mathbb{R}^N, \tag{3.78}$$

where

$$C = \begin{bmatrix} 0.25 & 0.25 & & & \\ -0.25 & 0 & 0.25 & & \\ & -0.25 & 0 & 0.25 & \\ & & \ddots & \ddots & \ddots \\ & & -0.25 & 0 & 0.25 \\ & & & -0.25 & -0.25 \end{bmatrix} \in \mathbb{R}^{N\times N}, \quad d = \begin{bmatrix} -0.5x_l \\ \mathbb{0}_{N-2} \\ 0.5x_u \end{bmatrix} \in \mathbb{R}^N. \tag{3.79}$$

That is, $\bar{r}$ can be interpreted as a particular measurement of the MAS positions with measurement matrix C and bias d. In turn, the convergence $x \to x^{ss}$ ensures the convergence $\bar{r} \to \bar{r}^{ss}$. By (3.78),

$$\bar{r}^{ss} = Cx^{ss} + d. \tag{3.80}$$

Computing $e_1^T\bar{r}^{ss}$, $e_N^T\bar{r}^{ss}$ and $e_i^T\bar{r}^{ss}$ (assuming $i \in \mathbb{N}_N\backslash\{1, N\}$) yields

$$\bar{r}^{ss} = Cx^{ss} + d = \frac{1}{2}\frac{x_u - x_l}{N}\mathbb{1}. \tag{3.81}$$

Inserting for x^{ss} in the agent depth expressions (3.43)-(3.45) yields

$$r_i^{ss} = \frac{1}{2}\frac{x_u - x_l}{N}, \ \forall i \in \mathbb{N}_N. \tag{3.82}$$

I.e. $\bar{r}_i^{ss} = r_i^{ss}$ for all $i \in \mathbb{N}_N$. (3.81) and (3.82) verif (3.77) and imply the stronger result

$$\lim_{k\to\infty} \bar{r}_i(k) = \lim_{k\to\infty} r_i(k) = \frac{1}{N}\frac{x_u - x_l}{2}. \tag{3.83}$$

Consistent with the simulations in section 2.7, the MAS converges to consensus on $\bar{r}_i$ and r_i. Our conjecture of consensus value $\frac{1}{2N}$ provided $\mathcal{W} = [x_l, x_u] = [0, 1]$ was correct. The result is also unsurprising when revisiting figure 3.12. The following relation is somewhat less apparent.

$$\text{average}(\bar{r}(k)) = \frac{1}{N}\mathbb{1}^T\bar{r}(k) = \frac{1}{N}[\underbrace{\mathbb{1}^TC}_{=0}x(k) + \underbrace{\mathbb{1}^Td}_{=\frac{x_u-x_l}{2}}] = \frac{1}{N}\frac{x_u - x_l}{2}. \tag{3.84}$$

That is, the limit value $\bar{r}^{ss} = r^{ss}$ equals average$(\bar{r})$. Also, average$(\bar{r})$ is time-invariant and independent of initial positions $x(0)$. In fact the limit value only depends on the boundaries x_l, x_u of $\mathcal{W}$ and the number of agents N.

Remark 3.3.2. *It is interesting to note that $\bar{r}(k)$ is translationally invariant with respect to x in the sense that*

$$\begin{bmatrix} \hat{x} \\ \hat{x}_u \\ \hat{x}_l \end{bmatrix} = \begin{bmatrix} x \\ x_u \\ x_l \end{bmatrix} + t\begin{bmatrix} \mathbb{1}_N \\ 1 \\ 1 \end{bmatrix}, t \in \mathbb{R}, \tag{3.85}$$

implies

$$\bar{r}(k) = Cx + \begin{bmatrix} -0.5x_l \\ \mathbb{0}_{N-2} \\ 0.5x_u \end{bmatrix} = C\hat{x} + \begin{bmatrix} -0.5\hat{x}_l \\ \mathbb{0}_{N-2} \\ 0.5\hat{x}_u \end{bmatrix}. \tag{3.86}$$

If $\bar{r}(k)$ was the only measurement we had of MAS state, absolute positions $x(k)$ would therefore not be observable.

While the above results are sufficient to prove convergence of $\bar{r}(k)$ to consensus, we still pursue an approach of uncovering the dynamics of $\bar{r}(k+1) = A_{\bar{r}}(\alpha)\bar{r}(k)$ to highlight interesting connections to discrete time averaging systems.

First, assume the existence of some matrix $A_{\bar{r}}(\alpha)$ such that $\bar{r}(k+1) = A_{\bar{r}}(\alpha)\bar{r}(k)$. By now we expect the following properties:

(i) $(1, \mathbb{1})$ is a right eigenpair, i.e. $A_{\bar{r}}(\alpha)\mathbb{1} = \mathbb{1}$, in order to satisfy $\bar{r}^{ss} = A_{\bar{r}}(\alpha)\bar{r}^{ss} = A_{\bar{r}}\,\text{average}(\bar{r})\mathbb{1} = \text{average}(\bar{r})\mathbb{1}$

(ii) $(1, \mathbb{1}^T)$ is a left eigenpair, i.e. $\mathbb{1}^T A_{\bar{r}}(\alpha) = \mathbb{1}^T$, in order to satisfy

$$0 = \text{average}(\bar{r}(k+1)) - \text{average}(\bar{r}(k)) \tag{3.87}$$

$$= \frac{1}{N}\mathbb{1}^T[A_{\bar{r}} - I]\bar{r}(k) = \frac{1}{N}[\mathbb{1}^T A_{\bar{r}} - \mathbb{1}^T]r(k). \tag{3.88}$$

(iii) From the two former properties, $A_{\bar{r}}(\alpha)$ must be doubly stochastic.

(iv) Since $\bar{r}(k)$ converges to consensus, $A_{\bar{r}}(\alpha)$ must be semi-convergent.

To find the matrix $A_{\bar{r}}$, let the $\bar{r}_i(k+1)$'s be given by the Chebyshev radii expressions (3.40)-(3.42) and replace all instances of $x_i(k+1)$'s with the closed loop agent position dynamics (3.48). We omit the derivations as these are easy albeit somewhat tedious. By following the outline procedure, we arrive at

$$\bar{r}(k+1) = A_{\bar{r}}(\alpha)\bar{r}(k) = (\alpha A_{\bar{r}} + (1-\alpha)I)\bar{r}(k) \tag{3.89}$$

with

$$A_{\bar{r}} = \begin{bmatrix} 0.75 & 0.25 & & & \\ 0.25 & 0.50 & 0.25 & & \\ & 0.25 & 0.50 & 0.25 & \\ & & \ddots & \ddots & \ddots \\ & & 0.25 & 0.50 & 0.25 \\ & & & 0.25 & 0.75 \end{bmatrix}. \tag{3.90}$$

Inspecting the matrix $A(\alpha) = (\alpha A_{\bar{r}} + (1-\alpha)I)$, it is apparent that the first three conjectured properties are indeed true. We also make the following observations:

(i) $A(\alpha)$ is symmetric real implying that all its eigenvalues are real.

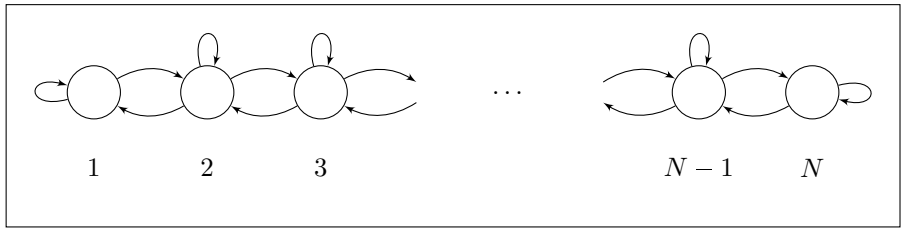

Figure 3.13: The graph associated with the matrix $A_{\bar{r}}(\alpha)$.

(ii) Additionally, by theorem 3.1 all eigenvalues of $A_{\bar{r}}$ must be in the interval $[0.25, 1]$. Since all eigenvalues of $A_{\bar{r}}$ are real, positive and less or equal to 1 all eigenvalues of $A_{\bar{r}}(\alpha)$ will also be.

(iii) The directed graph $\mathcal{G}(A_{\bar{r}}(\alpha))$ associated with $A_{\bar{r}}(\alpha)$ is illustrated in figure 3.13. Observe that $\mathcal{G}(A_{\bar{r}}(\alpha))$ is strongly connected. The presence of self-loops ensures aperiodicity. By theorem 3.3, $A_{\bar{r}}(\alpha)$ is therefore primitive.

The third observation is important for the following result, verifying the fourth conjectured property.

Theorem 3.9 (Convergence to consensus on $\bar{r}$ in 1D)**.** *The MAS converges to consensus on $\bar{r}$ with consensus value*

$$\lim_{k\to\infty} \bar{r}(k) = \frac{1}{N}\mathbb{1}^T\bar{r}(0)\mathbb{1} = \text{average}(\bar{r}(0))\mathbb{1} = \frac{1}{N}\frac{x_u - x_l}{2}\mathbb{1} \tag{3.91}$$

Proof. The graph $\mathcal{G}(A_{\bar{r}}(\alpha))$ associated with $A_{\bar{r}}(\alpha)$, illustrated in figure 3.13, is strongly connected and aperiodic. Therefore $A_{\bar{r}}(\alpha)$ is primitive by theorem 3.3. Since $A_{\bar{r}}(\alpha)$ is primitive, the statement follows from theorem 3.4. □

Having found $A_{\bar{r}}$, we can compute the convergence factor associated with $\bar{r}(k)$. Let the essential radius of $A_{\bar{r}}(\alpha))$, $\rho_{ess}(A_{\bar{r}}(\alpha))$, be the magnitude of the second largest eigenvalue of $A(\alpha)$. By theorem 3.4, $\rho_{ess}(A(\alpha)) < 1$. $\rho_{ess}(\cdot)$ has the same role in determining the convergence factor of $\bar{r}(k)$ as $\rho(\cdot)$ had in determining the convergence factor of $x(k)$. To see this, consider the norm of the error dynamics $\|\bar{r}(k) - \text{average}(\bar{r}(0))\mathbb{1}\|$. Since $A_{\bar{r}}(\alpha)$ is symmetric real, it admits a modal decomposition $A_{\bar{r}}(\alpha) = VD(\alpha)V^T$ where $V = [\frac{1}{\sqrt{N}}\mathbb{1}, v_2, \cdots, v_N]$, $VV^T = V^TV = I$ and $D(\alpha)$ is a diagonal matrix of eigenvalues μ_i^α.

Therefore

$$\|\bar{r}(k) - \text{average}(\bar{r}(0))\mathbb{1}\| = \|A_{\bar{r}}(\alpha)\bar{r}(k-1) - \text{average}(\bar{r}(0))\mathbb{1}\| \tag{3.92}$$

$$= \left\| \sum_{i\in\mathbb{N}_N} (\mu_i^\alpha)^k (v_i^T \bar{r}(0)) v_i - \text{average}(\bar{r}(0))\mathbb{1} \right\| \tag{3.93}$$

$$= \left\| \left[\frac{1}{N} \mathbb{1}^T \bar{r}(0)\mathbb{1} - \text{average}(\bar{r}(0))\mathbb{1} \right] + \sum_{i\in\mathbb{N}_N\setminus\{1\}} (\mu_i^\alpha)^k (v_i^T \bar{r}(0)) v_i \right\| \tag{3.94}$$

$$= \left\| \sum_{i\in\mathbb{N}_N\setminus\{1\}} (\mu_i^\alpha)^k (v_i^T \bar{r}(0)) v_i \right\| \tag{3.95}$$

$$\leqslant \rho_{ess}^k(A_{\bar{r}}(\alpha))\|\bar{r}(0)\| \,. \tag{3.96}$$

This result is analogous to theorem 3.8.

3.3.5 Concluding remarks on 1D convergence

The specialized 1D theoretical results comply with the behavior exhibited in the 1D motivating examples of section 2.7, and provide the mathematical background to understand the structural properties. In particular we have shown asymptotic convergence to an unique static Chebyshev configuration where all agents are in consensus on their Chebyshev radii and agent depths. The asymptotic configuration is invariant to initial conditions, and only depend on the boundaries of the interval $\mathcal{W}$ and the number of agents N. The results highlight the frameworks' connection to discrete time averaging systems. In particular we show how the 1D MAS dynamics can be translated to a form amenable to analysis by standard tools from this field. In fact, the closed loop MAS position dynamics and Chebyshev radii dynamics are equivalent particular discrete time averaging system.

While we cannot expect all properties to carry over, a natural question is whether similar properties hold in the multi-dimensional case. From the motivating examples of section 2.7 we know, for instance, that asymptotic configurations are not invariant to initial conditions and choice of controller gains α_i. Meanwhile, consensus-like behavior on Chebyshev radii and agent depth can be observed in the 2D numerical examples. Thus it is not unreasonable to expect that some generalization of the consensus-property holds in the non-linear multi-dimensional case.

Recall that several of the results in section 3.3 rely on the assumption of single integrator agent dynamics and linear control laws. As we will see in 3.4, this assumption can be relaxed. We now turn to convergence results for deployment to multi-dimensional environments.

3.4 Convergence in multi-dimensional environments

Whereas convergence is relatively easy to grasp in $\mathbb{R}$, the situation is considerably more complicated in two or more dimensions. Analytic closed loop dynamic equations are no longer available, and we have to resort to different tools.

We consider an N-agent MAS where each agent has dynamics (2.47) satisfying the regularity conditions in assumption 2.2.1. The agents utilize decentralized controllers $\mathcal{K}_1, \dots, \mathcal{K}_N$ satisfying the control law requirements (2.68)-(2.70). $\mathcal{W}$ is convex, polytopic and full-dimensional. The initial agent states are distinct elements of $\mathcal{W}$, i.e.

$$x(0) \in \mathcal{X}_{\mathrm{D}} = \{x^T = [x_1^T \cdots x_N^T] \mid x_i \in \mathcal{W} \ \forall i \in \mathbb{N}_N, x_i \neq x_j \ \forall j \neq i \in \mathbb{N}_N\}. \tag{3.97}$$

Judging from the 2D motivating examples in section 2.7, the MAS does not converge to a particular pre-defined final state. Rather we expect convergence towards the set of Chebyshev Configurations, $\mathcal{X}_{\mathrm{CC}}$. To this end, proving non-increase and convergence to zero of the energy-like function

$$V(x(k), \mathcal{W}) = \sum_{i \in \mathbb{N}_N} \bar{r}_i(k) - r_i(k), \tag{3.98}$$

would be sufficient. However, most quantities within the present framework do not exhibit the necessary monotonicity. E.g. both $\bar{r}_i(k)$ and $r_i(k)$ may increase and decrease with time. The same holds for the time-varying upper bound $\bar{r}_M(k)$. See figures 2.15 and 2.16 for illustrative examples. As such, it is non-trivial to show convergence of $V(x(k), \mathcal{W})$ to zero.

Meanwhile, certain quantities exhibit some degree of monotonicity. $r_m(k)$, the lower bound on agent depth, is provably non-decreasing. This is intuitive from the simulations in section 2.7, and will be shown formally in the sequel. By this result alone, the MAS moves towards smaller and smaller subsets of $\mathcal{X}_{\mathrm{D}}$. For any fixed $r > 0$, the set of configurations $\mathcal{X}_m(r) = \{x \in \mathcal{W}^N \mid r_i \geqslant r \ \forall i \in \mathbb{N}_N\} \subset \mathcal{X}_{\mathrm{D}}$ is an invariant set with respect to the MAS dynamics. I.e.

$$x(k) \in \mathcal{X}_m(r) \implies x(k+1) \in \mathcal{X}_m(r). \tag{3.99}$$

Additionally, if $r_m(k+1) > r_m(k)$ then

$$x(k+1) \in \mathcal{X}_m(r_m(k+1)) \subset \mathcal{X}_m(r_m(k)). \tag{3.100}$$

We still need to uncover the additional structure which gives rise to the consensus among subsets of agents as well as the mechanisms steering the MAS towards a Chebyshev configuration. Convergence of $r_m(k)$ alone is not sufficient to explain this behavior. As we will see, graph theoretical notions similar to those exploited in the 1D-case turn out to be central in explaining this behavior.

The forthcoming presentation is structured as follows:

1. In section 3.4.2 we prove the convergence of $r_m(k)$ and analogous time-varying lower bounds on $\tilde{r}_i(k)$ and $\bar{r}_i(k)$.

2. Section 3.4.3 elaborates on the convergence of $r_m(k)$ and relates this to optimality of limit configurations.
3. Section 3.4.4 introduces a novel MAS interaction graph notion to the present framework. Furthermore we relate the topology of static configurations to the connectivity properties of this graph. In this manner, we show how convergence to static configurations is associated with convergence to consensus on $\bar{r}_i$ and r_i for disjoint subsets of agents.
4. Section 3.4.5 is used to consider the notion of information propagation through the interaction graph. We illustrate how imbalances in agent depth propagates through a connected interaction graph and eventually leads to an increase in r_m.
5. In section section 3.4.6 we exploit the preceding results as well as standard results from real analysis to show convergence to consensus provided the interaction graph remains connected for all time.

All results rely on more low level bounds on intra-agents distances and agent depth. We begin our pursuit of convergence results in $\mathbb{R}^d$ by exploring these relations.

3.4.1 Bounding intra-agent distances and agent depths

The connection between agent depths and intra-agent distances can be used to derive useful bounds for both quantities. First, depth with respect to some polyhedron $P = \{x \mid a_i^T x \leqslant b_i, i = 1, \dots, m\} \subset \mathbb{R}^d$. Revisiting (2.37) for the definition of depth $x \in P$, we observe the relations

$$\begin{aligned} \operatorname{depth}(x, P) &= \min\{b_1 - a_i^T x, \dots b_m - a_m^T x\} && (3.101)\\ &= \min\{\operatorname{dist}(x, \partial\{\hat{x} \mid a_1^T \hat{x} \leqslant b_1\}), \dots, \operatorname{dist}(x, \partial\{\hat{x} \mid a_m^T \hat{x} \leqslant b_m\})\} && (3.102)\\ &= \min\{\operatorname{depth}(x, \{\hat{x} \mid a_1^T \hat{x} \leqslant b_1\}), \dots, \operatorname{depth}(x, \{\hat{x} \mid a_m^T \hat{x} \leqslant b_m\})\}. && (3.103) \end{aligned}$$

Next, recall the use of this notion in the context of agent positions in their respective cells,

$$r_i(k) = \operatorname{depth}(x_i(k), \mathbb{V}_i(k)). \tag{3.104}$$

For some Voronoi cell $\mathbb{V}_i$, normalizing the inequality constraint associated with some agent $j \neq i$ yields the half plane representation

$$H_{ij} = \{w \in \mathbb{R}^d \mid \frac{(x_j - x_i)^T}{\|x_j - x_i\|} w \leqslant \frac{(x_j - x_i)^T}{\|x_j - x_i\|} \left(\frac{x_i + x_j}{2} \right)\}. \tag{3.105}$$

Compared to the Voronoi cell representation given in (2.54), we have also used $\|x_j\|^2 - \|x_i\|^2 = (x_j - x_i)^T (x_i + x_j)$. In turn

$$\operatorname{dist}(x_i, \partial H_{ij}) = \frac{(x_j - x_i)^T}{\|x_j - x_i\|} \left[\frac{x_i + x_j}{2} - x_i \right] = \frac{1}{2} \|x_j - x_i\|. \tag{3.106}$$

That is, the distance from either agent to the hyperplane separating them is simply half the intra-agent distance $\|x_j - x_i\|$. Therefore

$$r_i(k) = \text{depth}(x_i(k), \mathbb{V}_i(k)) \tag{3.107}$$

$$= \min\{\text{dist}(x_i(k), \partial\mathcal{W}), \min_{j \neq i} \frac{1}{2}\|x_j(k) - x_i(k)\|\}. \tag{3.108}$$

Note that the depth with respect to $\mathcal{W}$ is accommodated by $\text{dist}(x_i(k), \partial\mathcal{W})$. By the redundancy of constraints arising from agents $j \notin \mathcal{N}_i(k)$

$$r_i(k) = \min\{\text{dist}(x_i(k), \partial\mathcal{W}), \min_{j \in \mathcal{N}_i(k)} \frac{1}{2}\|x_j(k) - x_i(k)\|\}. \tag{3.109}$$

Exploiting this final expression, it is easy to see how intra-agent distances at time k can be lower bounded via agent depths.

Lemma 3.4.1. *The distance* $\text{dist}(x_i(k), x_j(k))$ *between any pair of agents* $i \neq j$ *satisfies the inequality*

$$\text{dist}(x_i(k), x_j(k)) \geqslant 2\max\{r_i(k), r_j(k)\}. \tag{3.110}$$

Proof. By the definition of $r_i(k)$ and $r_j(k)$,

$$\frac{1}{2}\|x_j(k) - x_i(k)\| \geqslant r_i(k) \ \forall j \neq i, \quad \frac{1}{2}\|x_i(k) - x_j(k)\| \geqslant r_j(k) \ \forall i \neq j \tag{3.111}$$

implying the result $\|x_j(k) - x_i(k)\| \geqslant 2\max\{r_i(k), r_j(k)\}$. □

Correspondingly, we are interested in lower bounding the intra-agent distances at time $k+1$ as a function of the quantities available at time k. To this end, recall the definition

$$\tilde{r}_i(k) = \text{depth}(x_i(k+1), \mathbb{V}_i(k)). \tag{3.112}$$

Even though the depth is with respect to the Voronoi cell at time k, we can find a lower bound on intra-agent distance at time $k+1$ by exploiting that the interiors of the agent Voronoi cells are pairwise disjoint.

Lemma 3.4.2. *The distance* $\text{dist}(x_i(k+1), x_j(k+1))$ *between any pair of agents* $i \neq j$ *satisfies the inequality*

$$\text{dist}(x_i(k+1), x_j(k+1)) \geqslant \tilde{r}_i(k) + \tilde{r}_j(k). \tag{3.113}$$

Proof. Consider the N distinct balls $\mathbb{B}_{\tilde{r}_i(k)}(x_i(k+1)) \subset \mathbb{V}_i(k) : i \in \mathbb{N}_N$. Observe that $\text{int}(\mathbb{B}_{\tilde{r}_i(k)}(x_i(k+1))) \cap \text{int}(\mathbb{B}_{\tilde{r}_j(k)}(x_j(k+1))) = \varnothing$ since $\text{int}(\mathbb{V}_i(k)) \cap \text{int}(\mathbb{V}_j(k)) = \varnothing$ provided $i \neq j$. Thus for any two agents $i \neq j, \|x_i(k+1) - x_j(k+1)\| \geqslant \tilde{r}_i(k) + \tilde{r}_j(k)$. □

Moreover, $\tilde{r}_i(k)$ bounds the distance to $\partial\mathcal{W}$ at time $k+1$.

Lemma 3.4.3. *The distance from* $x_i(k+1)$ *to the boundary of* $\mathcal{W}$ *satisfies*

$$\text{dist}(x_i(k+1), \partial\mathcal{W}) \geqslant \tilde{r}_i(k). \tag{3.114}$$

Proof. Since $\mathbb{V}_i(k) \subset \mathcal{W}$ and by the time-invariance of $\mathcal{W}$,

$$\tilde{r}_i(k) = \operatorname{depth}(x_i(k+1), \mathbb{V}_i(k)) \tag{3.115}$$
$$\leqslant \operatorname{depth}(x_i(k+1), \mathcal{W}) = \operatorname{dist}(x_i(k+1), \partial\mathcal{W}). \tag{3.116}$$

□

Combining lemma 3.4.2 and lemma 3.4.3 yields the following lower bound on $r_i(k+1)$.

Lemma 3.4.4. *For all agents $i \in \mathbb{N}_N$, $r_i(k+1)$ satisfies the inequality*

$$r_i(k+1) \geqslant \min\{\tilde{r}_i(k), \min_{j \in \mathcal{N}_i(k+1)} \frac{\tilde{r}_i(k) + \tilde{r}_j(k)}{2}\}. \tag{3.117}$$

Proof. By definition,

$$r_i(k+1) = \min\{\operatorname{dist}(x_i(k+1), \partial\mathcal{W}), \min_{j \in \mathcal{N}_i(k+1)} \frac{1}{2}\big\|x_j(k+1) - x_i(k+1)\big\|\}. \tag{3.118}$$

By lemma 3.4.2, $\min_{j \in \mathcal{N}_i(k+1)} \frac{1}{2}\big\|x_j(k+1) - x_i(k+1)\big\| \geqslant \min_{j \in \mathcal{N}_i(k+1)} \frac{\tilde{r}_i(k) + \tilde{r}_j(k)}{2}$. By lemma 3.4.3, $\operatorname{dist}(x_i(k+1), \partial\mathcal{W}) \geqslant \tilde{r}_i(k)$. The result follows. □

3.4.2 Convergence of the minimal agent depth

Unfortunately, the intricate structure of the bound in lemma 3.4.4 makes it difficult to extract useful information regarding the individual agent depth trajectories. In particular the minimization over $\mathcal{N}_i(k+1)$ is impractical. To remove this dependence, let us define

$$\tilde{r}_m(k) = \min_{i \in \mathbb{N}_N} \tilde{r}_i(k). \tag{3.119}$$

Note that

$$\min_{j \in \mathcal{N}_i(k+1)} \tilde{r}_j(k) \geqslant \min_{i \in \mathbb{N}_N} \tilde{r}_j(k) = \tilde{r}_m(k). \tag{3.120}$$

Thus

$$r_i(k+1) \geqslant \min\{\tilde{r}_i(k), \frac{\tilde{r}_i(k) + \tilde{r}_m(k)}{2}\} \geqslant \frac{\tilde{r}_i(k) + \tilde{r}_m(k)}{2} \geqslant \tilde{r}_m(k), \tag{3.121}$$

where we also used that $\tilde{r}_i(k) \geqslant \tilde{r}_m(k)$ by construction. While this bound is not particularly tight, it is sufficiently so to show

(i) $r_m(k) = \min_{i \in \mathbb{N}_N} r_i(k)$ is non-decreasing and convergent.

(ii) $\bar{r}_m(k) = \min_{i \in \mathbb{N}_N} \bar{r}_i(k)$ is convergent.

First note that the $\bar{r}_i(k)$'s and $r_i(k)$'s are all bounded since $\mathcal{W}$ is bounded. Let $\gamma(\mathcal{W}) = r_c(\mathcal{W})$ be the Chebyshev radius of $\mathcal{W}$. Necessarily

$$\gamma(\mathcal{W}) \geqslant \bar{r}_i(k) \ \forall i \in \mathbb{N}_N. \tag{3.122}$$

Also note that

$$\gamma(\mathcal{W}) \geqslant \bar{r}_i(k) \geqslant \tilde{r}_i(k) \geqslant r_i(k) \ \forall i \in \mathbb{N}_N. \tag{3.123}$$

The rightmost inequality follows from the control law requirements (2.68) and (2.69), whereas the middle inequality follows from $\tilde{r}(k) \in [r_i(k), \bar{r}_i(k)]$ by the control law requirement (2.70). First we show the non-decrease and convergence of $r_m(k)$.

Theorem 3.10. *$r_m(k)$ is non-decreasing and converges to its finite supremum $r_m^\infty = \sup_k r_m(k)$. I.e. $r_m(k+1) \geqslant r_m(k)$ and $\lim_{k\to\infty} r_m(k) = r_m^\infty = \sup_k r_m(k)$.*

Proof. For the non-decrease, consider the bounds (3.123). The ordering is preserved when taking the individual minimums over i. I.e.

$$\gamma(\mathcal{W}) \geqslant \min_{i\in\mathbb{N}_N} \bar{r}_i(k) \geqslant \min_{i\in\mathbb{N}_N} \tilde{r}_i(k) \geqslant \min_{i\in\mathbb{N}_N} r_i(k) \tag{3.124}$$

which by definition is equivalent to

$$\gamma(\mathcal{W}) \geqslant \bar{r}_m(k) \geqslant \tilde{r}_m(k) \geqslant r_m(k). \tag{3.125}$$

Taking the minimum over i in the inequality (3.121) and combining this with $\tilde{r}_m(k) \geqslant r_m(k)$ shows the non-decrease of $r_m(k)$,

$$r_m(k+1) = \min_{i\in\mathbb{N}_N} r_i(k+1) \geqslant \tilde{r}_m(k) \geqslant r_m(k). \tag{3.126}$$

Next we prove the convergence of $r_m(k)$. Define $r_m^\infty = \sup_k r_m(k)$. The supremum is finite since $r_m(k)$ is upper bounded. Assume, for the sake of contradiction, the existence of some $\epsilon > 0$ such that $r_m^\infty - r_m(k) > \epsilon$ for infinitely many k. By the non-decrease of $r_m(k)$, this must hold for all k. But then $r_m^\infty - \epsilon$ is an upper bound for the entire sequence $\{r_m(k)\}_{k=0}^\infty$, contradicting the definition of the supremum. Thus $\lim_{k\to\infty} r_m(k) = \sup_k r_m(k) = r_m^\infty$. □

Revisiting figures 2.15 and 2.16, it can be concluded that the simulations in section 2.7 are consistent with and illustrative for this result. $r_m(k)$ is non-decreasing in both cases.

From (3.126) in the preceding proof, we also inherit a convergence result for $\tilde{r}_m(k)$.

Corollary 3.10.1. *The sequence $\tilde{r}_m(k)$ converges and $\lim_{k\to\infty} \tilde{r}_m(k) = \lim_{k\to\infty} r_m(k) = r_m^\infty$.*

Proof. Follows from taking the limit of

$$r_m(k+1) \geqslant \tilde{r}_m(k) \geqslant r_m(k). \tag{3.127}$$

Then $r_m^\infty \geqslant \lim_{k\to\infty} \tilde{r}_m(k) \geqslant r_m^\infty$. □

Let $I_m(k)$ be the indices of agents with $r_i(k) = r_m(k)$. I.e.

$$i \in I_m(k) \iff r_i(k) = r_m(k). \tag{3.128}$$

The inequality

$$r_m(k+1) \geqslant \tilde{r}_m(k) \geqslant r_m(k) \tag{3.129}$$

is stricter whenever $\bar{r}_i(k) > r_i(k)\ \forall i \in I_m(k)$. By the control law requirement (2.68),

$$\bar{r}_i(k) > r_i(k)\ \forall i \in I_m(k) \implies \tilde{r}_i(k) > r_i(k)\ \forall i \in I_m(k). \tag{3.130}$$

For the other agents, $i \in \mathbb{N}_N \backslash I_m(k)$, the control law requirements (2.68) and (2.69) ensure

$$\tilde{r}_i(k) \geqslant r_i(k) > r_m(k)\ \forall i \in \mathbb{N}_N \backslash I_m(k). \tag{3.131}$$

Thus $\tilde{r}_m(k) > r_m(k)$ whenever $\bar{r}_i(k) > r_i(k)\ \forall i \in I_m(k)$. In turn this leads to strict increase of $r_m(k)$,

$$r_m(k+1) \geqslant \tilde{r}_m(k) > r_m(k) \text{ when } \bar{r}_i(k) > r_i(k)\ \forall i \in I_m(k). \tag{3.132}$$

Since $\bar{r}_m(k) > r_m(k) \iff \bar{r}_i(k) > r_i(k)\ \forall i \in I_m(k)$, we therefore go further and state the convergence result for $\bar{r}_m(k)$ as another corollary of theorem 3.10.

Corollary 3.10.2. *The sequence $\bar{r}_m(k)$ converges and $\lim_{k\to\infty} \bar{r}_m(k) = \lim_{k\to\infty} r_m(k) = r_m^\infty$.*

Proof. By the control law requirement (2.70) and by definition of $\tilde{r}_m(k)$,

$$\tilde{r}_m(k) = \min_i \big[(1-\alpha_i(k))r_i(k) + \alpha_i(k)\bar{r}_i(k)\big] \tag{3.133}$$

$$\geqslant (1-\alpha_{i^\star(k)}(k))r_m(k) + \alpha_{i^\star(k)}(k)\bar{r}_m(k). \tag{3.134}$$

$i^\star(k)$ is the index of some agent $i \in \mathbb{N}_N$ such that $\tilde{r}_i(k) = \tilde{r}_m(k)$. The index or actual value of $\alpha_{i^\star(k)}$ is not important. From the inequality (3.129) and exploiting $\bar{r}_m(k) \geqslant r_m(k)$,

$$r_m(k+1) \geqslant (1-\alpha_{i^\star(k)}(k))r_m(k) + \alpha_{i^\star(k)}(k)\bar{r}_m(k) \geqslant r_m(k). \tag{3.135}$$

Rewriting and dividing by $\alpha_{i^\star(k)}(k)$ yields

$$\frac{1-\alpha_{i^\star(k)}(k)}{\alpha_{i^\star(k)}(k)}\big[r_m(k+1) - r_m(k)\big] + r_m(k+1) \geqslant \bar{r}_m(k) \geqslant r_m(k). \tag{3.136}$$

Note that the division by $\alpha_{i^\star(k)}$ is valid since $\alpha_i(k) > 0\ \forall i \in \mathbb{N}_N\ \forall k$ by construction. The results follows from taking the limits on both sides, then

$$r_m^\infty \geqslant \lim_{k\to\infty} \bar{r}_m(k) \geqslant r_m^\infty. \tag{3.137}$$

□

3.4.3 Optimality of limit configurations

The convergence of $r_m(k)$ illustrates how local interactions between agents yield convergence to a set of globally optimal configurations in the sense that

$$\lim_{k\to\infty} x(k) \tag{3.138}$$

is a local optimum of the global optimization problem

$$\max_{x_1,\ldots,x_N} \min_{i\in\mathbb{N}_N} \operatorname{depth}(x_i, \mathbb{V}_i(x_1,\ldots,x_N,\partial\mathcal{W})). \tag{3.139}$$

By the derivations in section 3.4.1, we can remove the dependence on the Voronoi partition. In particular the relation

$$\operatorname{depth}(x_i, \mathbb{V}_i(x_1,\ldots,x_N,\partial\mathcal{W})) = \min\{\operatorname{dist}(x_i,\partial\mathcal{W}), \min_{j\neq i} \frac{1}{2}\|x_j - x_i\|\} \tag{3.140}$$

allows us to define

$$\mathcal{H}_{\text{sp}}(x_1,\ldots,x_N,\mathcal{W}) = \min_{i\in\mathbb{N}_N} \min_{j\neq i} \min\{\operatorname{dist}(x_i,\partial\mathcal{W}), \min_{j\neq i} \frac{1}{2}\|x_j - x_i\|\} \tag{3.141}$$

and finally rewrite (3.139) to

$$\max_{x_1,\ldots,x_N\in\mathcal{W}} \mathcal{H}_{\text{sp}}(x_1,\ldots,x_N,\mathcal{W}) \tag{3.142}$$

In [Bullo et al., 2009], $\mathcal{H}_{\text{sp}}$ is referred to as a *sphere packing multicenter function*. They justify this terminology by highlighting the connection to classic sphere packing problems. Typically one is interested in finding the maximal number of non-overlapping equal-radius open spheres which fit inside some connected region of $\mathbb{R}^d$. Inspecting $\mathcal{H}_{\text{sp}}$, observe that the value of $\mathcal{H}_{\text{sp}}(x_1,\ldots,x_N,\mathcal{W})$ is the largest radius guaranteeing that N equal-radius open spheres centered at points $x_1,\ldots,x_N$ in $\mathcal{W}$ are non-overlapping and contained in $\mathcal{W}$.

The connection to sphere packing opens for interesting interpretations and applications of the present framework. It can be seen as, and used as, an optimization scheme (iterative procedure) to find a local optimum of the geometric optimization problem (3.142). We refer the interested reader to [Bullo et al., 2009] and its references for more information on the sphere packing problem.

However, the convergence to a local optimum of (3.142) is not sufficient to show the stronger result of convergence to the set of Chebyshev configurations. Neither does it explain the consensus-like behavior we conjecture from the earlier simulations. To strengthen the results on convergence, we proceed by introducing the notion of an interaction graph.

3.4.4 Interaction graph

The interaction graph encodes the agents ability to affect each others Chebyshev radii. In this sense it generalizes the graph associated with the $A_{\bar{r}}$ extensively used for 1D convergence.

Definition 3.4.1 (Interaction graph)**.** *Let the interaction graph $\mathcal{G} = (\mathcal{V}, \mathcal{E})$ be the undirected graph with nodes $\mathcal{V} = \mathbb{N}_N$ and edges $\mathcal{E} \subset \mathcal{V} \times \mathcal{V}$. To all ordered pairs of nodes $(i, j) \in \mathcal{V} \times \mathcal{V} : i \neq j$, we associate a unit normal*

$$n_{ij} = \frac{x_j - x_i}{\|x_j - x_i\|} \in \mathbb{R}^d, \tag{3.143}$$

and edge set

$$\mathcal{E} = \{(i, j) \in \mathcal{V} \times \mathcal{V} \mid n_{ij}^T(\bar{x}_j - \bar{x}_i) = \bar{r}_i + \bar{r}_j, i \neq j\}. \tag{3.144}$$

Observe that $\mathcal{G}$ is undirected as a consequence of the symmetry of the edge membership criterion. I.e. $(i, j) \in \mathcal{E} \iff (j, i) \in \mathcal{E}$ since

$$n_{ij}^T(\bar{x}_j - \bar{x}_i) = \bar{r}_i + \bar{r}_j \iff n_{ji}^T(\bar{x}_i - \bar{x}_j) = \bar{r}_i + \bar{r}_j. \tag{3.145}$$

To gain insight into what edge set membership entails, it is instructive to define the corresponding directed interaction graph.

Definition 3.4.2 (Directed interaction graph)**.** *Let the undirected interaction graph $\tilde{\mathcal{G}} = (\mathcal{V}, \tilde{\mathcal{E}})$ be the directed graph with nodes $\mathcal{V} = \mathbb{N}_N$ and edges $\tilde{\mathcal{E}}$. To all ordered pairs of nodes $(i, j) \in \mathcal{V} \times \mathcal{V} : i \neq j$, we associate a half space*

$$H_{ij} = \{w \in \mathbb{R}^d \mid n_{ij}^T w \leqslant n_{ij}^T(\frac{x_i + x_j}{2})\}, \tag{3.146}$$

where

$$n_{ij} = \frac{x_j - x_i}{\|x_j - x_i\|} \in \mathbb{R}^d. \tag{3.147}$$

The edge set is defined as

$$\tilde{\mathcal{E}} = \{(i, j) \in \mathcal{V} \times \mathcal{V} \mid \operatorname{dist}(\bar{x}_i, \partial H_{ij}) = \bar{r}_i, i \neq j\}, \tag{3.148}$$

with

$$\operatorname{dist}(\bar{x}_i, \partial H_{ij}) = n_{ij}^T[\frac{x_i + x_j}{2} - \bar{x}_i]. \tag{3.149}$$

That is, $(i, j) \in \tilde{\mathcal{E}}$ provided the distance from $\bar{x}_i$ to the half space of $\mathbb{V}_i$ associated with $j \neq i$ is equal to the Chebyshev radius. For some fixed i, $\{j \mid (i, j) \in \tilde{\mathcal{E}}\}$ is the set of agents constraining its Chebyshev radius. Assume that $(i, j) \in \tilde{\mathcal{E}}$ and $(j, i) \in \tilde{\mathcal{E}}$. Then

$$n_{ij}^T[\frac{x_i + x_j}{2} - \bar{x}_i] = \bar{r}_i, \tag{3.150}$$

$$-n_{ij}^T[\frac{x_i + x_j}{2} - \bar{x}_j] = \bar{r}_j, \tag{3.151}$$

since $n_{ij} = -n_{ji}$. Summing these equations yields

$$n_{ij}^T[\bar{x}_j - \bar{x}_i] = \bar{r}_i + \bar{r}_j. \tag{3.152}$$

Thus the interaction graph and its corresponding directed version are related by

$$(i,j) \in \tilde{\mathcal{E}} \text{ and } (j,i) \in \tilde{\mathcal{E}} \iff (i,j) \in \mathcal{E}. \tag{3.153}$$

That is, $(i,j) \in \mathcal{E}$ provided the i and j constrain each others Chebyshev radii via their separating hyperplane $\partial H_{ij} = \partial H_{ji}$.

We remark that $\mathcal{G}$ is a sub-graph of the so-called Delaunay graph $\mathcal{G}_D = (\mathbb{N}_N, \mathcal{E}_D)$ in which two nodes $i, j \in \mathbb{N}_N$ are adjacent provided they are Voronoi neighbors. Formally $\mathcal{E}_D = \{(i,j) \mid \mathbb{V}_i \cap \mathbb{V}_j \neq \varnothing, i \neq j \in \mathbb{N}_N\}$.

The interaction graph is inherently time-varying since the edge set $\mathcal{E}$ is constructed based on the time-varying quantities $x_i(k)$, $\bar{x}_i(k)$ and $\bar{r}_i(k)$. Correspondingly, the interaction graph is time-invariant for all static configurations $x \in \mathcal{X}_{\text{SC}}$. Thus we may exploit the interaction graph to uncover the topology of static MAS configurations.

Theorem 3.11. *Consider some static MAS configuration $x \in \mathcal{X}_{SC}$ and its associated interaction graph $\mathcal{G} = (\mathcal{V}, \mathcal{E})$. For all connected components $\mathcal{G}_0 = (\mathcal{V}, \mathcal{E})$ of $\mathcal{G}$, $\bar{r}_i = \bar{r}_j$ for all pairs $(i,j) \in \mathcal{V}_0 \times \mathcal{V}_0$.*

Proof. Recall that $x \in \mathcal{X}_{\text{SC}} \implies \mathcal{X}_{\text{CC}}$ by proposition 3.2.1. Let $\mathcal{G}_0 = (\mathcal{V}_0, \mathcal{E}_0)$ be any connected component of $\mathcal{G}$. If $|\mathcal{V}_0| = 1$, the results holds trivially. If $|\mathcal{V}_0| > 1$, consider any edge $(i,j) \in \mathcal{E}_0$. Since $x \in \mathcal{X}_{\text{CC}} \implies x_i = \bar{x}_i$ (for some fixed agent Chebyshev center $\bar{x}_i$) and $r_i = \bar{r}_i$ for all $i \in \mathbb{N}_N$,

$$n_{ij}^T[\bar{x}_j - \bar{x}_i] = \frac{(x_j - x_i)^T}{\|x_j - x_i\|}(x_j - x_i) = \|x_j - x_i\| = \bar{r}_i + \bar{r}_j = r_i + r_j. \tag{3.154}$$

Assume, for the sake of contradiction, that $r_i \neq r_j$. Without loss of generality, assume $r_i > r_j$. Applying the result of lemma 3.4.1 yields

$$\|x_j - x_i\| \geqslant 2\max\{r_i, r_j\} = 2r_i > r_i + r_j. \tag{3.155}$$

This contradicts (3.154), proving

$$r_i = r_j \ \forall (i,j) \in \mathcal{E}_0. \tag{3.156}$$

Since $\mathcal{G}_0$ is connected, there exists a path $\{v_m\}_{m=0}^M$ in $\mathcal{G}_0$ between any two distinct nodes $v_0, v_M \in \mathcal{V}_0$. Along the path, $r_{v_{m-1}} = r_{v_m}$ for all $m = 1, \ldots, M$ by (3.156). Thus $r_{v_0} = r_{v_M}$. Since v_0 and v_M can be chosen arbitrarily, $r_i = r_j \ \forall j \in \mathcal{V}_0$ for any $i \in \mathcal{V}_0$. The result follows when re-applying $\bar{r}_i = r_i \ \forall i \in \mathbb{N}_N$ and noting that the derivations hold for any connected component of $\mathcal{G}$. □

Thus convergence to a static configuration will necessarily lead to consensus on the radii $\bar{r}_i$ and r_i within each connected component of $\mathcal{G}$. This can be seen as a generalization of

the 1D result of section 3.3 showing consensus on $\bar{r}_i$ and r_i in the static configuration. As we expected from the motivating illustrations in section 2.7, the associated multi-dimensional result is of a similar yet more general nature. While the concept of consensus is applicable in both cases, deployment to multi-dimensional environments entails a more general type of consensus-behavior with consensus in between subsets of agents rather than the entire MAS.

Figure 3.14 shows the interaction graphs for the final configurations of all three 2D simulations in section section 2.7.

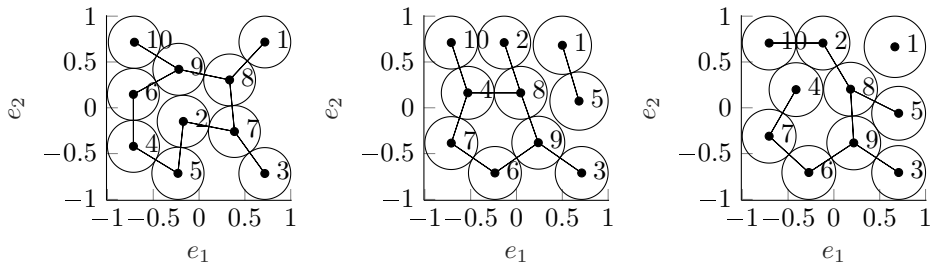

(a) 2D simulation 1. The graph consists of a single connected component.

(b) 2D Simulation 2. The graph consists of two connected components.

(c) 2D simulation 3. The graph consists of two connected components.

Figure 3.14: Interaction graphs associated with the final configurations of the 2D simulations. The dots are the agent positions and the circles are agent Chebyshev balls. There is a line between two agents i, j provided the edge (i, j) exists in the edge set.

Inspecting these illustrative graphs reveals how theorem 3.11 explains the consensus patterns observed for $\bar{r}_i$ and r_i with respect to the final configurations.

- For 2D simulation 1, figure 3.14a reveals that the interaction graph consists of a single connected component. Consistent with this connectivity pattern, figure 2.15 supports consensus on agent depth.
- For 2D simulation 2, the interaction graph in figure 3.14b consists of two disconnected components - the subgraphs induced by $\mathcal{V}_0^1 = \{1, 5\}$ and $\mathcal{V}_0^2 = \mathbb{N}_{10} \backslash \{1, 5\}$ respectively. Correspondingly, the agent depth trajectories in figure 2.16 exhibit convergence to two distinct values.
- Finally, for 2D simulation 3, the interaction graph consists of two connected components. Agent 1 clearly has greater agent depth than the other agents. Agents $\mathbb{N}_{10} \backslash \{1\}$ are in the same connected component, and exhibit consensus on agent depths.

Obviously the multi-dimensional interaction graph notion also applies in 1D. The 1D interaction graph is straightforward to find. Exploiting the explicit equations for Chebyshev centers and Chebyshev radii, it is easy to verify that for all $i \in \{1, 2, \dots, N-1\}$

$$\bar{x}_j(k) - \bar{x}_i(k) = \bar{r}_i(k) + \bar{r}_j(k) \iff j = i + 1 \ \forall k \in \{0, 1, 2, \dots\}. \tag{3.157}$$

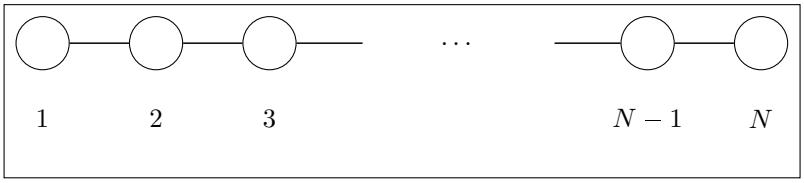

Figure 3.15: The interaction graph w.r.t. MAS deployment to $\mathbb{R}$. The graph is time invariant and connected.

I.e. there is an edge between two agents provided they have neighboring Voronoi cells[1]. The resulting graph is shown in figure 3.15. Remark that this is simply $\mathcal{G}(A_{\bar{r}}) = (\mathcal{V}, \hat{\mathcal{E}}, W)$ from figure 3.13 disregarding weights and self-loops. Formally the interaction graph is $\mathcal{G} = (\mathcal{V}, \mathcal{E})$ where

$$(i,j) \in \mathcal{E} \iff (i,j) \in \{(i,j) \in \hat{\mathcal{E}} \mid i \neq j\}. \tag{3.158}$$

In this sense, the interaction graph generalizes $\mathcal{G}(A_{\bar{r}})$ to the multi-dimensional case. At the same time, the 1D interaction graph has some useful particularities. It can be constructed on the basis of initial conditions and importantly it is time-invariant since the edge set is the same for all time steps k. This is useful for the construction of analytic results such as the ones presented in section 3.3.

The treatment of convergence in one-dimensional environments in section 3.3 is constrained to single integrator agent dynamics and linear control laws. We can extend several of the results to more general agent dynamics and controllers by utilizing the results on multi-dimensional convergence. In this regard, the following result is useful:

Proposition 3.4.1. *Let Σ be an N-agent MAS deployed to $\mathcal{W} = [x_l, x_u] \subset \mathbb{R}$, $x_u > x_l$. The MAS is subjected to the controllers $\mathcal{K}_1, \ldots, \mathcal{K}_N$ where each satisfy the control law requirements* (2.68)-(2.70)*. Then Σ has an unique Chebyshev configuration, and consequently an unique static configuration, x^{ss}. The entries of x^{ss} are given by $x_i^{ss} = (2i-1)\frac{x_u - x_l}{2N} + x_l$.*

Proof. Assume that Σ is in a static configuration and let $\mathcal{G}$ be the interaction graph associated with the MAS. $\bar{r}$ and r denote the vectors collecting agent Chebyshev radii and agent depths respectively (as in section 3.3). Since $\mathcal{G}$ is time-invariant and connected, theorem 3.11 ensures that $\bar{r} = r = \beta\mathbb{1}$ for some constant $\beta > 0$. Then the average of the Chebyshev radii is $\frac{1}{N}\mathbb{1}^T\bar{r} = \beta$. (3.78) ensures that $\frac{1}{N}\mathbb{1}^T\bar{r}(k) = \frac{1}{N}\frac{x_u - x_l}{2}$, invariant to MAS state. Thus $\beta = \frac{1}{N}\frac{x_u - x_l}{2}$ when the MAS is in a static configuration. In turn x^{ss}, with entires $x_i^{ss} = (2i-1)\frac{x_u - x_l}{2N} + x_l$, is the unique static configuration. Σ satisfies the assumptions of proposition 3.3.1, and thus Σ is in a Chebyshev configuration if and only if it is in a static configuration. I.e. the uniqueness of the static configuration implies uniqueness of the Chebyshev configuration. That is, Σ has an unique static Chebyshev configuration. The result follows. □

[1]Recall that we assume the ordering $x_1 < x_2 < \cdots < x_N$ in 1D.

The uniqueness of x^{ss} shown in section 3.3 can be seen as a special case of proposition 3.4.1.

The next step is to uncover mechanisms steering agents within the same connected component to consensus on r_i and $\bar{r}_i$. Just like we were able to prove convergence to consensus in 1D by exploiting connectivity properties of $\mathcal{G}(A_{\bar{r}})$, we would like to find more general results for $\mathbb{R}^d$ by exploiting connectivity properties of the interaction graph. In a sense we are generalizing the 1D results. However, in $\mathbb{R}^d$ we necessarily need to account for the fact that the interaction graph may not be connected.

3.4.5 Information propagation

First we investigate how imbalances in $\bar{r}_i$ and r_i propagate through the graph. Assume that for some configuration $x(0) \in \mathcal{X}_{\mathrm{D}}$ the corresponding interaction graph consists of a fixed number $N_c \leqslant N$ of connected components with node sets $\mathcal{V}_0^{(1)}, \dots, \mathcal{V}_0^{(N_c)}$ which are time-invariant along the trajectory of the MAS. It is clear from proposition 3.11 that convergence to a static configuration must be associated with convergence to consensus on $\bar{r}_i$ and r_i within each connected component of $\mathcal{G}$. Equivalently, assuming convergence to some static configuration $\mathcal{X}_{\mathrm{SC}}$,

$$\lim_{k\to\infty} x(k) \in \mathcal{X}_{\mathrm{SC}} \implies \max_{i\in\mathcal{V}_0} \bar{r}_i(k) = \min_{i\in\mathcal{V}_0} r_i(k) \ \forall \mathcal{G}_0 = (\mathcal{V}_0, \mathcal{E}_0) \in \{\mathcal{G}_0^{(1)}, \dots, \mathcal{G}_0^{(N_c)}\}. \quad (3.159)$$

As a stepping stone to such a result, we illustrate information propagation through some interaction graph $\mathcal{G}$ which is connected along the trajectory of the MAS.

Consider the set

$$L(k,\tau) = \{l \in \mathbb{N}_N \mid \bar{r}_l(k+\tau) > r_m(k)\}, \quad (3.160)$$

indexed by $k \in \{0,1,2,\dots\}$ and a finite offset $\tau \in \{0,1,2,\dots\}$. Intuitively $L(k,\tau)$ contains the indices of agents whose Chebyshev radius is greater than the baseline $r_m(k)$ at time $k+\tau$. By $\bar{r}_i \geqslant r_i$, $L(k,\tau)$ will also contain the indices of agents with agent depth greater than $r_m(k)$ at time $k+\tau$.

Also define

$$\Delta(k,\tau) = \begin{cases} \min_{l\in L(k,\tau)} \bar{r}_l(k+\tau) - r_m(k) & |L(k,\tau)| > 0, \\ 0 & |L(k,\tau)| = 0. \end{cases} \quad (3.161)$$

$\Delta(k,\tau)$ measures the smallest non-zero deviation between the Chebyshev radii and $r_m(k)$. If there are no non-zero deviations, i.e. if $L(k,\tau)$ is empty, then $\Delta(k,\tau) = 0$ by convention.

First we illustrate what set membership in $L(k,\tau)$ entails in terms of agent depth trajectories. This intermediate result will be used several times in the sequel.

Lemma 3.4.5. *For all agents $l \in L(k,\tau)$,*

$$r_l(k+\tau+1) \geqslant \frac{\alpha_l(k+\tau)}{2}\Delta(k,\tau) + r_m(k) > r_m(k). \quad (3.162)$$

Proof. Exploiting the bound (3.117) from lemma 3.4.4 yields

$$r_i(k+\tau+1) \geqslant \min\{\tilde{r}_i(k+\tau), \min_{j\in\mathcal{N}_i(k+\tau+1)} \frac{\tilde{r}_i(k+\tau)+\tilde{r}_j(k+\tau)}{2}\}. \tag{3.163}$$

Since $\tilde{r}_j(k+\tau) \geqslant r_m(k+\tau) \geqslant r_m(k)$ by the construction of $\tilde{r}_j(k)$ and the non-decrease of $r_m(k)$,

$$r_i(k+\tau+1) \geqslant \min\{\tilde{r}_i(k+\tau), \frac{\tilde{r}_i(k+\tau)}{2} + \frac{r_m(k)}{2}\}. \tag{3.164}$$

The minimization can be removed when using $\tilde{r}_i(k+\tau) \geqslant r_m(k)$ once more,

$$r_i(k+\tau+1) \geqslant \frac{\tilde{r}_i(k+\tau)}{2} + \frac{r_m(k)}{2}. \tag{3.165}$$

Consider now $\tilde{r}_i(k+\tau)$. Exploiting $r_m(k)$ yet again yields the following bound:

$$\tilde{r}_i(k+\tau) = (1-\alpha_i(k+\tau))r_i(k+\tau) + \alpha_i(k+\tau)\bar{r}_i(k+\tau) \tag{3.166}$$
$$\geqslant (1-\alpha_i(k+\tau))r_m(k) + \alpha_i(k+\tau)\bar{r}_i(k+\tau) \tag{3.167}$$

By construction $\bar{r}_l(k+\tau) \geqslant \Delta(k,\tau) + r_m(k)$ for all $l \in L(k,\tau)$. Therefore

$$\tilde{r}_l(k+\tau) \geqslant (1-\alpha_i(k+\tau))r_m(k) + \alpha_i(k+\tau)[\Delta(k,\tau) + r_m(k)] \tag{3.168}$$
$$\geqslant r_m(k) + \alpha_i(k+\tau)\Delta(k,\tau) \tag{3.169}$$

for all agents $l \in L(k,\tau)$. Thus,

$$r_l(k+\tau+1) \geqslant \frac{\alpha_i(k+\tau)}{2}\Delta(k,\tau) + r_m(k). \tag{3.170}$$

for all agents $l \in L(k,\tau)$. Since $\exists l \in L(k,\tau) \implies \Delta(k,\tau) > 0$ and $\alpha_i(k) > 0$ by construction,

$$r_l(k+\tau+1) \geqslant \frac{\alpha_i(k+\tau)}{2}\Delta(k,\tau) + r_m(k) > r_m(k) \tag{3.171}$$

as claimed. □

The study of $L(k,\tau)$ and $\Delta(k,\tau)$ is motivated by the following result - relating the cardinality of $L(k,\tau)$ with increase in $r_m(k)$.

Lemma 3.4.6. *If $L(k,\tau)$ has cardinality $|L(k,\tau)| = N$ then $r_m(k+\tau+1) > r_m(k)$.*

Proof. By lemma 3.4.5 and the fact that $i \in L(k,\tau)\ \forall i \in \mathbb{N}$,

$$r_i(k+\tau+1) \geqslant \frac{\alpha_i(k+\tau)}{2}\Delta(k,\tau) + r_m(k). \tag{3.172}$$

Taking the minimum over i yields the desired result,

$$r_m(k+\tau+1) = \min_{i\in\mathbb{N}_N} r_i(k+\tau+1) \geqslant \frac{\min_i \alpha_i(k+\tau)}{2}\Delta(k,\tau) + r_m(k) > r_m(k). \tag{3.173}$$

□

Hence we can use $L(k,\tau)$ to prove strict increase of $r_m(k+\tau+1)$ versus the baseline $r_m(k)$ provided the cardinality of $L(k,\tau)$ reaches N. We first show the non-decrease of $|L(k,\tau)|$ in τ.

Lemma 3.4.7. $L(k,\tau) \subseteq L(k,\tau+1)$.

Proof. By lemma 3.4.5

$$r_l(k+\tau+1) \geqslant \frac{\alpha_i(k+\tau)}{2}\Delta(k,\tau) + r_m(k) \ \forall l \in L(k,\tau). \tag{3.174}$$

That is

$$\bar{r}_l(k+\tau+1) \geqslant r_l(k+\tau) > r_m(k) \ \forall l \in L(k,\tau). \tag{3.175}$$

I.e. $l \in L(k,\tau+1) \ \forall l \in L(k,\tau)$. □

Proposition 3.4.2. $|L(k,\tau+1)| \geqslant |L(k,\tau)|$.

Proof. $|L(k,\tau+1)| \geqslant |L(k,\tau)|$ since $L(k,\tau) \subseteq L(k,\tau+1)$ by lemma 3.4.7. □

Next we want to establish conditions under which $|L(k,\tau)|$ increases. To this end we exploit the interaction graph $\mathcal{G}(k)$. We also define the complement of $L(k,\tau)$ as

$$L_c(k,\tau) = \mathbb{N}_N \backslash L(k,\tau). \tag{3.176}$$

Lemma 3.4.8. *Assume that*

(i) $\mathcal{G}(k+\tau)$ *is connected for all* $\tau \in \{0,1,2,\dots\}$.

(ii) $|L(k,0)| > 0$. *I.e. at least one Chebyshev radius is strictly higher than* $r_m(k)$ *at time* k.

Then $\bar{r}_{l_c}(k+\tau+1) > r_m(k)$ *for at least one* $l_c \in L_c(k,\tau)$ *provided* $L_c(k,\tau) \neq \varnothing$.

Proof. First observe that $L(k,\tau)$ is non-empty at the particular τ in question by $|L(k,0)| > 0$ and the non-decrease in cardinality by lemma 3.4.7.

Since $\mathcal{G}(k+\tau)$ and $\mathcal{G}(k+\tau+1)$ are connected and $|L_c(k,\tau)| > 1$, there exists at least one edge $(l,l_c) \in \mathcal{E}(k+\tau+1)$ such that $l_c \in L_c(k,\tau)$ and $l \in L(k,\tau)$. Pick any such edge.

Assume for the sake of contradiction that

$$\bar{r}_{l_c}(k+\tau+1) = r_m(k). \tag{3.177}$$

Due to $\bar{r}_{l_c}(k+\tau+1) \geqslant r_{l_c}(k+\tau+1) \geqslant r_m(k)$ we have $\bar{r}_{l_c}(k+\tau+1) = r_{l_c}(k+\tau+1) = r_m(k)$. That is, the agent l_c is at at Chebyshev center and has Chebyshev radius $r_m(k)$. In this case the distance from $\bar{x}_{l_c}(k+\tau+1) = x_{l_c}(k+\tau+1)$ to all hyperplanes constraining $\bar{r}_{l_c}(k+\tau+1)$ is $r_m(k)$. Thus for all $\{l_n,l_c\} \in \mathcal{E}(k+\tau+1)$,

$$\frac{\operatorname{dist}(x_{l_c}(k+\tau+1), x_{l_n}(k+\tau+1))}{2} = \bar{r}_{l_c}(k+\tau+1) = r_{l_c}(k+\tau+1) = r_m(k). \tag{3.178}$$

Meanwhile, for any pair of agents $i \neq j$ and any k,

$$\operatorname{dist}(x_i(k), x_j(k)) \geqslant 2\max\{r_i(k), r_j(k)\} \tag{3.179}$$

by lemma 3.4.1. Consider now the particular edge $\{l, l_c\}$. By the bound (3.179),

$$\frac{1}{2}\operatorname{dist}(x_{l_c}(k+\tau+1), x_l(k+\tau+1)) \geqslant \max\{r_{l_c}(k+\tau+1), r_l(k+\tau+1)\} \tag{3.180}$$

$$\geqslant \max\{r_m(k), \frac{\Delta(k,\tau)}{2} + r_m(k)\} \tag{3.181}$$

$$\geqslant \frac{\Delta(k,\tau)}{2} + r_m(k) > r_m(k). \tag{3.182}$$

From the first to second step we use the non-decrease of $r_m(k)$ and the bound from lemma 3.4.5. The inequality (3.182) contradicts (3.178). Thus $\bar{r}_{l_c}(k+\tau+1) \neq r_m(k)$. Furthermore $\bar{r}_{l_c}(k+\tau+1) \geqslant r_m(k+\tau+1) \geqslant r_m(k)$ by the non-decrease of r_m. Therefore the only possibility is $\bar{r}_{l_c}(k+\tau+1) > r_m(k)$ as claimed. □

This result can easily be extended to a result on increase in cardinality of $L(k,\tau)$

Proposition 3.4.3. *Under the same assumptions as in lemma 3.4.8,* $|L(k,\tau+1)| > |L(k,\tau)|$.

Proof. By proposition 3.4.2, $l \in L(k,\tau+1)\ \forall l \in L(k,\tau)$. By proposition 3.4.8 there exists at least one $l \in L(k,\tau+1)$ such that $l \in L_c(k,\tau)$. Thus $|L(k,\tau+1)| > |L(k,\tau)|$ whenever $0 < |L(k,\tau)| < N$. □

Under the same set of assumptions, its now apparent that we can find a finite τ which guarantees $|L(k,\tau)| = N$.

Proposition 3.4.4. *Under the same assumptions as in lemma 3.4.8,* $|L(k,N-1)| = N$.

Proof. Consider the worst case. Namely

- $|L(k,0)| = 1$, which is the lowest possible cardinality satisfying the assumptions.
- By proposition 3.4.2, $|L(k,\tau+1)| > |L(k,\tau)|$. Thus in the worst case $|L(k,\tau+1)| = |L(k,\tau)| + 1$.

Then $|L(k,\tau)| \geqslant \tau + 1$ and the result follows. □

Remark 3.4.1. *Under the same assumptions as in lemma 3.4.8, proposition 3.4.4 can be stated in a more general from stating* $\exists K \in \{0,1,\dots,N-1\}$ *such that* $|L(k,K)| = N$.

The final result of this section is simply a summary of the preceding results.

Theorem 3.12. *Assume*

(i) $\mathcal{G}(k+\tau)$ *is connected for all* $\tau \in \{0,1,2,\dots\}$.

(ii) $|L(k,0)| > 0$.

Then

$$r_m(k+N) > r_m(k). \tag{3.183}$$

Proof. By proposition 3.4.4, $|L(k, N-1)| = N$. The result follows by lemma 3.4.6. □

Recall the 1D information propagation simulation in section 2.7. It illustrates that the propagation of a deviation $\bar{r}_M(k) > r_m(k)$ to an increase in r_m such that $r_m(k+K) > r_m(k)$, for some $K \in \mathbb{N}$, can at best happen after $K = N$ steps in the general case. The results of the present section are sufficient to establish that, for deployment to $\mathbb{R}$, N indeed represents a worst case delay K between the time at which $\bar{r}_M(k) > r_m(k)$ until $r_m(k+K) > r_m(k)$. In particular theorem 3.12 applies since the interaction graph for a 1D MAS is time-invariant and connected. The simulation represents an instance of the edge case considered in the proof of proposition 3.4.4. In particular, $|L(0,0)| = 1$ and the cardinality $|L(0,\tau)|$ increases by exactly one per increase in offset τ until $\tau = N-1$. Interestingly we see that the same mechanics driving the propagation of a deviation $\bar{r}_M(k) > r_m(k)$ to an increase in r_m generalize to the multi-dimensional case provided the interaction graph is connected.

Based on theorem 3.12, it is apparent that convergence to some Chebyshev configuration can be proved whenever the interaction graph is connected along the trajectory of the MAS. Informally $\bar{r}_M(\infty) > r_m(\infty)$ in a sense contradicts the convergence of $r_m(k)$ as then $r_m(\infty + N) > r_m(\infty) = r_m^\infty$. Showing this in a formal manner is the topic of the next section.

3.4.6 Convergence over connected interaction graphs

The following theorem is the main convergence result of this manuscript.

Theorem 3.13. *Let $x(0) \in \mathcal{X}_D$ be some initial MAS configuration with an associated interaction graph $\mathcal{G}(0)$ which stays connected along the trajectory of the MAS. I.e. $\mathcal{G}(k)$ is connected for all $k \in \{0, 1, 2, \dots\}$. Then*

$$\lim_{k\to\infty} x(k) \in \mathcal{X}_{CC} \tag{3.184}$$

and

$$\lim_{k\to\infty} \bar{r}_M(k) = \lim_{k\to\infty} \max_i \bar{r}_i(k) = \lim_{k\to\infty} r_m(k) = r_m^\infty. \tag{3.185}$$

I.e. the MAS converges to a Chebyshev Configuration where all agents attain consensus on Chebyshev radii and agent depths.

We prove this theorem by via two different procedures. First by showing that $\bar{r}_M(k)$ has an unique accumulation point corresponding to r_m^∞. Next we use a fixed point theorem like procedure where we show convergence of a particular decreasing subsequence of $\bar{r}_M(k)$. While either approach is valid, they differ in their interpretation and complexity.

Proof - Unique accumulation point approach. Consider the sequence $\{\bar{r}_M(k)\}_{k\in\mathbb{N}}$. This is a bounded sequence in $\mathbb{R}$, $\bar{r}_M(k) \in [r_m(k), \gamma(\mathcal{W})] \subseteq [0, \gamma(\mathcal{W})] \subset \mathbb{R}$. By theorem 3.6, $\{\bar{r}_M(k)\}_{k\in\mathbb{N}}$ has at least one accumulation point.

The inequalities $\gamma(\mathcal{W}) \geqslant \bar{r}_M(k) \geqslant r_m(k)$ ensures that any accumulation point r_M^∞ of $\{r_M(k)\}$ must be in the interval $\bar{r}_M^\infty \in [r_m^\infty, \gamma(\mathcal{W})]$. Assume that $\{\bar{r}_M(k)\}$ has an accumulation point $\bar{r}_M^\infty$ strictly greater than r_m^∞. Then, by definition, there exists a subsequence $\{\bar{r}_M(k_l)\}_{l\in\mathbb{N}}$ such that

$$\lim_{l\to\infty} \bar{r}_M(k_l) = \bar{r}_M^\infty > r_m^\infty. \tag{3.186}$$

Using the same sequence of indices $\{k_l\}_{l\in\mathbb{N}}$, we consider the subsequence $\{r_m(k_l)\}_{l\in\mathbb{N}}$ of $\{r_m(k)\}_{k\in\mathbb{N}}$. Since $r_m(k)$ is convergent, it has an unique accumulation point r_m^∞ by lemma 3.1.2. By the same lemma, all subsequences of $\{r_m(k)\}_{k\in\mathbb{N}}$ converge to r_m^∞. In particular

$$\lim_{l\to\infty} r_m(k_l) = r_m^\infty. \tag{3.187}$$

For $\bar{r}_M^\infty > r_m^\infty$ to hold, there has to exist a MAS configuration where $r_m(k)$ is constant despite $\bar{r}_M(k) > r_m(k)$. By theorem 3.12 and by the assumptions on interaction graph connectivity, $\bar{r}_M(k) > r_m(k) \implies |L(k,0)| > 0 \implies r_m(k+N) > r_m(k)$ thus contradicting the existence of such a configuration.

As such, any accumulation point $\bar{r}_M^\infty$ of $\{\bar{r}_M(k)\}_{k\in\infty}$ must satisfy $r_m^\infty \geqslant \bar{r}_M^\infty \geqslant r_m^\infty$. Therefore $\{\bar{r}_M(k)\}_{k\in\mathbb{N}_N}$ has a single unique accumulation point $\bar{r}_M^\infty = r_m^\infty$. Subsequently $\{\bar{r}_M(k)\}_{k\in\mathbb{N}_N}$ is convergent by lemma 3.1.2 and

$$\lim_{k\to\infty} \bar{r}_M(k) = \lim_{k\to\infty} r_m(k) = r_m^\infty. \tag{3.188}$$

That is, the MAS converges to a configuration

$$x \in \{x \mid \max_{i\in\mathbb{N}_N} \bar{r}_i(\mathbb{V}_i) = \min_{i\in\mathbb{N}_N} r_i(x, \mathbb{V}_i)\} \subseteq \mathcal{X}_{\mathrm{CC}}. \tag{3.189}$$

□

Proof - Fixed point approach. Even though $\bar{r}_M(k)$ is not non-increasing, it is possible to construct a convergent sequence upper bounding $\bar{r}_M(k)$.

Three cases will have to be dealt with in order to construct a convergent subsequence.

i) For a sequence with infinitely many peaks, let $\{\bar{r}_M(k_l)\}_{l\in\mathbb{N}}$ be the subsequence of these peaks. Obviously, the subsequence is non-increasing and convergent.

ii) For a sequence with finitely many peaks K, we construct a subsequence in the following manner: Let the first K indices of the subsequence be the peaks $k_1, \ldots, k_K$. Since the sequence has a finite number of peaks, there exists a minimal index $k^\star > k_K$ such that the value $\bar{r}_M(k^\star)$ is repeated infinitely many times and $\bar{r}_M(k) \leqslant \bar{r}_M(k^\star)\ \forall k > k^\star$. Thus the subsequence will be completed with the indices beyond index k_K with corresponding

sequence value $\bar{r}_M(k^\star)$. The obtained subsequence yields a non-increasing, bounded and convergent subsequence of $\bar{r}_M(k)$.

iii) The last case to be considered is that of a sequence which has no peaks. Following the definition of peaks, absence of peaks yields $\nexists l : \bar{r}_M(k) < \bar{r}_M(l)\ \forall k > l$. In this case,

$$\forall k\ \exists l > k : \bar{r}_M(k) \leqslant \bar{r}_M(l). \tag{3.190}$$

As such there exists at at least one non-decreasing subsequence of $\bar{r}_M(k)$. A particular such subsequence can be constructed effectively starting at index $k_1 = 0$ and picking indices k_{l+1} such that $\bar{r}_M(k_{l+1}) \geqslant \bar{r}_M(k_l)$. By construction

$$\lim_{l\to\infty} \bar{r}_M(k_l) = \sup_k \bar{r}_M(k). \tag{3.191}$$

Whether $\bar{r}_M(k)$ exhibits peaks or not, we have now shown that $\bar{r}_M(k)$ has a specific convergent subsequence $\{\bar{r}_M(k_l)\}$. Define the limit of this sequence by $\bar{r}_M^\infty$,

$$\lim_{l\to\infty} \bar{r}_M(k_l) = \bar{r}_M^\infty. \tag{3.192}$$

Using the same sequence of indices $\{k_l\}_{l\in\mathbb{N}}$, we consider the subsequence $\{r_m(k_l)\}_{l\in\mathbb{N}}$ of $\{r_m(k)\}_{k\in\mathbb{N}}$. Since $r_m(k)$ is convergent, it has an unique accumulation point r_m^∞ by lemma 3.1.2. By the same lemma, all subsequences of $\{r_m(k)\}_{k\in\mathbb{N}}$ converge to r_m^∞. In particular

$$\lim_{l\to\infty} r_m(k_l) = r_m^\infty. \tag{3.193}$$

The sub-sequence of $\bar{r}_M(k)$ is constructed in a manner which allows us to bound the original sequence $\bar{r}_M(k)$.

- Assuming $\bar{r}_M(k)$ has at least one peak, i.e. cases i) and ii) above, then for any index k_l of the subsequence, $\bar{r}_M(k) \leqslant \bar{r}_M(k_l)\ \forall k > k_l$,
- Assuming $\bar{r}_M(k)$ has no peaks, i.e. case iii), then still $\bar{r}_M(k) \leqslant \sup_l \bar{r}_M(k_l)\ \forall k$.

Thus we know that the original sequence converges to the interval

$$\lim_{k\to\infty} \bar{r}_M(k) \in [r_m^\infty, \bar{r}_M^\infty]. \tag{3.194}$$

Consider now the limits of the subsequences. Assume that $\bar{r}_M^\infty > r_m^\infty$. For this to hold, there has to exist some configuration (associated with the limit) where $r_m(k_l)$ is constant despite $\bar{r}_M(k_l) > r_m(k_l)$. By theorem 3.12 and by the assumptions on interaction graph connectivity, $\bar{r}_M(k_l) > r_m(k_l) \implies |L(k_l, 0)| > 0 \implies \exists k_{l'} > k_l + N : r_m(k_{l'}) > r_m(k_l)$ contradicting the existence of such a configuration. I.e. $r_m^\infty \geqslant \bar{r}_M^\infty \geqslant r_m^\infty$. In turn $\lim_{k\to\infty} \bar{r}_M(k) \in [r_m^\infty, \bar{r}_M^\infty] = [r_m^\infty, r_m^\infty]$ and therefore

$$\lim_{k\to\infty} \bar{r}_M(k) = r_m^\infty. \tag{3.195}$$

That is, the MAS converges to a configuration

$$x \in \{x \mid \max_{i\in\mathbb{N}_N} \bar{r}_i(\mathbb{V}_i) = \min_{i\in\mathbb{N}_N} r_i(x, \mathbb{V}_i)\} \subseteq \mathcal{X}_{\mathrm{CC}}. \tag{3.196}$$

□

Since any admissible 1D MAS has a time-invariant and connected interaction graph, convergence to some Chebyshev configuration follows. Combined with proposition 3.4.1, we now know that any admissible MAS converges to the unique static 1D configuration given in section 3.3. Thus we now formally understand the behavior of the 1D MAS simulation illustrated in figure 2.9c, where the agent controllers have time-varying gains.

We can strengthen the theorem provided the agent Chebyshev centers are unique along the trajectory of the MAS.

Corollary 3.13.1. *Let $x(0) \in \mathcal{X}_D$ be some initial MAS configuration with an associated interaction graph $\mathcal{G}(0)$ which preserves connectivity along the trajectory of the MAS. I.e. $\mathcal{G}(k)$ is connected for all $k \in \{0, 1, 2, \dots\}$. Additionally, the agent Chebyshev centers satisfy assumption 3.2.1. I.e. all agent Chebyshev centers are unique at all time steps. Then*

$$\lim_{k \to \infty} x(k) \in \mathcal{X}_{SC}. \tag{3.197}$$

I.e. the MAS converges to a static configuration.

Proof. By theorem 3.13,

$$\lim_{k \to \infty} x(k) \in \mathcal{X}_{\mathrm{CC}}. \tag{3.198}$$

Since assumption 3.2.1 is satisfied, 3.2.2 applies and thus $x \in \mathcal{X}_{\mathrm{CC}} \iff x \in \mathcal{X}_{\mathrm{SC}}$. The result follows. □

2D simulation 1 in section 2.7 satisfy the assumptions of corollary 3.13.1. In particular the Chebyshev centers are unique and the interaction is graph connected along the trajectory of the MAS. Thus the simulation is illustrative for the corollary. As expected, the MAS converges to a Chebyshev static configuration with consensus on $\bar{r}_i$ and r_i.

3.4.7 Extension to multiple connected components

Intuitively we expect a result similar to theorem 3.13 to hold for all connected components of $\mathcal{G}$. However, the situation is complicated by the fact that lack of connectivity in $\mathcal{G}$ only inhibits mutual influence. Agents $i \neq j$ in two separate connected components of $\mathcal{G}$ may still exhibit inter-dependence. 2D Simulations 2 and 3 in section 2.7 are practical illustrations of this situation. In figure 2.13b, the Chebyshev radii of agents 1 and 5 are constrained by agents in $\mathbb{N}_{10} \backslash \{1, 5\}$. Similarly, agent 1 in figure 2.14b is constrained by agent 8. These dependencies are not reflected in the interaction graph.

Meanwhile, said dependencies are reflected in the directed interaction graph $\tilde{G} = (\mathcal{V}, \tilde{\mathcal{E}})$. The directed interaction graph for both simulations are shown in figure 3.16. For simulation 2, the edges $(1, 2)$ and $(5, 9)$ reflect that their Chebyshev radii are constrained by agents 2 and 9 respectively. Likewise for simulation 3, the edge $(1, 8)$ mirror the fact that $\bar{r}_1$ is constrained by agent 8.

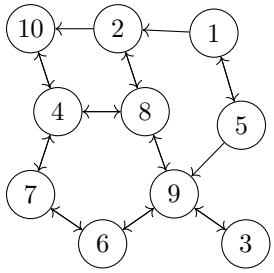

(a) 2D Simulation 2.

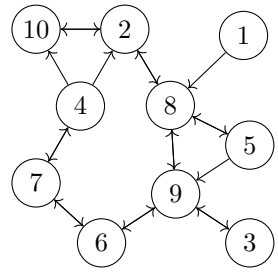

(b) 2D simulation 3.

Figure 3.16: Directed interaction graphs associated with the final configurations of 2D simulations 2 and 3. An arrow from agent i to agent j implies the existence of an edge (i, j) in the graph edge set.

Thus convergence results when $\mathcal{G}$ consists of multiple disconnected components necessarily must account for edges in $\tilde{\mathcal{G}}$. A relatively simple extension in this respect, is to consider the situation where there are no edges in the directed interaction graph between connected components of the undirected version.

Proposition 3.4.5. *Let $x(0) \in \mathcal{X}_D$. $\mathcal{G} = (\mathcal{V}, \mathcal{E})$ and $\tilde{\mathcal{G}} = (\mathcal{V}, \tilde{\mathcal{E}})$ is respectively the interaction graph and the directed interaction graph associated with the MAS. Suppose that:*

(i) Along the MAS trajectories, $\mathcal{G}$ consists of a fixed number of $N_c \leqslant N$ connected components.

(ii) For each connected component $\mathcal{G}_0^{(l)} = (\mathcal{V}_0^{(l)}, \mathcal{E}_0^{(l)})$ of $\mathcal{G}$, $l \in \mathbb{N}_{N_c}$, the node sets $\mathcal{V}_0^{(l)}$ are time-invariant along the MAS trajectory.

(iii) Along the MAS trajectories, $\nexists (i, j) \in \tilde{\mathcal{E}}$ such that $i \in \mathcal{V}_0^{(l_1)}$ and $j \in \mathcal{V}_0^{(l_2)}$ for $l_1 \neq l_2$.

(iv) Along the MAS trajectories, for each connected component $\mathcal{G}_0^{(l)} = (\mathcal{V}_0^{(l)}, \mathcal{E}_0^{(l)})$, for each $i \in \mathcal{V}_0^{(l)}$, $\min\{\min_{j \in \mathcal{V}_0^{(l)}} \|x_j - x_i\|, \operatorname{dist}(x_i, \partial\mathcal{W})\} \leqslant \min_{j \in \mathbb{N}_N \setminus \mathcal{V}_0^{(l)}} \|x_j - x_i\|$. I.e. for any agent, its depth does not improve when disregarding agents belonging to other connected components than that of agent i.

Then

$$\lim_{k \to \infty} x \in \mathcal{X}_{SC} \tag{3.199}$$

and

$$\max_{i \in \mathcal{V}_0} \bar{r}_i(k) = \min_{i \in \mathcal{V}_0} r_i(k) \ \forall \mathcal{G}_0 = (\mathcal{V}_0, \mathcal{E}_0) \in \{\mathcal{G}_0^{(1)}, \ldots, \mathcal{G}_0^{(N_c)}\} \tag{3.200}$$

Proof sketch. The assumptions of the proposition are constructed in such a manner that $\bar{r}_i$ and r_i can be computed independently of all other agents but the ones in the same

connected component of $\mathcal{G}$ as agent i. To see this, consider any connected component $\mathcal{G}_0^{(l)}$ of $\mathcal{G}$ and note that:

- By assumption (iv),

$$r_i(k) = \min\{\text{dist}(x_i(k), \partial\mathcal{W}), \min_{j\neq i} \frac{1}{2}\big\|x_j(k) - x_i(k)\big\|\} \tag{3.201}$$

$$= \min\{\text{dist}(x_i(k), \partial\mathcal{W}), \min_{j\in\mathcal{V}_0^{(l)}\setminus\{i\}} \frac{1}{2}\big\|x_j(k) - x_i(k)\big\|\} \tag{3.202}$$

$$\tag{3.203}$$

- Assuming some Chebyshev center $\bar{x}_i(k)$ is given,

$$\bar{r}_i(k) = \text{depth}(\bar{x}_i(k), \mathbb{V}_i(x(k), \mathcal{W})) \tag{3.204}$$

$$= \text{depth}(\bar{x}_i(k), \mathbb{V}_i(x_i(k), \{x_j(k) \mid j \in \mathcal{V}_0^{(l)}\}, \mathcal{W})) \tag{3.205}$$

  where $\mathbb{V}_i(x_i(k), \{x_j(k) \mid j \in \mathcal{V}_0^{(l)}\}, \mathcal{W})$ is defined as

$$\{w \in \mathcal{W} \mid \|x_i(k) - w\| \leqslant \big\|x_j(k) - w\big\| \; \forall j \in \mathcal{V}_0^{(l)}\setminus\{i\}\}. \tag{3.206}$$

  Disregarding $j \notin \mathcal{V}_0^{(l)}$ is valid by assumption (iii). At $\bar{x}_i(k)$ the distance to half planes of $\mathbb{V}_i$ associated with agents $j \notin \mathcal{V}_0^{(l)}$ is greater than $\bar{r}_i(k)$ by construction.

The illustrated independence ensures that we may construct quantities analogous to $r_m(k), \bar{r}_m(k)$ and $\bar{r}_M(k)$ for each connected component of $\mathcal{G}$ which, locally to the connected component in question, inherits the important properties of its global counterparts. In particular the non-decrease and convergence of the local variant of $r_m(k)$ is vital. The result follows from applying a modified version of theorem 3.13 to each connected component using these specialized component-local quantities in place of the regular global $r_m(k)$ and $\bar{r}_M(k)$ in the proof of theorem 3.13 as well as in the other results the theorem relies on. □

A complete proof involves the rewriting of a trove the results related to d-dimensional convergence into a the specialized form required by the theorem using quite heavy notation and restrictive assumptions. This is outside the scope of the thesis. Meanwhile, the theorem as well as the proof sketch highlights some of the elements to keep in mind for generalizations.

While the assumptions of the theorem are quite restrictive, we have already seen one example where it applies. Recall 2D simulation 4 in figure 2.17a in section 2.7 - the example illustrating the degenerate case with non-unique Chebyshev centers. After a few iterations, the agent radii are independent of one another. Consistent with the theorem, the MAS converges to a set of Chebyshev configurations.

3.4.8 Concluding remarks on multi-dimensional convergence

The theoretical developments of section 3.4 for multi-dimensional target environments formally establish asymptotic MAS convergence to the set of Chebyshev configurations over time-varying connected interaction graphs. The deployment objective of convergence to optimal static configurations is achieved under the sufficient condition of unique agent Chebyshev centers along the trajectory of the MAS. Convergence for single-dimensional target environments is a special case in which the assumptions of the results always hold. In particular we establish convergence to an unique static Chebyshev configuration for a wider class of agent dynamics and agent control laws than assumed for analogous results in section 3.3. As such convergence to optimal static configurations for deployment to one-dimensional environments is now a solved problem.

Furthermore, the results verify that consensus-mechanisms are central for the convergence of the MAS to the set of Chebyshev configurations. Over time-varying and connected interaction graphs, the subsets of Chebyshev configurations to which the MAS converges are associated with consensus on Chebyshev radii and agent depth. Again deployment to one-dimensional environments represents a special case. The analogous multi-dimensional result can be seen as a generalization from 1D in the following sense: When imposing the connectedness-property inherent in the 1D case to the multi-dimensional case, the property of convergence to consensus on Chebyshev radii and agent depth is maintained.

3.4.9 Towards generalized convergence proofs

The novel connection to consensus theory as well as the introduction of the interaction graph opens for several interesting lines of research.

An extension of the results in order to show convergence to consensus within each connected component of a time-varying interaction graph, starting from any arbitrary initial structure, stands out in this respect. Such a result would be sufficient to show MAS convergence to the set of Chebyshev centers in the general case.

The illustrative examples presented so far highlight key phenomena of the framework. With regards to the 2D simulations in section 2.7, extensions of the interaction graph based convergence results are needed to explain the exhibited convergence in respectively 2D simulation 2 in figure 2.13 and 2D simulation 3 in figure 2.14. In both cases the observed behavior is less surprising given the presented theoretical developments. In particular the simulations resemble situations with convergence to consensus among agents within the same connected component of a graph. However, the conditions are complicated by the asymmetric dependencies among the strongly connected components of the directed interaction graph. Moreover, the time-varying nature of the number of connected components as well as members in each connected component must be accounted for.

The issue with degeneracy exemplified in 2D simulation 4, figure 2.17, must be dealt with separately. It illustrates that convergence to the set of Chebyshev centers is not sufficient to ensure convergence to optimal static configurations. While any Chebyshev configuration is optimal in the sense discussed in section 3.4.3, Chebyshev configurations are not

inherently static in degenerate cases. Further to the goal of achieving the deployment objective, modifications are in order.

Lack of convergence to the set of static configurations in degenerate cases can be regarded as a deficiency in the framework specification. The MAS behavior is under-constrained when the dimension of the set of agent Chebyshev centers is non-zero. Ad-hoc solutions include constraining the agents to stay at their current state whenever they are at a Chebyshev center. However, such a scheme could steer agents to configurations which do not exhibit the desired degree of symmetry. See figure 3.17 for an example. In both cases depicted, the agents are in a Chebyshev configuration. Still figure 3.17b exhibits a better coverage of the target region.

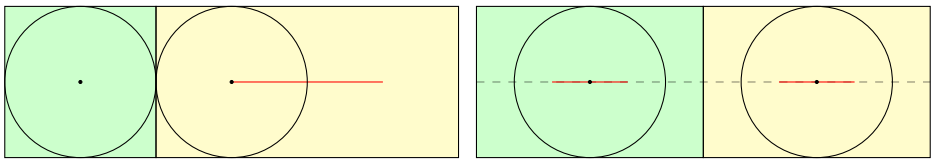

(a) MAS in Chebyshev center configuration. (b) MAS in general center configuration.

Figure 3.17: Symmetry of MAS Chebyshev configurations in a degenerate case. Dots indicate agents positions. Circles are Chebyshev balls. Red lines indicate sets of agent Chebyshev centers. Voronoi cells are indicated by colored regions.

Figure 3.17b shows an example of a *general center configuration* of a MAS, in which all agents are at a *general center* of their respective cells. The general center was introduced in [Nguyen, 2016] and an algorithm for its computation was derived in [Hatleskog, 2017]. The general center of a cell can be found by recursively computing the Chebyshev center within the previous set of Chebyshev centers, starting with the Chebyshev centers of the original cell as the first set[2]. The reader is referred to [Hatleskog, 2017] for details. For the case of figure 3.17b, observe that the set of Chebyshev centers of the original agent Voronoi cells are depicted with red lines. Additionally both agents are at a Chebyshev center of these line segments.

In [Nguyen, 2016] the author outlines a promising approach for achieving MAS convergence to a general center configuration. The author proposes the use of control actions ensuring a particular kind of contraction of each agent towards their current general center. A linear controller $\alpha_i(x_i^g - x_i)$, where x_i^g is the agents' current general center and $\alpha_i \in (0, 1]$, satisfies the above requirement. For the particular case of single integrator dynamics and such linear agent controllers, the conjectured property of MAS convergence to a general center configuration is supported by simulations in [Hatleskog, 2017].

Subsequent to such an adaption of the framework, the framework convergence results must be revisited once more. This time with the goal of proving convergence to a general center configuration. To accommodate the more complex inter-agent dependencies induced by

[2] A projection is necessary for embedding the polytopic set of Chebyshev centers in a space in which it is full-dimensional. Next the Chebyshev center within this set is computed in the normal manner by utilizing this latter embedding.

the general center, the interaction graph notion will have to be extended. Observe from 3.17b that the general centers of the agents depend on the half-plane separating the agents. This is not reflected in the MAS interaction graph. Meanwhile the same figure indicates that an appropriate extension of the interaction graph notion can have some explanatory power. Observe that the MAS configuration with respect to the 1D environment indicated by the dashed line in the middle of the figure is the unique static 1D configuration.

To summarize, we propose the following program for completing the convergence proofs as well as remedying the degeneracy issue:

1. Extend results on convergence to Chebyshev configurations over time-varying connected interaction graphs to convergence over time-varying graphs. A starting point would be to show convergence assuming the number of components and their members are time-invariant.
2. Modify the framework as suggested in [Nguyen, 2016] in order to steer the agents towards general center configurations.
3. Prove convergence of the MAS to the set of general center configurations by extending the interaction graph notion as well as related results on convergence to Chebyshev configurations.

If such a program were to succeed, the resulting deployment framework would have formal proofs of convergence to configurations satisfying the deployment objective.

This finalizes the discussion on convergence in multi-dimensional target environments. We refer the interested reader to section 3.5 for chapter notes. Next the thesis conclusion follows in chapter 4.

3.5 Chapter notes

The interaction graph is a novel notion for the framework discussed in this thesis. Meanwhile, the naming is inspired by graphs used in related settings. For instance the authors of [Mesbahi and Egerstedt, 2010] define particular interaction graphs for use in the context of formation control. As the interaction graph defined in this manuscript, the interaction graphs in [Mesbahi and Egerstedt, 2010] encode inter-dependencies between agents.

[Mesbahi and Egerstedt, 2010] also discusses the notion of *connectivity preserving control* in relation to formation control. Further to the introduction of the interaction graph to the present framework, a natural question is whether one can construct control laws maintaining interaction graph connectivity along the trajectory of the MAS. This is a topic for further research.

A topic which has not been addressed in any research works on Chebyshev center based deployment, is that of time-varying environments $\mathcal{W}$. In addition to being relevant for practical deployment scenarios, such a research direction could also inform the convergence results for time-varying disconnected interaction graphs. To see this, assume that a MAS has two strongly connected components in its directed interaction graph and also a globally reachable node. E.g. a globally reachable node in component one. In this case component one is unaffected by component two. Thus component two cannot affect component one, and the boundary component two has towards component one therefore resembles a time-varying environment boundary.

While we have chosen to use the section on convergence in multi-dimensional environments to generalize the 1D case beyond single integrator dynamics and linear controllers, several of the results derived in section 3.3 could also easily have been adapted in a direction of increased generality. E.g. theorem 3.8 could be adapted to accommodate the case of time varying gains α.

Further to the discussion on finite time convergence in section 3.3, a natural question is whether there exists any control scheme for the framework which guarantees finite time convergence. E.g. by having time-varying gains $\alpha_i(k)$. This is a topic for future research.

While we model agents as point masses, real agents obviously have a certain extent. The non-decrease of $r_m(k)$ is convenient in this context. Assume that $\bar{d}$ is the minimal distance between any pair of agents such that collision is avoided. Provided $r_m(0) \geqslant \bar{d}$, the non-decrease of $r_m(k)$ ensures collision avoidance.

In [Nguyen et al., 2017; Nguyen, 2016] the authors pursue a proof of MAS convergence to the set of Chebyshev configurations by showing the non-increase and convergence to zero of the energy-like function given in (3.98). However, a counterexample in [Hatleskog, 2017] illustrates that the result has certain limitations. These limitations are also difficult to fix, hence we chose to not follow this line of research.

Chapter 4

Conclusion

This thesis considers Voronoi-based multi-agent deployment utilizing the Chebyshev centers of the agents' Voronoi cells as the target points. Under mild assumptions, such a control policy leads to convergence of the multi-agent system (MAS) to particular static configurations. In these so-called static Chebyshev configurations, all agents are at a Chebyshev center of their associated Voronoi cell. The goal of the thesis is to provide a theoretical framework for the characterization of Chebysev configurations and convergence properties. While the subject is not new, the current work provides several novel results contributing to both structural analysis and the qualitative characterization of the MAS dynamics and behavior.

For the special case of deployment to $\mathbb{R}$, we i) prove asymptotic convergence to an unique static Chebyshev configuration, and ii) prove that the MAS achieves consensus on the agent Chebyshev radii in this asymptotic configuration. For the general case of deployment to $\mathbb{R}^d$, we first extend an existing result on convergence of the minimal distance any agent has to its cell boundary. Next we prove convergence of the minimal Chebyshev radius. The most important contribution of the thesis is related to the introduction of a novel undirected time-varying interaction graph. Exploiting this graph, we show that consensus-like behavior is inherent to all static MAS configurations. In particular we prove that all subsets of agents within the same connected component of the interaction graph have consensus on their Chebyshev radii whenever the MAS is in a static configuration. The final result considers MAS deployment to $\mathbb{R}^d$ when the time-varying interaction graph remains connected along the MAS trajectories. We prove that the MAS converges to a Chebyshev configuration in which all agents achieve consensus with respect to the Chebyshev radii. The convergence results obtained for deployment in $\mathbb{R}$ and $\mathbb{R}^d$ represents a significant strengthening of theoretical convergence results pertaining to the framework at hand. These are the first results proving convergence to Chebyshev configurations for multi-agent systems with more than one agent. Moreover, the consensus-like behavior has not been uncovered in previous works.

In the context of the present framework, the deployment objective entails driving the MAS to a static Chebyshev configuration. As reiterated in the thesis, convergence to a Chebyshev configuration is necessary to fulfill this goal. In this respect, generalizing the new convergence results to interaction graphs with several connected components is a pertinent candidate for further research on the framework. Meanwhile, we also highlight the fact that convergence to the set of Chebyshev configurations does not imply convergence to a static configuration. In degenerate cases, additional constraints must be imposed. This follows from the non-uniqueness of Chebyshev centers. We point to previous work suggesting the so-called general center as a mean to solve this issue. Merging the new convergence results with the general center notion thus represents the second interesting line of research. Finally, the framework would also benefit from a relaxation of the regularity constraints imposed on the agent dynamics. All of the three mentioned extensions will be addressed in future work.

Appendix A

Generalizing dynamics

For completeness we briefly sketch how the assumptions on agent dynamics can be generalized. Notably this generalization allows agents to have dynamics of higher dimension than the space to which they are deployed. The generalization proposed here follows Nguyen [2016].

Recall from section 2.1 that the assumptions on agent dynamics are motivated by the control law requirements (2.68)-(2.70) ensuring the following:

(i) By (2.69): If an agent is at a Chebyshev center of its Voronoi cell $\mathbb{V}_i(k)$, it can pursue a trajectory such that $x_i(k+1)$ remains in the set of Chebyshev centers of $\mathbb{V}_i(k)$. Thus for all $x_i \in \mathcal{W}$ all agents must have sufficient control authority to ensure that $x_i(k+1) = x_i(k)$ can hold.

(ii) By (2.68): If an agent is not at a Chebyshev center of its cell, it may be steered to some state $x_i(k+1)$ such that $\text{depth}(x_i(k+1), \mathbb{V}_i(k)) > \text{depth}(x_i(k), \mathbb{V}_i(k))$. This is ensured provided the agent can move from the boundary and to the interior of any full-dimensional convex set.

The first generalization is to consider deployment in the agents output space rather than their state space. I.e. all agent outputs evolve in a common output space $\mathbb{R}^d$. The agents are deployed to the target environment $\mathcal{W} \subset \mathbb{R}^d$. Assume that the dynamics of all agents $i \in \mathbb{N}_N$ are governed by the discrete time linear time-invariant equations

$$v_i(k) = A_i v_i(k) + B_i u_i(k) \in \mathbb{R}^{n_i} \tag{A.1}$$

$$x_i(k) = C_i v_i(k) \in \mathbb{R}^d \tag{A.2}$$

where $A_i \in \mathbb{R}^{n_i \times n_i}$, $u_i \in \mathbb{R}^{m_i}$, $B_i \in \mathbb{R}^{n_i \times m_i}$ and $C_i \in \mathbb{R}^{d \times n_i}$. This notation is somewhat non-standard since one usually would let x_i denote state and y_i denote output. By letting x_i be the output, most of the definitions and derivations of the previous chapters still make sense. For instance, the Voronoi cells are still computed with respect to the x_i's. The same goes for agent depth and Chebyshev radii. However, the interpretation of x_i changes from agent state to agent output.

The control law requirements also remain the same. The next step is to impose a new set of regularity constraints on the dynamics in order to ensure that the control law requirements (2.68)-(2.70) can be met.

Assumption A.0.1 (Regularity conditions for output space deployment)**.**

(i) *The pair* (A_i, B_i) *is controllable for all* $i \in \mathbb{N}_N$.

(ii) *The pair* (C_i, A_i) *is observable for all* $i \in \mathbb{N}_N$.

(iii) *For all* $\hat{x}_i \in \mathbb{R}^d$ *and for all* i *there exists* $(\hat{v}_i, \hat{u}_i)$ *such that* $\hat{x}_i = C_i(A_i\hat{v}_i + B_i\hat{u}_i)$. *I.e. the system*

$$\bar{v}_i = A_i\bar{v}_i + B_i\bar{u}_i \tag{A.3}$$
$$\bar{y}_i = C_i\bar{x}_i \tag{A.4}$$

is feasible for any $y_i \in \mathcal{W}$.

(iv) *For all agents* i, *any full-dimensional convex set* $P \subset \mathbb{R}^d$ *is output controlled* λ*-contractive with respect to the agent dynamics. I.e. for any* $x_i \in \text{int}(P)$ *and any admissible* v_i *satisfying* $C_iv_i = x_i$ *there exists* u_i *such that*

$$C_i(A_iv_i + B_iu_i) \in \lambda(P \oplus \{-x_i\}) \oplus x_i \tag{A.5}$$

for some $\lambda \in [0, 1)$ *whenever* $x_i \in P$.

Now (2.69) is satisfied by (iii) in assumption A.0.1. Simple adjustments to the proof of 2.5.2 shows that also (2.68) is satisfied.

Still, particularly (iv) in assumption A.0.1 is relatively restrictive. In order to relax this condition, Nguyen [2016] introduces the following notion:

Definition A.0.1. *A full-dimensional convex set* $P \subset \mathbb{R}^d$ *is* K*-step controlled* λ*-contractive with respect to the dynamics of an individual agent* $i \in \mathbb{N}_N$ *if for any* $x_i(0) \in \text{int}(P)$ *and any admissible* $v_i(0)$ *satisfying* $C_iv_i(0) = x_i(0)$ *there exists an input sequence* $\{u_i(0), \ldots, u_i(K-1)\}$ *such that*

$$x_i(K) = C_i(A_iv_i(K-1) + B_iu_i(K-1)) \in \lambda(P \oplus \{-x_i(0)\}) \oplus x_i(0) \tag{A.6}$$

for some $\lambda \in [0, 1)$ *whenever* $x_i \in P$.

The following statement holds by theorem 4.1 in Nguyen [2016]: For any agent satisfying regularity conditions (i), (ii) and (iii) in assumption A.0.1 there exists a finite integer $K(\lambda)$ such that any full-dimensional convex set $P \subset \mathbb{R}^d$ is $K(\lambda)$-step controlled λ-contractive for any $\lambda \in (0, 1)$.

Thus the non-standard notion of K-step controlled λ-contractiveness can be exploited to relax the regularity conditions even further.

We end this section by outlining how deployment while exploiting this notion could be conducted. In this outline, we assume that all agents can communicate over a centralized

communications channel. Start from some static initial configuration $x(0)$. At time zero each agent computes its Voronoi cell and a trajectory which will steer it to some output with increased depth with respect to its cell. Next the regular deployment framework is bypassed until all agents have reached such an output, still with respect to their time-zero Voronoi cells. I.e. all agents simply follow the trajectories they have computed at time zero. Once all agents have messaged over the centralized communications channel that they have reached their respective targets, the procedure restarts with the present configurations as a new initial condition. Agents which are at at Chebyshev center at time zero can simply message that they have reached their target immediately. By theorem 4.1 in Nguyen [2016], the procedure will restart within some finite time $K \in \mathbb{N}$. In a sense, we vary the clock speed of the deployment framework. Each tick starts after all agents have communicated that they have reached their former targets. The time between each tick is finite by theorem 4.1 in Nguyen [2016].

Note that for any practical scenario, the strict assumption of having a centralized communications channel should be replaced in favor of a distributed scheme. It is beyond the scope of the thesis to discuss the details of the modifications. In fact, it is an open research problem to carve out the details of such a scheme. We refer to Nguyen [2016] for more on this proposal.

Bibliography

Alsalih, W., Islam, K., Rodríguez, Y. N., and Xiao, H. (2008). Distributed voronoi diagram computation in wireless sensor networks. In *SPAA*, page 364.

Bakolas, E. and Tsiotras, P. (2013). Optimal partitioning for spatiotemporal coverage in a drift field. *Automatica*, 49(7):2064–2073.

Bash, B. A. and Desnoyers, P. J. (2007). Exact distributed voronoi cell computation in sensor networks. In *Proceedings of the 6th international conference on Information processing in sensor networks*, pages 236–243. ACM.

Blanchini, F. and Miani, S. (2008). *Set-theoretic methods in control*. Springer.

Boyd, S. and Vandenberghe, L. (2004). *Convex optimization*. Cambridge University Press.

Bullo, F. (2018). *Lectures on Network Systems*. CreateSpace. With contributions by J. Cortes, F. Dorfler, and S. Martinez. Electronically available at http://motion.me.ucsb.edu/book-lns.

Bullo, F., Cortes, J., and Martinez, S. (2009). *Distributed Control of Robotic Networks*. Applied Mathematics Series. Princeton University Press. Electronically available at http://coordinationbook.info.

Cortes, J. and Bullo, F. (2005). Coordination and geometric optimization via distributed dynamical systems. *SIAM Journal on Control and Optimization*, 44(5):1543–1574.

Cortes, J., Martinez, S., and Bullo, F. (2005). Spatially-distributed coverage optimization and control with limited-range interactions. *ESAIM: Control, Optimisation and Calculus of Variations*, 11(4):691–719.

Cortes, J., Martinez, S., and Bullo, F. (2006). Robust rendezvous for mobile autonomous agents via proximity graphs in arbitrary dimensions. *IEEE Transactions on Automatic Control*, 51(8):1289–1298.

Cortes, J., Martinez, S., Karatas, T., and Bullo, F. (2002). Coverage control for mobile sensing networks. In *Robotics and Automation, 2002. Proceedings. ICRA'02. IEEE International Conference on*, volume 2, pages 1327–1332. IEEE.

Cortes, J., Martinez, S., Karatas, T., and Bullo, F. (2004). Coverage control for mobile sensing networks. *IEEE Transactions on robotics and Automation*, 20(2):243–255.

Francis, B. (2014). The robot rendezvous problem. In *53rd IEEE Conference on Decision and Control*, pages 1–3.

Fukuda, K. (2004). Frequently asked questions in polyhedral computation, 2004. Technical report, ETH.

Fukuda, K. (2016). Lecture notes: Polyhedral computation, spring 2016.

Grünbaum, B. (2003). *Convex polytopes*. Springer-Verlag, New York,.

Hatleskog, J. (2017). Optimization based control for multi-agent deployment. Technical report, NTNU.

Herceg, M., Kvasnica, M., Jones, C. N., and Morari, M. (2013). Multi-parametric toolbox 3.0. In *Control Conference (ECC), 2013 European*, pages 502–510. IEEE.

Kolmogorov, A. and Fomin, S. (1975). *Introductory real analysis*. Dover Publications, New York,.

Kwok, A. and Martinez, S. (2010). Deployment algorithms for a power-constrained mobile sensor network. *International Journal of Robust and Nonlinear Control*, 20(7):745–763.

Martinez, S., Cortes, J., and Bullo, F. (2007). Motion coordination with distributed information. *IEEE Control Systems*, 27(4):75–88.

Mesbahi, M. and Egerstedt, M. (2010). *Graph theoretic methods in multiagent networks*. Princeton University Press.

Moarref, M. and Rodrigues, L. (2014). An optimal control approach to decentralized energy-efficient coverage problems. *IFAC Proceedings Volumes*, 47(3):6038–6043.

Murray, R. M. (2007). Recent research in cooperative control of multivehicle systems. *Journal of Dynamic Systems, Measurement, and Control*, 129(5):571–583.

Nguyen, M. T. (2016). *Safe predictive control for Multi-Agent dynamical systems*. Phd, CentraleSupelec.

Nguyen, M. T. and Maniu, C. S. (2016). Voronoi based decentralized coverage problem: From optimal control to model predictive control. In *Control and Automation (MED), 2016 24th Mediterranean Conference on*, pages 1307–1312. IEEE.

Nguyen, M. T., Maniu, C. S., and Olaru, S. (2017). Optimization-based control for multi-agent deployment via dynamic voronoi partition. *IFAC-PapersOnLine*, 50(1):1828–1833.

Nocedal, J. and Wright, S. J. (2006). *Numerical optimization*. Springer, 2 edition.

Rakovic, S., Grieder, P., and Jones, C. (2004). Computation of voronoi diagrams and delaunay triangulation via parametric linear programming. Technical report, ETH.

Ren, W. and Beard, R. W. (2008). *Distributed consensus in multi-vehicle cooperative control*. Springer.

Ritter, A., Elbert, P., and Onder, C. (2017). *How to Use the IDSCreport LaTeX Class*. Institute for Dynamic Systems and Control (IDSC), ETH Zürich, Switzerland.

Schlömer, N. (2008). matlab2tikz. *File Exchange-MATLAB Central*.

Schwager, M., Slotine, J.-J., and Rus, D. (2011). Unifying geometric, probabilistic, and potential field approaches to multi-robot coverage control. In *Robotics research*, pages 21–38. Springer.

Song, Y., Wang, B., Shi, Z., Pattipati, K. R., and Gupta, S. (2014). Distributed algorithms for energy-efficient even self-deployment in mobile sensor networks. *IEEE Transactions on Mobile Computing*, 13(5):1035–1047.

Tanner, H. G. (2004). Flocking with obstacle avoidance in switching networks of interconnected vehicles. In *IEEE International Conference on Robotics and Automation*, volume 3, pages 3006–3011. IEEE.

Tanner, H. G., Jadbabaie, A., and Pappas, G. J. (2007). Flocking in fixed and switching networks. *IEEE Transactions on Automatic control*, 52(5):863–868.

Voronoï, G. (1908). Nouvelles applications des paramètres continus à la théorie des formes quadratiques. deuxième mémoire. recherches sur les parallélloèdres primitifs. *Journal für die reine und angewandte Mathematik*, 134:198–287.

Yan, Y. and Mostofi, Y. (2012). Utilizing mobility to minimize the total communication and motion energy consumption of a robotic operation. *IFAC Proceedings Volumes*, 45(26):180–185.

Yun, X. and Yamamoto, Y. (1992). On feedback linearization of mobile robots. Technical report, University of Pennsylvania.

Ziegler, G. M. (2012). *Lectures on polytopes*. Springer Science & Business Media.